ornl

OAK RIDGE NATIONAL LABORATORY

UNION CARBIDE

NUREG/CR-1530, Part 2
ORNL/NUREG-80/P2

MASTER

Potential Radiological Impact of Tornadoes on the Safety of Nuclear Fuel Services' West Valley Fuel Reprocessing Plant

2. Reentrainment and Discharge of Radioactive Materials

W. Davis, Jr.

Prepared for the
U.S. Nuclear Regulatory Commission
Division of Fuel Cycle and Material Safety
Office of Nuclear Material Safety and Safeguards
Under Interagency Agreement DOE 40-549-75

OPERATED BY
UNION CARBIDE CORPORATION
FOR THE UNITED STATES
DEPARTMENT OF ENERGY

Printed in the United States of America. Available from
National Technical Information Service
U.S. Department of Commerce
5285 Port Royal Road, Springfield, Virginia 22161

Available from

GPO Sales Program
Division of Technical Information and Document Control
U.S. Nuclear Regulatory Commission
Washington, D.C. 20555

NUREG/CR-1530, Part 2
ORNL/NUREG-80/P2

Contract No. W-7405-eng-26

CHEMICAL TECHNOLOGY DIVISION

NUREG/CR--1530-Pt.2

TI86 000954

POTENTIAL RADIOLOGICAL IMPACT OF TORNADOES ON THE SAFETY OF NUCLEAR FUEL SERVICES' WEST VALLEY FUEL REPROCESSING PLANT

2. REENTRAINMENT AND DISCHARGE OF RADIOACTIVE MATERIALS

W. Davis, Jr.

Manuscript Completed: November 1979

Date Published: July 1981

Prepared for the
U.S. Nuclear Regulatory Commission
Division of Fuel Cycle and Material Safety
Office of Nuclear Material Safety and Safeguards
Washington, D.C. 20555
Under Interagency Agreement DOE 40-549-75
NRC FIN No. B0102

Prepared by the
OAK RIDGE NATIONAL LABORATORY
Oak Ridge, Tennessee 37830
operated by
UNION CARBIDE CORPORATION
for the
DEPARTMENT OF ENERGY

CONTENTS

ACKNOWLEDGMENTS

I am very pleased to acknowledge the guidance of A. T. Clark, L. S. Person, and C. J. Haughney of the Office of Nuclear Material Safety and Safeguards, U.S. Nuclear Regulatory Commission, during the development of this report. Calculations with the TVENT and SOLA-ICE codes were performed by L. J. Holloway and R. W. Andrae, authors of Part 1 of this report. I thank Alden Pierce, Clyde Alday, and their colleagues at Nuclear Fuel Services for providing details of the head-end cells of the plant, for the new data on dose rates in these cells, and for obtaining the cladding hulls and wipe samples from the Central Purpose Cell. Finally, I thank C. W. Nestor, Jr., of the Computer Sciences Division, for valuable discussions concerning several mathematical aspects of this report and members of the ORNL Analytical Chemistry Division for gamma-ray spectroscopic and particle counting data on the samples obtained from Nuclear Fuel Services.

POTENTIAL RADIOLOGICAL IMPACT OF TORNADOES ON THE SAFETY OF NUCLEAR FUEL SERVICES' WEST VALLEY FUEL REPROCESSING PLANT 2. REENTRAINMENT AND DISCHARGE OF RADIOACTIVE MATERIALS

W. Davis, Jr.

ABSTRACT

This report describes results of a parametric study of quantities of radioactive materials that might be discharged by a tornado-generated depressurization on contaminated process cells within the presently inoperative Nuclear Fuel Services' (NFS) fuel reprocessing facility near West Valley, New York. The study involved the following tasks: determining approximate quantities of radioactive materials in the cells and characterizing particle-size distribution; estimating the degree of mass reentrainment from particle-size distribution and from air speed data presented in Part 1; and estimating the quantities of radioactive material (source term) released from the cells to the atmosphere. The study has shown that improperly sealed manipulator ports in the Process Mechanical Cell (PMC) present the most likely pathway for release of substantial quantities of radioactive material in the atmosphere under tornado accident conditions at the facility.

---

1. SUMMARY AND CONCLUSIONS

This is the second of a two-part report on methods used to estimate the potential radiological impacts of a tornado strike at the presently inoperative Nuclear Fuel Services' (NFS) fuel reprocessing plant near West Valley, N.Y. This part includes estimating the quantities of radioactive materials (irradiated nuclear fuels) in the Process Mechanical Cell (PMC) and the the General Purpose Cell (GPC) and evaluating the degree of reentrainment of these materials. Finally, estimated ranges of reentrainment are combined with the near-floor wind speeds presented in Part 1 to derive source terms for tornadoes with maximum wind speeds of 100, 200, and 300 mph. Estimates of quantities of radioactive materials in the PMC and GPC are based on combining measured in-cell gamma-ray dose-rate measurements with a defined reference fuel and calculations with the ORIGEN and SDC computer codes. Parametric reentrainment calculations are based on several factors, including previously reported particle-size distributions and particulate terminal settling and threshold friction speeds.

In Part 1 it is concluded that the most direct pathway involves the discharge of air through inadequately sealed manipulator ports in the PMC. From the volume of air so discharged, we conclude that no radioactive material will be discharged if the tornado has a maximum speed of 100 mph. However, radioactive materials will be discharged from the PMC when wind speeds are 200 or 300 mph whether building walls surrounding this cell remain intact or are destroyed. With the walls and doors intact, the quantities of fission products dicharged into the PMC operating aisles will be in the order of 60 to 4000 Ci at 200 mph and 200 to 10,000 Ci at 300 mph. Corresponding quantities of actinides are 10 to 800 Ci and 50 to 2000 Ci. This material would most likely settle in the operating aisle; however, winds accompanying the tornado could generate high enough air flows in the corridors to carry the radioactive particles out of the building. With the building walls and doors destroyed, still larger quantities of radioactive materials would be discharged directly to the environment.

The average age of the reactor fuel particles in which these radioactive materials are contained is $\sim$10 years as of November 1978. Three cladding hulls and three wipe samples obtained from NFS were analyzed by gamma-ray spectroscopy. Frequencies of particle sizes on the wipe samples are shown to conform to a lognormal distribution.

The analyses of the two parts of this report show clearly that the simplest method for eliminating any potential for significant radiological impact from a tornado strike at the NFS plant would be to install secure plugs in all manipulator ports of the PMC and GPC that are now lightly covered with cardboard or plywood, including the port in the GPC now used as an inlet for a hose carrying carbon dioxide for fire extinguishing. Analysis of the facility with these proposed modifications included indicates that radiological releases from the head-end cells during a tornado strike would essentially be eliminated by these alterations.

2. INTRODUCTION

Nuclear Fuel Services (NFS), Inc., established the first commercial facility for processing irradiated Nuclear fuels at West Valley, New York, on the property of the Western New York Nuclear Service Center (WNYNSC) in 1966. The plant was operated until 1972 during which time 640 metric tons of irradiated fuel were processed. The plant was originally shut down in 1972 because of plans to expand capacity; on Septebmer 22, 1976, NFS announced its decision to withdraw from the nuclear fuel reprocessing business. The history of the WNYNSC and the interactions of local residents, and local, state, and federal agencies have been documented in ref. 1.

The NRC is concerned with the ability of the NFS plant in its present shutdown status to contain radioactive materials within the head-end processing cells in the event of a tornado strike at the facility.[2] Gamma-ray dose rate measurements have shown that there are significant quantities of radioactive materials in the Process Mechanical Cell (PMC), the General Purpose Cell (GPC), and the Chemical Process Cell (CPC). The NRC has sponsored a study by Los Alamos Scientific Laboratory (LASL) of tornado-induced air flow in nuclear facilities in an effort to learn how radioactive materials might be transferred through ventilation systems under tornado conditions.[3] The LASL study led to the development of the TVENT computer code[3,4] used in Part 1 of this two-part analysis.[5] This Part 2 describes a complimentary study of the quantities of radioactive materials in the head-end cells and of the reentrainment of this material by tornado-induced air flows.

The need for this study arises from the fact that there is radioactive material in the head-end cells, but no detailed analyses have been made of factors that could lead to the transport of this material into the atmosphere. The scope of this report includes identifying these factors, estimating ranges of their numerical values, and finally, estimating ranges of the quantities of radioactive materials that could be discharged from the head-end cells as a result of tornadoes defined in Part 1. The steps in this procedure are as follows:

1. Defining a mass-averaged reference fuel, including burnup and decay time, on the basis of documented information pertaining to fuels processed at NFS.

2. Obtaining gamma-ray dose-rate measurements in the head-end cells at known distances from surfaces on which radioactive materials are believed to be located (obtained by the staff of NFS).

3. Using the ORIGEN code to calculate the gamma-ray spectrum of the reference fuel at a series of decay times spanning the time at which the gamma-ray dose measurements were made.

4. Utilizing a gamma-ray shielding code, the SDC code in this case, to calculate dose conversion factors applicable to the gamma-ray spectrum obtained in step 3.

5. Using the measured dose rates and the dose-conversion factors to estimate the quantities of radioactive materials on head-end cell horizontal surfaces.

6. Estimating the particle size distribution of radioactive materials on head-end cell surfaces. The particulate matter of significance in this report was derived, primarily, from shearing irradiated light-water reactor (LWR) fuels which consist of UO_2. It is presumed to have the same size distribution ranges as obtained from analyses of sieve fractions from laboratory-scale shearing of single-irradiated LWR fuel rods.

7. Obtaining near-floor air speeds in head-end cells for each case in which discharge of radioactive materials cannot be ruled out. As described by Holloway and Andrae in Part 1,[5] the calculations were performed by use of the SOLA-ICE code.

8. Combining near-floor wind speeds, particle-size distribution data, and terminal settling and threshold friction speeds to estimate the fractional (weight) reentraiment of UO_2 particles as a function of wind speed.

9. Combining information from steps 5 and 8 to calculate the quantity of radioactive material that becomes airborne per unit surface area.

10. Defining the shape of the air space within each head-end cell from which air will be discharged. From this and the volume of air discharged, as defined in Part 1, calculate the dimensions of the air space. In particular, determine whether the air space intersects the floor. If the air space does not intersect the floor, conclude that no radioactive material is discharged from the cell. If air space intersects the floor, calculate the extent of reentrainment. Assume that all radioactive material reentrained from this segment of the floor is contained in the air discharged from the cell.

One topic not analyzed in either part of this report concerns the structural integrity of process building walls and doors under tornado-induced loadings. The potential radiological consequences of a tornado are much greater if exterior walls and doors are destroyed than if they remain intact.

3. RADIOACTIVE MATERIALS IN NFS CELLS

The primary reason for analyzing the potential radiological impacts of a tornado strike at the Nuclear Fuel Services' (NFS) fuel reprocessing plant is the presence of considerable quantities of radioactive materials in the head-end cells [Process Mechanical Cell (PMC), General Purpose Cell (GPC), and Chemical Process Cell (CPC)].[6] A quantitative estimate of the potential radiological impact requires an estimate of the quantity of radioactive material in each cell, particularly the PMC and the GPC, wherein the highest dose rates were measured. The CPC is of only minor importance in this analysis since most of the radioactivity in this cell is believed to be contained within various process vessels. In this section we describe the successive steps in making such estimates and the various assumptions at each step.

3.1 Elemental and Nuclide Composition

During the period April 22, 1966, to December 12, 1971, reprocessing of 28 batches of nuclear fuel was initiated at NFS. Only two types of fuel were represented in these 28 batches, namely LWR fuels and New Production Reactor (NPR) fuels from Hanford, Washington. A summary of the distribution of fuels processed at the NFS plant that will be significant in this report, from Table I-2-2 of ref. 7, the Safety Analysis Report of the NFS facility, is as follows:

Reactor type	No. of batches	Total weight (MTU)	Total burnup (MWd)	Average burnup (MWd/MTU)
NPR	11	379.4	774,481	2,041
LWR	16	245.1	2,848,674	11,623
Indian Pt-1 (special case)	1	16 (U + Th)		

Fuel from the NPR consisted of uranium in Zircaloy cladding; all of the LWR fuels, including the special ThO_2-UO_2 test fuel from the Indian Point-1 reactor, were in the form of metal oxide. From the above summary we calculate that the LWR oxide fuels (including the Indian Point-1 special material) constituted about 41 wt % of the fuel reprocessed at NFS and (excluding the ThO_2-UO_2 from Indian Point-1) in excess of 79% of the burnup.

In Sect. 4 we will be concerned with the reentrainment of radioactive particles as a result of abnormal flow of air near the floors of the GPC and PMC. Distribution of oxide particle sizes from the shearing of LWR fuels has been characterized, as will be discussed.[8] In addition, data have been presented concerning the fraction of fuel that is dislodged from segments of cladding as a function of the lengths into which single fuel rods are sheared.[8] No similar quantitative characterization of the sizes of particles from shearing NPR fuel has been performed. Finney,[9] using unirradiated NPR fuels, and Dymmel,[10] at the NFS plant, observed that the product from shearing this material, was in the form of chunks and that fine particles constituted only a small fraction of the total. From burnup data, a specified radiation dose rate would require about 4 times as much NPR fuel as power reactor fuel. Based particularly on this datum and the observations of Finney and Dymmel, we have made the apparently conservative assumption that all radiation in the PMC and GPC is derived from oxide fuel. The contribution of NPR to radiation dose rate is assumed to be within the large uncertainties inherent in this analysis.

On the basis of the above analysis, the sources of radioactivity in the head-end cells are assumed to be spent oxide fuel (excluding noble gases) and pieces of Zircaloy cladding. More specifically, the fuel-to-cladding ratio is assumed to be the same as that of the reference PWR

described by Croff et al.[11] It should be noted that no separation of uranium and/or plutonium from fission products occurred in the PMC or GPC, or in the dissolver of the CPC, during the operational life of the NFS plant. Thus, whether the fuel in the GPC was simply dislodged from pieces of cladding or was partly deposited as dissolver solution from the CPC, the nuclide and elemental composition will be essentially that of the irradiated fuel (excluding noble gases).

The reference fuel is assumed to have been UO_2, enriched to about 3.3 wt % in ^{235}U, irradiated at an average power density of 30 MW/MTU to a burnup of 16,171 MWd/MTU. The burnup value is an average for lots 13, 15, 16, 17, 19, 20, 23, 24, 25, and 26 of Table I-2-2 of the Safety Analysis Report of NFS.[7] The fuel is assumed to have been removed from reactors an average of 10 years prior to the radiation measurements made November 6, 1978. Of the fuels processed at NFS assumed not to contribute to the reference fuel, the Indian Point-1 material was the most unusual.

The significance of the uncertainty in the assumption of an average fuel age of 10 years at the time of dose-rate measurements was analyzed two ways. First, we compared data in Table I-2-2 of ref. 7 with similar data in US LWR Spent Fuel Inventory and Projection.[12] Such comparisons are possible only for the 4 reactors listed in Table 1. It should be noted that batches 4 and 5 of this table were used only to ensure cross identification, not to obtain an average age. From Table 1 the calculated mass-weighted average age of spent fuel in batches 13, 15, 16, 17, 19, 20, 24, and 26 in November 1978 was about 10 years and 4 months.

The second analysis of the effect of the uncertainty concerning average decay time was made by performing ORIGEN calculations[11] for decay times of 9, 10, and 11 years. Information pertinent to subsequent dose-rate calculations is summarized in Tables 2-4. An examination of numerical values or primcipal nuclide listings shows that "Total source strength" decreases only 5 to 6% per year and that there are only minor changes in the relative importance of various radioactive nuclides. Both analyses support the use of an average decay time of 10 years. Also, it is apparent that fission-product photons are by far the most important in dose-rate measurements and calculations.

3.2 Dose-Rate Calculations

Calculations of radiation dose rates to be expected from the reference fuel were performed with the Shield Design Code (SDC).[13] Variables in these calculations are as follows: (1) the fuel γ-ray spectrum, defined by the mean energy (column 1) and source strength (column 8 and note c) information in Tables 2-4; (2) the distribution of radioactive materials on surfaces, assumed to be uniform; (3) the dose rate measured at any point in a head-end cell, assumed to be expressible in terms of a perpendicular distance (D_o) from dose-rate meter to the center of a disk source, of radius r_o, the effective value of which is a function of the cell dimensions. Tables 5-7 summarize results of the

Table 1. Data on fuels reprocessed at NFS and dates of fuel discharge and initiation of reprocessing

Entries from NFS Table I-2-2						Entries from Y/OWI/SUB-77/42500							
Lot No.	Reactor	Date of start of fuel reproc.	Fuel weight (MTU)	Total Pu (kg)	Average burnup (MWd/MTU)	Discharge date (month/year)	Assemblies discharged Number	Assemblies discharged (MTHM)	Discharge burnup (MWd/MTHM)	Discharge isotopic data ^{235}U (%)	Discharge isotopic data Total Pu (kg)	Discharge isotopic data Fissionable Pu (%)	Time from discharge to 11/78 (years/months)
19	Big Rock Point (BWR)	11/26/70	18.4	72.8	9,212	4/66	24	3.34	5,000	2.42	13	95.0	12/7
						9/66	36	5.00	7,000	2.31	22	95.3	12/2
						5/67	30	4.17	8,000	2.26	20	92.0	11/6
						2/68	39	5.39	12,310	2.04	30	90.0	10/9
								17.90	8,460		85		
26		11/30/71	5.8	27.9	13,567	6/68	48	6.64	11,870	2.06	37	83.4	10/5
						- - - - - - - - - - - -							
A	Dresden-1 (BWR)	11/12/66	50.0	191.0	8,500	11/62	7	0.79	6,680	1.73	3	84.1	16/0
							1	0.11	6,380	1.68	1	84.0	
							182	20.30	6,480	0.68	76	82.0	
						4/64	5	0.56	6,000	1.70	2	85.0	14/7
							3	0.33	10,270	1.54	1	82.0	
							89	9.90	9,590	0.63	48	79.6	
						3/65	97	10.78	10,320	0.62	55	78.7	13/8
							1	0.11	14,630	1.32	1	79.0	
							102	11.38	7,820	1.60	50	83.0	
							487	54.26	8,120		237		
15		10/01/69	21.5	104.6	10,900	1/67	17	1.89	12,200	0.58	11	75.0	11/10
							2	0.20	12,307	0.76	1	76.0	
							4	0.37	8,590	1.40	2	79.0	
							83	9.21	12,200	0.58	53	76.0	
						9/68	65	7.23	8,960	0.64	34	78.8	10/2
							27	2.73	15,050	0.70	17	76.5	
							4	0.37	11,820	1.23	2	76.0	
							202	22.00	11,425		120		
						- - - - - - - - - - - -							
16	Indian Point-1 (PWR)	11/23/69	15.6	107.6	15,794	9/67	40	7.95	12,670	1.51	50	82.8	11/2
						2/70	40	7.90	19,040	1.50	63	81.6	8/9
							80	15.85	15,845		113		
20		01/11/71	7.6	68.1	23,445	12/70	40	7.64	23,460	1.82	66	80.5	7/11
						- - - - - - - - - - - -							
5	Yankee Rowe (PWR)	06/07/67	49.8	185.1	11,200	5/62	74	20.59	8,470	2.70	85	88.2	16/6
						7/63	40	11.13	10,150	2.60	66	86.4	15/4
						8/64	36	9.99	12,900	2.80	64	85.9	14/3
						8/65	38	10.22	16,500	2.50	72	84.7	13/3
							188	51.93	11,265		287		
13		05/14/69	19.6	176.0	20,500	10/66	36	9.68	17,270	2.40	73	84.9	12/1
						3/68	36	9.62	22,520	2.10	71	84.5	10/8
							72	19.30	19,885		144		
17		06/02/70	9.3	95.6	24,381	8/69	36	9.61	24,450	2.00	89	84.3	9/3
24		07/16/71	9.5	95.7	23,653	10/70	36	9.62	23,190	2.10	86	84.9	8/1

Table 2. Energy-dependent γ-ray source strength data, from ORIGEN calculations, 9 years after fuel discharge[a]

Photon mean energy (MeV)	Heavy metals		Cladding and hardware		Fission products		Total source strength[b,c] (phot $s^{-1}MTU^{-1}$)
	Source strength[b] (phot $s^{-1}MTU^{-1}$)	Principal nuclides	Source strength[b] (phot $s^{-1}MTU^{-1}$)	Principal nuclides	Source strength[b] (phot $s^{-1}MTU^{-1}$)	Principal nuclides	
0.015	1.055E13	Am-241, Pu-238 Pu-240, Pu-241					1.055E13
0.025	5.990E11	Am-241, Np-239					5.990E11
0.0375	6.101E10	Am-241					6.101E10
0.0575	8.753E12	Am-241					8.753E12
0.085	4.997E10	Am-243, Np-239					4.997E10
0.125	3.989E10	Np-239, U-237					3.989E10
0.150			1.349E12	Sb-125, Co-60 Te-125m	9.820E14	Y-90, Sr-90, Cs-137 Eu-154, Ba-137m, Rh-106 Eu-155, Sb-125, Pr-144	9.833E14
0.225	2.573E10	Np-239, U-237					2.573E10
0.375	4.580E09	Np-239	1.196E12	Sb-125	9.213E13	Y-90, Sb-125, Rh-106 Pr-144	9.333E13
0.575	5.253E08		1.533E12	Sb-125	1.668E15	Ba-137m, Cs-134, Y-90 Sb-125, Rh-106, Eu-154	1.670E15
0.850	2.819E08		4.664E10	Mn-54	9.957E13	Cs-134, Eu-154, Y-90 Rh-106	9.962E13
1.25	1.299E08		8.707E13	Co-60	3.191E13	Eu-154, Cs-134, Y-90	1.190E14
1.75	1.566E07		3.366E07		1.112E12		1.112E12
2.25	1.076E06		4.614E08		1.104E11	Pr-144	1.109E11
2.75	1.459E07		1.428E06		4.035E09		4.051E09
3.50	5.565E05		0		5.176E08		5.182E08
Total	2.009E13		9.119E13		2.875E15		2.986E15
MeV/sec	6.964E11		1.104E14		1.268E15		1.379E15

[a]Calculations were made with the ORIGEN version described by Croff et al. (ref. 11). The reference fuel is analyzed as though it had been in a PWR with initial U-235 content of 3.2%, irradiated to a burnup of 16,171 MWd/MTU at a specific power of 30 MW/MTU, where MTU means metric tons of uranium charged to the reactor. Croff et al. use the terminology Metric Ton Initial Heavy Metal (MTIHM); in this case heavy metal and uranium are synonymous since no plutonium recycle or thorium utilization occurs.

[b]Phot = photons.

[c]To compensate for the fact that the lowest energy accepted by SDC is 0.1 MeV, as well as to reduce the number of energy groups to 12 (the maximum accepted by SDC) or less, the first 5 groups were converted to an approximate equivalent of a 0.1-MeV group by multiplying each of the 5 source strengths by the square of the ratio (group energy/0.1). This was done at the suggestion of E. D. Arnold, one of the authors of the SDC code. The result is 3.213E12 photons $s^{-1}MTU^{-1}$ at 0.1 MeV.

Table 3. Energy-dependent γ-ray source strength data, from ORIGEN calculations, 10 years after fuel discharge[a]

Photon mean energy (MeV)	Heavy metals		Cladding and hardware		Fission products		Total source strength[b,c] (phot $s^{-1}MTU^{-1}$)
	Source strength[b] (phot $s^{-1}MTU^{-1}$)	Principal nuclides	Source strength[b] (phot $s^{-1}MTU^{-1}$)	Principal nuclides	Source strength[b] (phot $s^{-1}MTU^{-1}$)	Principal nuclides	
0.015	1.091E13	Am-241, Pu-238 Pu-240, Pu-241					1.091E13
0.025	6.474E11	Am-241, Np-239					6.474E11
0.0375	6.490E10	Am-241					6.490E10
0.0575	9.465E12	Am-241					9.465E12
0.085	5.031E10	Am-243, Np-239					5.031E10
0.125	4.013E10	Np-239, U-237					4.013E10
0.150			1.099E12	Sb-125, Co-60 Te-125m	9.461E14	Y-90, Sr-90, Cs-137 Ba-137m, Eu-154, Eu-155 Rh-106, Sb-125, Pr-144	9.472E14
0.225	2.554E10	Np-239, U-237					2.554E10
0.375	4.607E09	Np-239	9.317E11	Sb-125	8.707E13	Y-90, Sb-125, Rh-106 Pr-144	8.801E13
0.575	5.389E08		1.194E12	Sb-125	1.599E15	Ba-137m, Cs-134, Y-90 Sb-125, Eu-154, Rh-106	1.600E15
0.850	2.854E08		4.536E10	Mn-54	7.868E13	Cs-134, Eu-154, Y-90 Rh-106	7.873E13
1.25	1.296E08		7.634E13	Co-60	2.852E13	Eu-154, Y-90, Cs-134	1.049E14
1.75	1.565E07		3.049E07		1.001E12		1.001E12
2.25	1.049E06		4.046E08		4.783E10	Pr-144	4.824E10
2.75	1.485E07		1.252E06		2.022E09		2.038E09
3.50	5.421E05		0		2.602E08		2.607E08
Total	2.120E13		7.961E13		2.740E15		2.841E15
MeV/sec	7.440E11		9.666E13		1.198E15		1.295E15

[a]Calculations were made with the ORIGEN version described by Croff et al. (ref. 11). The reference fuel is analyzed as though it had been in a PWR with initial U-235 content of 3.2%, irradiated to a burnup of 16,171 MWd/MTU at a specific power of 30 MW/MTU, where MTU means metric tons of uranium charged to the reactor. Croff et al. use the terminology Metric Ton Initial Heavy Metal (MTIHM); in this case heavy metal and uranium are synonymous since no plutonium recycle or thorium utilization occurs.

[b]Phot = photons.

[c]To compensate for the fact that the lowest energy accepted by SDC is 0.1 MeV, as well as to reduce the number of energy groups to 12 (the maximum accepted by SDC) or less, the first 5 groups were converted to an approximate equivalent of a 0.1-MeV group by multiplying each of the 5 source strengths by the square of the ratio (group energy/0.1). This was done at the suggestion of E. D. Arnold, one of the authors of the SDC code. The result is 3.461E12 photons $s^{-1}MTU^{-1}$ at 0.1 MeV.

Table 4. Energy-dependent γ-ray source strength data, from ORIGEN calculations, 11 years after fuel discharge[a]

Photon mean energy (MeV)	Heavy metals		Cladding and hardware		Fission products		Total source strength[b,c] (phot $s^{-1}MTU^{-1}$)
	Source strength[b] (phot $s^{-1}MTU^{-1}$)	Principal nuclides	Source strength[b] (phot $s^{-1}MTU^{-1}$)	Principal nuclides	Source strength[b] (phot $s^{-1}MTU^{-1}$)	Principal nuclides	
0.015	1.124E13	Am-241, Pu-238 Pu-240, Pu-241					1.124E13
0.025	6.933E11	Am-241, Np-239					6.933E11
0.0375	6.860E10	Am-241					6.860E10
0.0575	1.014E13	Am-241					1.014E13
0.085	5.063E10	Am-243, Np-239					5.063E10
0.125	4.035E10	Np-239, U-237					4.035E10
0.150			8.983E11	Sb-125, Co-60 Te-125m	9.161E14	Y-90, Sr-90, Cs-123 Ba-137m, Eu-154, Eu-155 Sb-125, Rh-106, Pm-147	9.170E14
0.225	2.535E10	Np-239, U-237					2.535E10
0.375	4.632E09	Np-239	7.258E11	Sb-125	8.303E13	Y-90, Sb-125, Rh-106 Pr-144	8.376E13
0.575	5.516E08		9.296E11	Sb-125	1.541E15	Ba-137m, Cs-134, Y-90 Sb-125, Eu-154, Rh-106	1.542E15
0.850	2.887E08		4.457E10	Mn-54	6.340E13	Cs-134, Eu-154, Y-90 Rh-106	6.344E13
1.25	1.293E08		6.693E13	Co-60	2.577E13	Eu-154, Y-90, Cs-134	9.270E13
1.75	1.562E07		2.792E07		9.202E11		9.202E11
2.25	1.023E06		3.547E08		2.091E10	Pr-144	2.127E10
2.75	1.502E07		1.098E06		1.014E09		1.030E09
3.50	5.283E05		0		1.308E08		1.313E08
Total	2.227E13		6.953E13		2.630E15		2.722E15
MeV/sec	7.892E11		8.464E13		1.142E15		1.227E15

[a]Calculations were made with the ORIGEN version described by Croff et al. (ref. 11). The reference fuel is analyzed as though it had been in a PWR with initial U-235 content of 3.2%, irradiated to a burnup of 16,171 MWd/MTU at a specific power of 30 MW/MTU, where MTU means metric tons of uranium charged to the reactor. Croff et al. use the terminology Metric Ton Initial Heavy Metal (MTIHM); in this case heavy metal and uranium are synonymous since no plutonium recycle or thorium utilization occurs.

[b]Phot = photons.

[c]To compensate for the fact that the lowest energy accepted by SDC is 0.1 MeV, as well as to reduce the number of energy groups to 12 (the maximum accepted by SDC) or less, the first 5 groups were converted to an approximate equivalent of a 0.1-MeV group by multiplying each of the 5 source strengths by the square of the ratio (group energy/0.1). This was done at the suggestion of E. D. Arnold, one of the authors of the SDC code. The result is 3.695E12 photons $s^{-1}MTU^{-1}$ at 0.1 MeV.

Table 5. Conversion factors for dose rate to surface contamination density for 9.0-year decayed reference fuel

Perpendicular distance between disk source center and dose rate meter		Ratio of disk-source radius to source distance							
		2/3		1		4/3		2	
(m)	(ft)	Specific dose rate $\left(\frac{R}{hr \cdot MTU}\right)$	Conversion factor x 100 $\left(\frac{kg\ U/m^2}{R/hr}\right)$	Specific dose rate $\left(\frac{R}{hr \cdot MTU}\right)$	Conversion factor x 100 $\left(\frac{kg\ U/m^2}{R/hr}\right)$	Specific dose rate $\left(\frac{R}{hr \cdot MTU}\right)$	Conversion factor x 100 $\left(\frac{kg\ U/m^2}{R/hr}\right)$	Specific dose rate $\left(\frac{R}{hr \cdot MTU}\right)$	Conversion factor x 100 $\left(\frac{kg\ U/m^2}{R/hr}\right)$
0.3	0.98	161,100	4.94	136,980	2.58	114,990	1.73	81,916	1.08
0.6	1.97	42,574	4.67	35,939	2.46	29,987	1.66	21,184	1.04
0.9	2.95	19,287	4.58	16,240	2.42	13,523	1.63	9,527	1.03
1.2	3.94	10,956	4.54	9,214	2.40	7,664	1.62	5,392	1.02
1.5	4.92	7,055	4.51	5,928	2.39	4,928	1.61	3,464	1.02
1.8	5.91	4,920	4.49	4,132	2.38	3,433	1.61	2,412	1.02
2.1	6.89	3,626	4.48	3,043	2.37	2,528	1.61	1,775	1.02
2.4	7.87	2,782	4.47	2,335	2.37	1,939	1.60	1,361	1.02
2.7	8.86	2,202	4.46	1,848	2.36	1,534	1.60	1,076	1.01
3.0	9.84	1,787	4.45	1,498	2.36	1,244	1.60	873	1.01

Table 6. Conversion factors for dose rate to surface contamination density for 10.0-year decayed reference fuel

Perpendicular distance between disk source center and dose rate meter		Ratio of disk-source radius to source distance							
		2/3		1		4/3		2	
(m)	(ft)	Specific dose rate $\left(\frac{R}{hr \cdot MTU}\right)$	Conversion factor x 100 $\left(\frac{kg\ U/m^2}{R/hr}\right)$	Specific dose rate $\left(\frac{R}{hr \cdot MTU}\right)$	Conversion factor x 100 $\left(\frac{kg\ U/m^2}{R/hr}\right)$	Specific dose rate $\left(\frac{R}{hr \cdot MTU}\right)$	Conversion factor x 100 $\left(\frac{kg\ U/m^2}{R/hr}\right)$	Specific dose rate $\left(\frac{R}{hr \cdot MTU}\right)$	Conversion factor x 100 $\left(\frac{kg\ U/m^2}{R/hr}\right)$
0.3	0.98	151,470	5.25	128,790	2.75	108,110	1.84	77,015	1.15
0.6	1.97	40,026	4.97	33,788	2.62	28,192	1.76	19,917	1.11
0.9	2.95	18,133	4.88	15,269	2.57	12,713	1.74	8,957	1.10
1.2	3.94	10,301	4.83	8,662	2.55	7,205	1.73	5,069	1.09
1.5	4.92	6,633	4.80	5,573	2.54	4,633	1.72	3,257	1.09
1.8	5.91	4,625	4.78	3,884	2.53	3,227	1.71	2,267	1.08
2.1	6.89	3,409	4.76	2,861	2.52	2,377	1.71	1,669	1.08
2.4	7.87	2,616	4.75	2,195	2.52	1,823	1.71	1,280	1.08
2.7	8.86	2,071	4.74	1,737	2.51	1,442	1.70	1,012	1.08
3.0	9.84	1,680	4.74	1,409	2.51	1,169	1.70	820	1.08

Table 7. Conversion factors for dose rate to surface contamination density for 11.0-year decayed reference fuel

Perpendicular distance between disk source center and dose rate meter		Ratio of disk-source radius to source distance							
		2/3		1		4/3		2	
(m)	(ft)	Specific dose rate $\left(\frac{R}{hr \cdot MTU}\right)$	Conversion factor x 100 $\left(\frac{kg\ U/m^2}{R/hr}\right)$	Specific dose rate $\left(\frac{R}{hr \cdot MTU}\right)$	Conversion factor x 100 $\left(\frac{kg\ U/m^2}{R/hr}\right)$	Specific dose rate $\left(\frac{R}{hr \cdot MTU}\right)$	Conversion factor x 100 $\left(\frac{kg\ U/m^2}{R/hr}\right)$	Specific dose rate $\left(\frac{R}{hr \cdot MTU}\right)$	Conversion factor x 100 $\left(\frac{kg\ U/m^2}{R/hr}\right)$
0.3	0.98	143,620	5.54	122,110	2.90	102,510	1.94	73,024	1.21
0.6	1.97	37,952	5.24	32,038	2.76	26,731	1.86	18,885	1.17
0.9	2.95	17,193	5.14	14,477	2.71	12,055	1.83	8,493	1.16
1.2	3.94	9,767	5.09	8,214	2.69	6,832	1.82	4,806	1.15
1.5	4.92	6,287	5.06	5,284	2.68	4,393	1.81	3,088	1.15
1.8	5.91	4,386	5.04	3,683	2.67	3,060	1.81	2,150	1.14
2.1	6.89	3,232	5.02	2,713	2.66	2,253	1.80	1,582	1.14
2.4	7.87	2,480	5.01	2,081	2.66	1,728	1.80	1,213	1.14
2.7	8.86	1,963	5.00	1,647	2.65	1,367	1.80	960	1.14
3.0	9.84	1,593	5.00	1,336	2.65	1,109	1.79	778	1.14

parametric calculations for decay times of 9, 10, and 11 years for air-filled spaces. In each table the parameters are (1) the perpendicular distance (D_o) between disk-source center and dose-rate meter (0.3 to 3.0 m), and (2) the ratio of disk-source radius to source distance (r_o/D_o = 2/3, 1, 4/3, or 2). Specific dose rates are expressed in R/(hr MTU). In each table and at each value of D_o and r_o/D_o a conversion factor, in units (kg U/m^2)/(R/hr), is listed. When any measured dose rate (R/hr) is multiplied by the appropriate conversion factor, an estimate is obtained of surface concentration of radioactive material in units of (kg U/m^2). By comparing corresponding factors in Tables 5-7, it is again apparent that calculated doses are relatively insensitive to the average decay age in the time frame 9 to 11 years. It is also apparent that the factors decrease only slightly with increasing distance, D_o, between dose-rate meter and source, an expected conclusion since air is the only material between source and meter. The most significant changes in Tables 5-7 are due to changes in r_o/D_o.

3.3 Surface Concentrations of Reference Fuel in Head-End Cells

As mentioned in Sect. 3.2, the ORIGEN and SDC calculations are summarized in terms of conversion factors, which, when multiplied by a measured dose rate, yield values of surface contamination in terms of kilograms of reference fuel per square meter of area. Dose rates, measured by staff of NFS, at various locations in PMC and GPC are presented in Tables 8 and 9; locations of measurements are further defined in Figs. 1 and 2. Surfaces to which contamination values apply are floors in many cases; in the PMC, other surfaces are the shear, the DIPO Table, and Saw Table (Fig. 1).

3.3.1 Concerning dose-rate measurements in the PMC (Table 8)

Measurements 1 and 2 (70 and 320 R/hr). These values might both be due to radioactive materials on the shear, which is about 4.3 by 2.5 ft^2. The radius of a circle of this same area (~10.75 ft^2) is 1.85 ft. Measurement 1 was taken 8 ft above the shear, in which case r_o/D_o = 1.85/8 = 0.23, and the dose-rate conversion factor, from Fig. 3, is in the order of 0.1 [(kg U/m^2)/(R/hr)]. Thus, measurement 1 is equivalent to ~7 kg U/m^2 (on the shear table), and to 7 kg U on the whole table, whose area is ~1 m^2. On this same basis, measurement 2 corresponds to r_o/D_o = 1.85/1.5 = 1.2, and the dose rate conversion factor is ~0.02 [(kg U/m^2)/(R/hr)]. Measurement 2 thus is equivalent to ~6.8 kg U/m^2, essentially the same as measurement 1. However, instead of being due only to 7 kg U on the shear table, measurements 1 and 2 could be due to a still larger quantity of fuel on the table and floor under and around the shear.

Table 8. Radiation dose rates measured in the PMC of the NFS Plant on November 6, 1978[a]

No.	Measurement location Detailed description	Measured dose rate (R/hr)
1	6 ft from north end, 5 ft from east wall, 8 ft above shear	70
2	18 in. directly above shear	320
3	18 in. south of shear at magazine opening level 5 ft above floor	370
4	8 ft south of shear, 5 ft above floor, 4 ft from east wall	145
5	5 ft from C window, directly in front, 16 in. from DIPO table	80
6	5 ft from west wall, even with saw blade 18 in. from table	185
7	Directly in front of B window, 2 ft above table, 1 ft above saw rail, 5 ft from window	240
8	Directly in front of PMC transfer port, center of cell, 4 ft above rail	335
9	Same as (8) but 1 ft above rail	450
10	3 ft from PMC port, 2.5 ft above rail level In front of B window.	600

[a]The radiation survey was made by staff of the Nuclear Fuel Services Company and reported to the U.S. Nuclear Regulatory Commission. Measurement numbers and locations are shown in Fig. 1.

Table 9. Radiation dose rates measured in the GPC of the NFS Plant on November 6, 1978[a]

No.	Measurement location Detailed description	Measured dose rate (R/hr)
1	Southwest corner, 18 in. from south wall, 3 ft from door at crane room floor level ∿12 ft above floor	65
2	2 ft from south wall, 3 ft from west wall, 5 ft above floor, 18 in. from basket	115
3	18 in. from hull hopper, middle of cell (N-S), 4 ft from floor	230
4	Same as (3), only 1 ft from floor (hulls on floor)	480
5	Middle of cell, 7 ft from floor, in front of cell cooler	175
6	Middle of cell, front of cell cooler, 2.5 from floor, 10 in. from top of scrap drum with empty lids, miscellaneous	435
7	Middle of cell, 11 ft above floor, in front of cell cooler	105
8	2 ft over No. 2 basket, 3 ft from south wall, ∿10 ft above floor	140
9	1 ft in front of No. 2 basket, 2.5 ft from floor, ∿7 ft from fuel chute	350
10	2.5 ft in front of No. 2 window, 2 ft from floor, just east of hull dumper	650
11	In front of No. 3 (west) window (2 ft from window), 18 in. from floor, 1 ft west of dumping station	500

[a]The radiation survey was made by the staff of the Nuclear Fuel Services Company and reported to the U.S. Nuclear Regulatory Commission. Measurement numbers and locations are shown in Fig. 2.

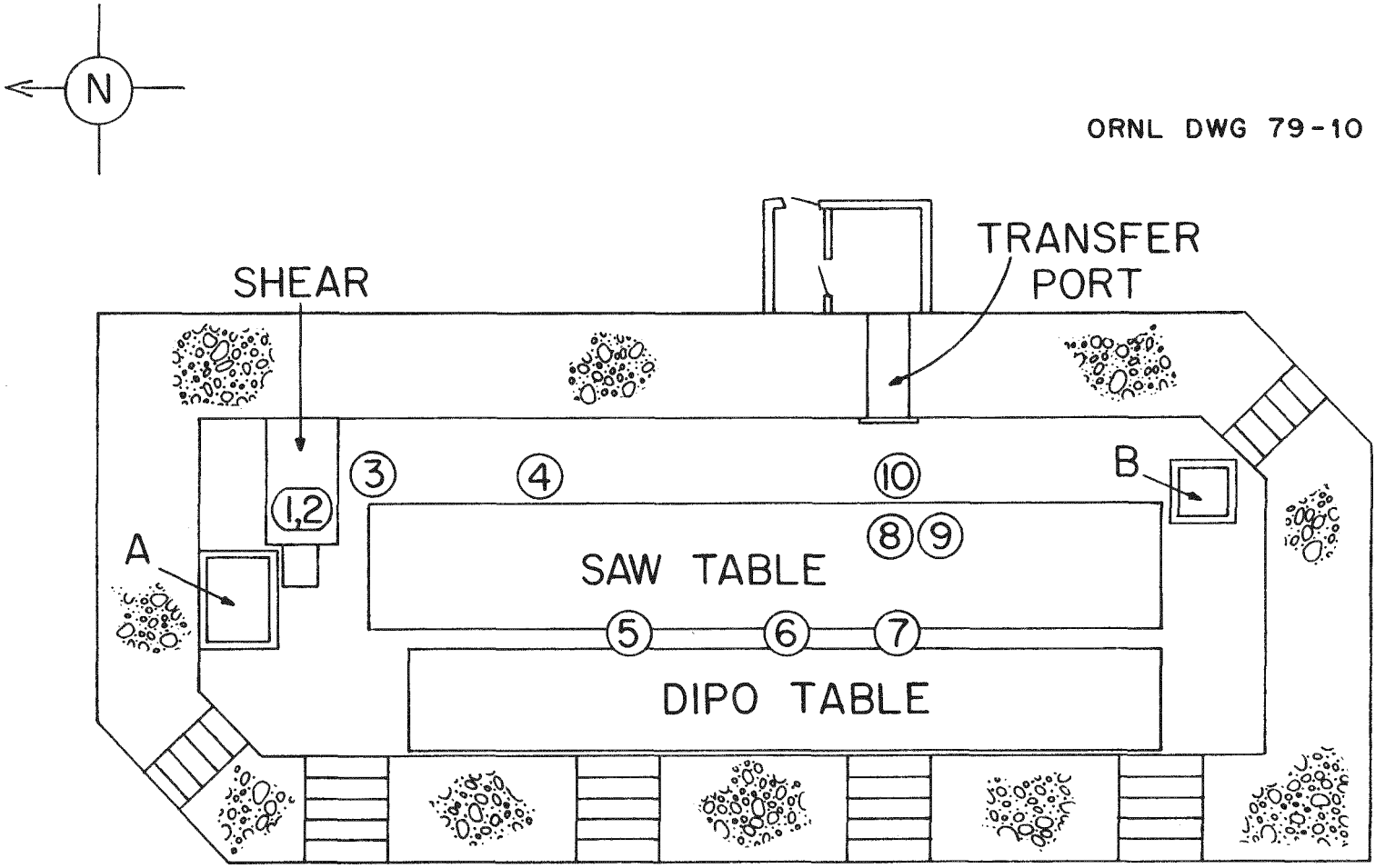

Fig. 1. Plan and dose-rate measurment locations: Process Mechanical Cell.

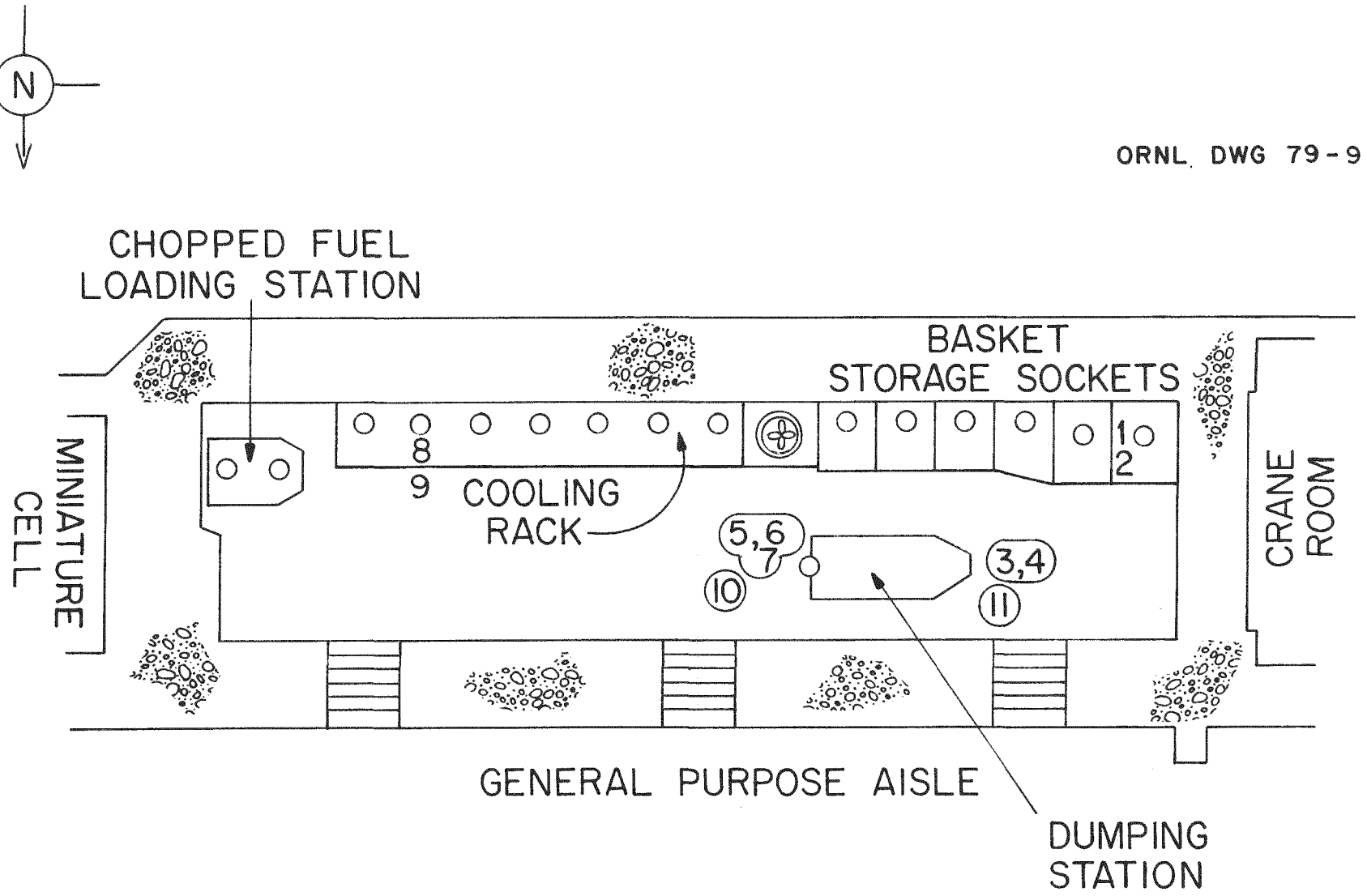

Fig. 2. Plan and dose-rate measurement locations: General Purpose Cell.

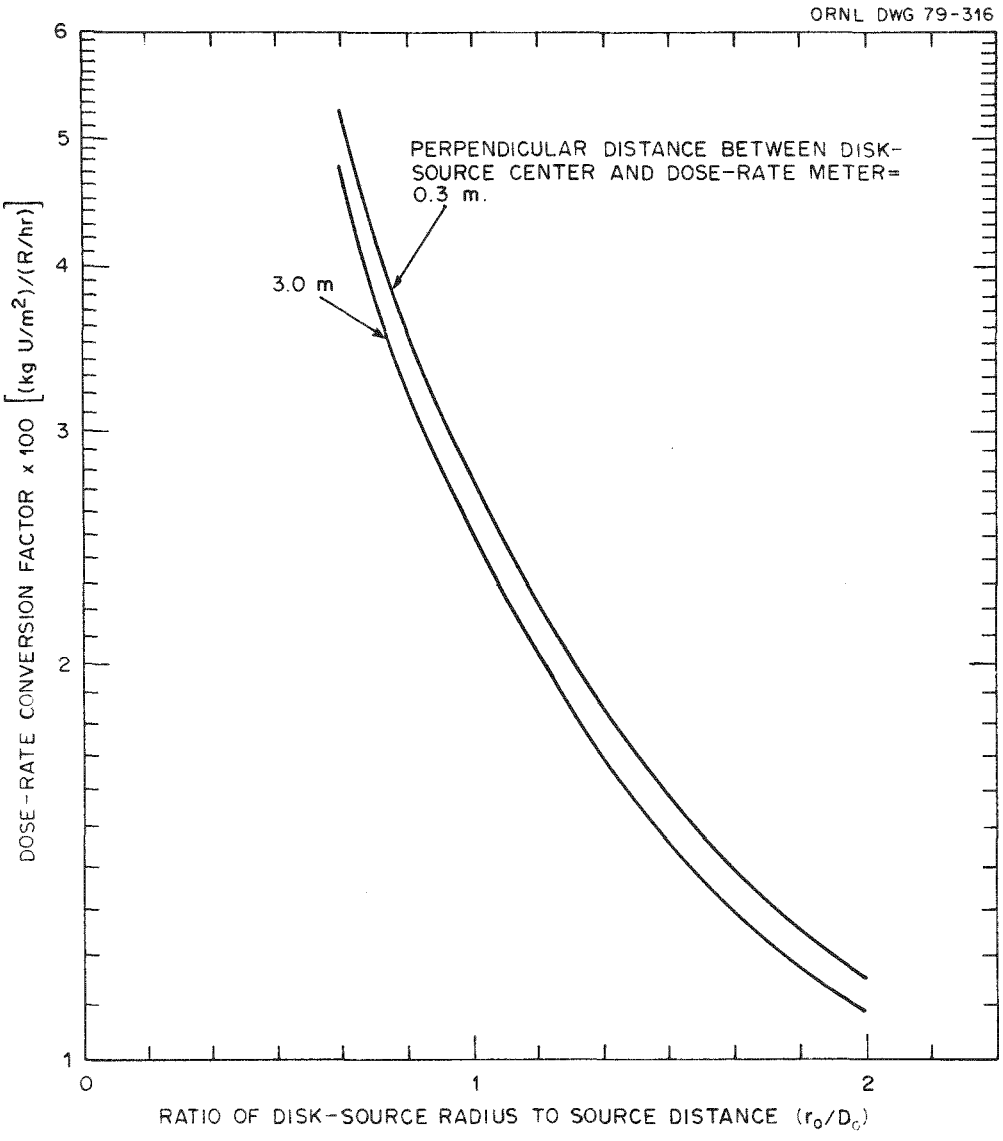

Fig. 3. Variation of dose-rate conversion factor with source-to-meter distance and with r_o/D_o.

Measurement 3 (370 R/hr). This measurement was taken at about the same height above the shear table as measurement 2, but offset 1.5 ft. While material on or under the shear table contributed to the 370 R/hr of measurement 3, other material, presumably on the floor or at the NE corner of the Saw Table must also have contributed. Using a source-to-meter distance of 2 to 5 ft, the dose-rate conversion factor from Fig. 3 changes from about 0.011 to 0.025-0.03 as r_o/D_o decreases from 2 to 1. Thus, the dose rate corresponds to 4 to 11 kg U/m^2.

Measurements 4 and 10 (145 and 600 R/hr). Between the Saw Table and the east wall of PMC is an area not normally visible through any viewing window. It is likely that fuel hardware fell from the Saw Table into this area and was not removed during normal cleaning operations employed to remove visible quantities of fuel and hardware. At a height of 5 ft above the floor for measurement 4 and an r_o/D_o of 1, the dose-rate conversion factor of 0.027 suggests ~4 kg U/m^2; by contrast, the 145 R/hr reading might be due to hardware and cladding from about 13 times that much fuel (the total source strength divided by hardware and cladding source strength, Table 3). Measurement 10 corresponds to 6 to 16 kg U/m^2 or to a correspondingly larger quantity of hardware and cladding.

Measurements 5 through 9 (80 to 450 R/hr). On the bases of $1 \leq r_o/D_o \leq 2$, all of these measurements (except 5) correspond to 2 to 10 kg U/m^2 or to appropriately larger quantities of hardware and cladding. Measurement 5 corresponds to 1 to 2 kg U/m^2.

3.3.2 Concerning dose-rate measurements in the GPC (Table 9)

Dose-rate measurements in the GPC are in the same range as in the PMC. Based on $1 \leq r_o/D_o \leq 2$, these readings correspond to a little less than 1 kg U/m^2 (measurement 1 with $r_o/D_o = 2$) to 18 kg U/m^2 (measurement 10 with $r_o/D_o = 1$). As discussed above, instead of being due primarily to fission products from these quantities of uranium, the measured dose rates in some cases may be due to the presence of correspondingly larger amounts of hardware and cladding.

In both PMC and GPC, contamination values range from 1 to >10 kg U/m^2; in Sects. 4.2 and 4.3, we used the range 5 to 15 kg U/m^2 for the purpose of calculating the source term for radioactive airborne releases from the PMC. It is apparent from the dose-rate measurements that surface concentrations of reference fuel in PMC and GPC are very nearly equal. Using floor surface dimensions of 12 by 52 ft^2 for the PMC and 11 by 46 ft^2 for the GPC, the total quantities of fuel on surfaces in these cells are calculated to be in the range of 60 to 600 kg in the PMC and 50 to 500 kg in the GPC; probable values are in the order of 200 kg in each cell. In both cells hardware and cladding, relatively free of fuel, may be making more of a contribution to estimated quantities of fuel than expected as a result of accumulation in unviewable areas.

The primary uncertainty in calculated values of surface contamination is due to uncertainty in the effective value of r_o/D_o. From cell dimensions and dose-rate meter locations, it is probable that the effective value of r_o/D_o is < 2 in many cases, particularly at the greater distances between meter and surfaces.

4. RESUSPENSION OR REENTRAINMENT

Resuspension or reentrainment is of primary concern in any analysis of the potential radiological consequences of a tornado grounding at a fuel reprocessing plant such as the NFS plant at West Valley, N.Y. Many authors, as summarized in refs. 14 and 15, have presented resuspension data* with values in the range 10^{-3} to 10^{-10} m^{-1}. These data would appear to be of uncertain utility in evaluating reentrainment of particles of irradiated nuclear fuel from the floors (and other surfaces) of head-end cells at the NFS plant, as noted by Andrae et al.[3] and by Healy.[16] There are varied reasons for this conclusion including dissimilarity between the material being resuspended (sand, ZnS, limestone, etc.) and UO_2, the absence of information on particle size distribution of material from which resuspension occurred and on resuspended matter, wind speeds, humidity, etc.

4.1 A Model of Reentrainment

The model of resuspension presented in this report is based on the concept that air, flowing close to the floor and other surfaces where irradiated UO_2/fission product particulate matter is located, will reentrain some of this matter. There are many variables that will influence the amount of particulate matter that is reentrained including: air speed; particle size distribution when shearing of fuel was performed; degree of agglomeration during the decade since shearing was performed (Appendix A); particle shape; the magnitude of eddy velocities. In the simplified approach used in this report, we assume that the eddy currents will be of sufficient magnitude to cause entrainment of any particle whose terminal settling speed is less than the local average air speed. Most of the concepts of such an approach to resuspension have been presented by Corn[17] and by Davies.[18-20] Table 10 and Fig. 4 show the variation of settling speeds in air of spherical particles of density 10 g/cm^3, namely the density of UO_2. These values are based on the following two equations presented by Davies:[20]

---

*A common representation is in terms of a resuspension factor K defined as [air concentration ($\mu Ci/m^3$)]/[surface deposit concentration ($\mu Ci/m^2$)].

Table 10. Relaxation times and terminal and threshold friction speeds of spheres of density 10.0 g/cm^3 in air at one atmosphere pressure and 20°C

Particle diameter (μm)	Relaxation time (τ) (s)[a]	Terminal speed of fall (V_s) (cm/s)	Friction speed at threshold (cm/s)[b]				Weight in sizes less than the indicated value (%)[c]	
			without interparticle cohesion		with interparticle cohesion			
			B≤0.22 [Eq. (4-5)]	0.22≤B≤10 [Eq. (4-6)]	B≤0.22 [Eq. (4-3)]	0.22≤B≤10 [Eq. (4-4)]	Minimum	Maximum
0.01	3.09 E-9	3.03 E-6	7.74 E-1	NA	1.81 E+3	NA	NS	0.000027
0.02	1.23 E-8	1.21 E-5	1.09 E+0	NA	1.27 E+3	NA	NS	0.00010
0.03	2.77 E-8	2.72 E-5	1.34 E+0	NA	1.04 E+3	NA	NS	0.00021
0.05	7.72 E-8	7.57 E-5	1.73 E+0	NA	7.98 E+2	NA	NS	0.00052
0.1	3.09 E-7	3.03 E-4	2.45 E+0	NA	5.58 E+2	NA	NS	0.0017
0.2	1.23 E-6	1.21 E-3	3.46 E+0	NA	3.89 E+2	NA	NS	0.0051
0.3	2.77 E-6	2.72 E-3	4.23 E+0	NA	3.15 E+2	NA	NS	0.011
0.5	7.72 E-6	7.57 E-3	5.46 E+0	NA	2.40 E+2	NA	0.0000024	0.031
1	3.09 E-5	3.03 E-2	7.70 E+0	NA	1.66 E+2	NA	0.000038	0.12
2	1.23 E-4	1.21 E-1	1.08 E+1	NA	1.14 E+2	NA	0.00045	0.39
5	7.72 E-4	7.57 E-1	1.64 E+1	NA	6.90 E+1	6.88 E+1	0.0091	1.54
10	3.08 E-3	3.02 E+0	2.15 E+1	NA	NA	4.65 E+1	0.056	3.71
15	6.88 E-3	6.75 E+0	2.45 E+1	2.42 E+1	NA	3.84 E+1	0.15	5.88
20	1.21 E-2	1.19 E+1	NA	2.49 E+1	NA	3.46 E+1	0.30	7.95
25	1.86 E-2	1.82 E+1	NA	2.56 E+1	NA	3.27 E+1	0.49	9.90
30	2.60 E-2	2.55 E+1	NA	2.63 E+1	NA	3.17 E+1	0.71	11.7
50	6.21 E-2	6.09 E+1	NA	2.89 E+1	NA	3.14 E+1	1.90	18.1
100	1.68 E-1	1.65 E+2	NA	3.54 E+1	NA	3.63 E+1	5.87	29.6
150	2.76 E-1	2.71 E+2	NA	4.13 E+1	NA	4.18 E+1	7.93	37.6
200	3.81 E-1	3.74 E+2	NA	4.66 E+1	NA	4.69 E+1	9.65	44.7
250	4.83 E-1	4.74 E+2	NA	5.14 E+1	NA	5.17 E+1	11.2	50.2
300	5.80 E-1	5.69 E+2	NA	NA	NA	NA	12.5	54.7
400	7.61 E-1	7.46 E+2	NA	NA	NA	NA	14.9	61.7
500	9.26 E-1	9.08 E+2	NA	NA	NA	NA	16.9	66.9
1000	1.58 E+0	1.55 E+3	NA	NA	NA	NA	24.2	80.7

[a]Calculated at $\tau = V_s/g$, where g = acceleration of gravity (980.7 cm/s^2).

[b]NA means "not applicable."

[c]NS means "not significant."

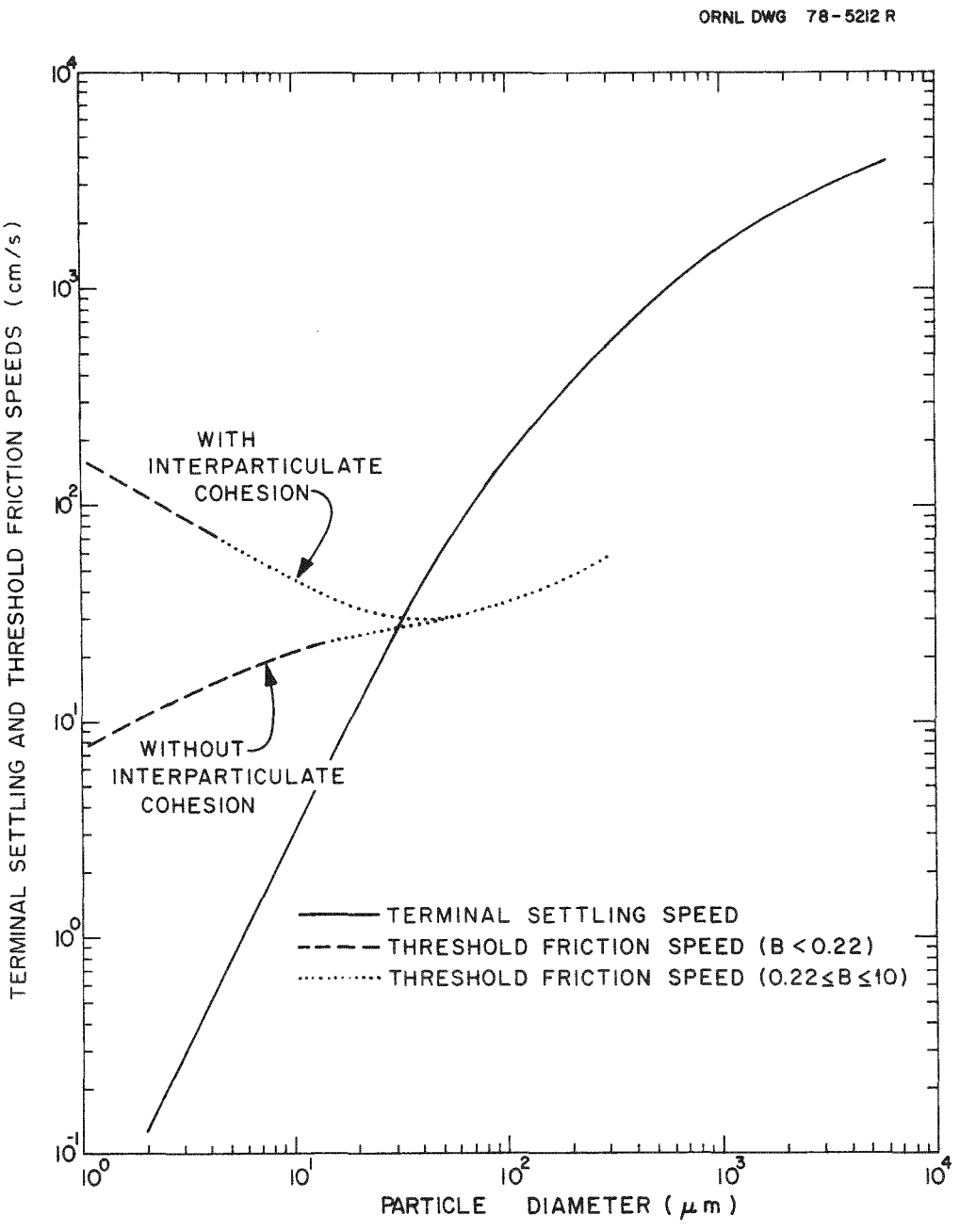

Fig. 4. Terminal settling and threshold friction speeds of spherical particles of density = 10 g/cm^3 in air at 20°C and 1 atm pressure.

For $N_{Re} < 4$,

$$N_{Re} = \Omega/24 - 2.3363 \times 10^{-4}\ \Omega^2 + 2.0154 \times 10^{-6}\ \Omega^3 - 6.9105 \times 10^{-9}\ \Omega^4; \quad (1)$$

For $3 \leq N_{Re} \leq 10^4$,

$$\log N_{Re} = -1.29536 + 0.986 \log \Omega - 4.6677 \times 10^{-2} \log \Omega^2 + 1.1235 \times 10^{-3} \log \Omega^3. \quad (2)$$

In these equations,

N_{Re} = Reynolds number,

$\Omega = C_D N_{Re}^2$,

and

C_D = drag coefficient.

Very small particles (smaller than ~30 μm for spheres of density 10 g/cm^3), however, do not become reentrained at air speeds as small as their settling speeds. Instead, there is for any particular size a threshold friction speed below which a particle will not move on the surface and will not become entrained; in turn, this speed depends on whether there is or is not any interparticulate cohesion. Iversen et al.[21] performed dust-resuspension experiments in wind tunnels and analyzed these and other data in terms of the threshold friction speed. Iversen et al.[22] used the resulting equations, given below, to estimate quantities of dust resuspended on Venus, Earth, and Mars.

<u>With interparticulate cohesion</u>:

(a) $B \leq 0.22$,

$$A = 0.266 \left(\frac{1 + 0.055/\rho_p g\ D_p^2}{1 + 2.123B} \right)^{1/2} \quad (3)$$

(b) $0.22 \leq B \leq 10$,

$$A = (0.108 + 0.0323/B - 0.00173/B^2)(1 + 0.055/\rho_p g D_p^2)^{1/2} \quad (4)$$

Without interparticulate cohesion:

(a) $B \leq 0.22$,

$$A = 0.266/(1 + 2.123B)^{1/2}. \quad (5)$$

(b) $0.22 \leq B \leq 10$,

$$A = 0.108 + 0.0323/B - 0.00173/B^2. \quad (6)$$

In Eqs. (3)-(6) the following definitions apply:

$$A = U_{xt}/[(\rho_p - \rho)gD_p/\rho]^{1/2} \text{ (threshold coefficient)} \quad (7)$$

$$B = U_{xt}\, D_p/\nu \text{ (particle friction Reynolds number)} \quad (8)$$

D_p = particle diameter

g = gravitational acceleration

$U*$ = friction speed $(\tau/\rho)^{1/2}$

$U*_t$ = friction speed at threshold

ρ = fluid (air) density

ρ_p = particle (UO_2) density

μ = viscosity

ν = kinematic viscosity

τ = shear stress

Friction threshold speeds are plotted in Fig. 4 and listed in Table 10, in both cases for the applicable range of values of B and for the presence or absence of interparticulate cohesion. It is apparent that essentially no resuspension of particles >1 μm will occur until the air speed attains a value in the order of 10 to 100 cm/s, depending on the strength of interparticulate cohesion.

The above calculations are based on the assumption that particles of UO_2/fission products are spherical. In fact, all photographs and photomicrographs of products obtained from shearing single rods from the H. B. Robinson-2 reactor and from the Peach Bottom-2 reactor show that the particles are not spherical; instead, they are elongated, as shown in Figs. 5 and 6 for H. B. Robinson fuel. (Burnup of fuel from the H. B. Robinson-2 reactor was in the range 11,000 to 28,000 MWd/Mg U and 9,000 to 11,000 MWd/Mg U from the Peach Bottom-2 reactor.[8]) However, ratios of maximum to minimum linear dimension rarely exceeded 3. Thus,

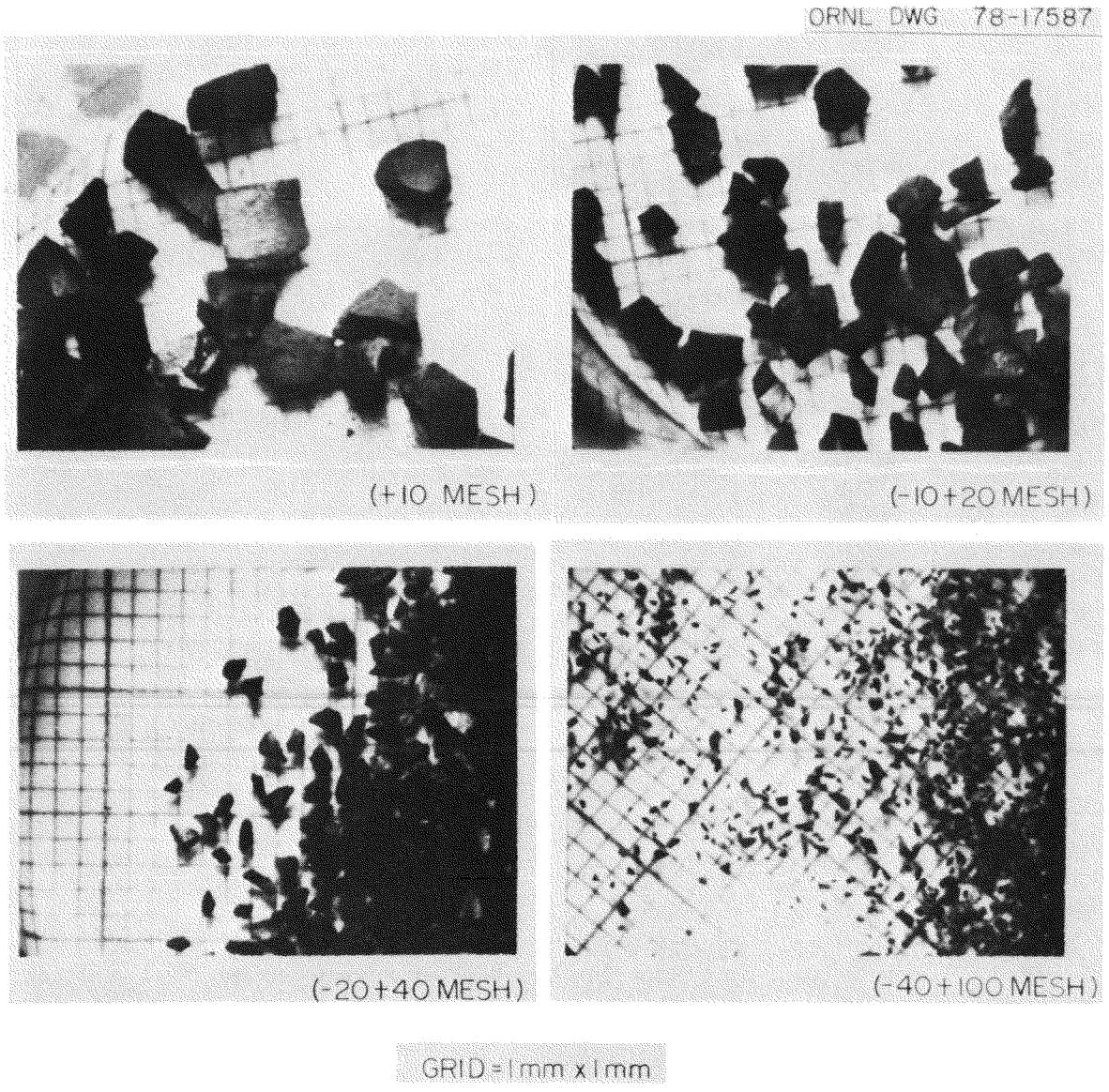

Fig. 5. Photomicrographs of sieve fractions from shearing one rod of irradiated fuel from the H. B. Robinson reactor.

ORNL DWG 78-17540

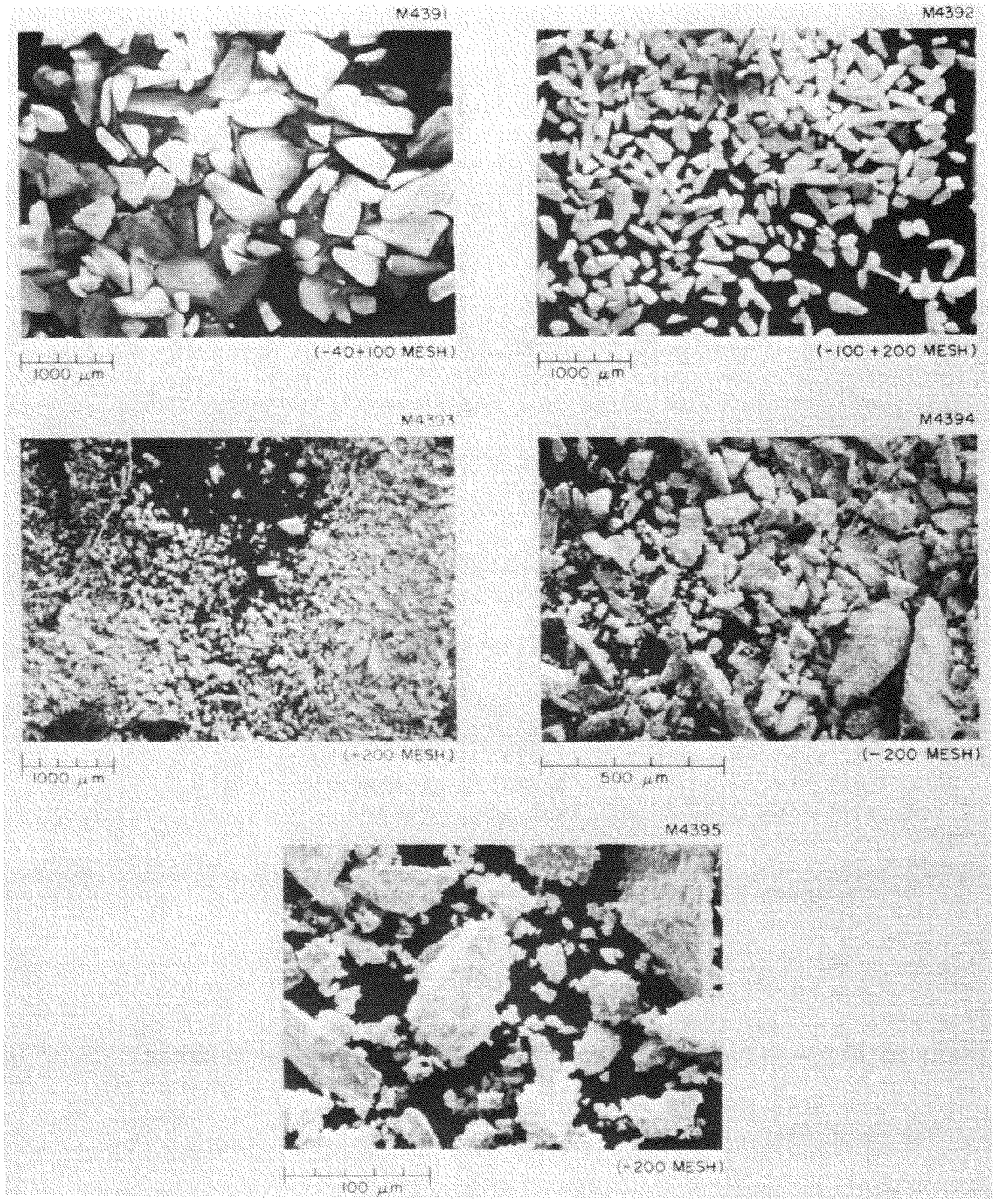

Fig. 6. Photomicrographs of fine particles from shearing H. B. Robinson fuel rods.

on the basis of Davies' sedimentation study,[20] fuel particles assumed to be representative of material that is on the floors (and other surfaces) of cells at NFS, are "spherical" within the accuracy of the model.

As noted previously, there is a considerable range in the parameters that define a lognormal distribution of particles produced by shearing unirradiated bundles or single irradiated rods of LWR fuels. The last two columns of Table 10 contain estimates of the minimum and maximum percentages of mass that will be of size less than values listed in column 1. In the present model we consider, for example, that a minimum of 0.30% and a maximum of 7.95% of the weight of dislodged fuel from the shearing of irradiated fuel will be in particle sizes of 20 μm or less.

As will be discussed in Sect. 4.2, the highest velocities of air near the floor in either the GPC or PMC under the worst tornado conditions considered in this report will be 450 cm/s (~15 fps). Thus, we will be concerned (Table 10) with the movement of particles up to 250 μm in size wherever these large velocities occur. As the air velocities decrease to about 30 cm/s (1 fps), particle movement becomes influenced by friction, in the presence or absence of interparticulate cohesion (Fig. 4); at still lower velocities, particles are nearly immobilized.

There is a question of response time that must be asked in analyzing the effects of a tornado strike, namely: "Will particles on the floor be exposed to higher-than-normal air velocities for a time long enough to become airborne?" Davies has presented values,[18] and a method for calculation of values, of a kind of relaxation time, τ, which is the time an isolated particle needs to adapt itself, or relax, to an applied force. For example, a spherical particle at rest and having a density of 10.0 g/cm^3 would acquire 1/e (~0.368) of the velocity of a suddenly applied air stream in the times listed in Table 10. For a 100-μm particle, this time is 0.17 s. Thus particles whose terminal settling or threshold friction speeds, Fig. 4, are exceeded will move, and are assumed to become airborne in the time frame of tornado effects, which are in the range of 0 to 20 or 30 s.

4.2 Reentrainment in the Head-End Cells

Four steps already taken in our evaluation of reentrainment of radioactive materials in head-end cells at NFS are as follows:

1. determining the distribution of particle sizes from shearing LWR oxide fuels;[8]

2. relating particle size with air velocity required to move and reentrain the particle (Sect. 4.1);

3. specifying the magnitude of the tornado, evaluating air flows at the boundaries when building walls remain intact and when they are destroyed, and identifying cases to be analyzed in more detail;[5]

4. obtaining air velocity data pertaining to near-floor locations by use of the SOLA-ICE code.[5,23]

As discussed by Holloway and Andrae,[5] air flows in head-end cells and tornado conditions requiring more detailed analysis involve discharge of air through manipulator ports into the PMC and GPC operating aisles, discharge of GPC ventilation air into the atmosphere via the adjoining Master Slave Manipulator building, with and without building walls remaining intact, and discharge of air from the CPC. Air flows and air paths are summarized in Table 11 and Fig. 7, as discussed in ref. 5.

Several aspects of the numbers in Table 11 need to be noted. First, when the building walls and doors remain intact, nearly as much air flows from the GPC to the PMC (Branch 4) as is discharged from the PMC to the operating aisles (Branch 3). Air flowing from the GPC to the PMC passes through a 4 by 3 ft^2 hatch that is located very close to the floor area directly below the lightly covered manipulator ports in the northwest corner of the PMC. For this reason, much of the air leaving the PMC (e.g., 1273 ft^3 in Case 1B1, Table 11) will have originated in the GPC. This does not mean, however, that 1142 ft^3 of the 1273 ft^3 discharged from the PMC in this case originated in the GPC. However, air flowing from the GPC to the PMC will largely originate from the upper volumes of the GPC, which is 19.5 ft high, where the only contaminant at the time of the tornado strike is radon. The point of these comments is that a significant, but unquantified, factor of conservatism will be introduced when it is assumed that all air discharged from the PMC actually was derived from air originally in the PMC; this assumption neglects dilution by air, initially containing no particulate matter, from the GPC.

Another aspect of the numbers in Table 11 that will be considered below is specification of the lightly covered ports in the PMC through which air will be discharged. When air discharged from the PMC is assumed to have been derived from a particular geometric shape, such as quarter sphere or truncated half cone, the parameters of that geometry will be a function of the volume. Thus, another factor that introduces an over estimation of the quantity of particulate matter discharged from the PMC is the assumption that all air is discharged through the three lightly covered ports in the northwest corner instead of equally through all seven lightly covered ports in this cell. This factor will be addressed below.

Finally, we note that numbers in the last column of Table 11 are the sums of discharges of contaminated and uncontaminated air.

The final step of the analysis involves combining the particle-size distribution data,[8] terminal settling and threshold friction speeds (Sect. 4.1), and the air-volumetric discharge and near-floor and spatial air-speed calculations presented by Holloway and Andrae.[5] The detail with which this combining can be performed is somewhat limited because of the complexity of the task and because the SOLA-ICE code is two-dimensional, not three-dimensional. For these reasons two simplified approaches have

Table 11. Air volumes discharged from cells during postulated tornado strike (from TVENT calculations)[a]

Case	Maximum tornado wind speed (mph)	Volume[b] released from PMC (ft^3)	Volume[b] released from GPC (ft^3)	Volume[b] released from CPC (ft^3)	Total discharge[c] to ambient from pathway (ft^3)
		Branch (3)	Branch (4)		Branch (1)
1A1 Outer	100	362	275	0	570
1B1 Walls	200	1273	1142	0	2300
1C1 Intact	300	1983	1922	0	3953
					Branches (2) and (3)
1A2 Outer	100	484	439	0	568
1B2 Walls	200	1947	2222	0	2792
1C2 Removed	300	3057	3913	0	5098
			Branch (7)	Branch (29)	Branch (28)
2A	100	0	0	896	919
2B	200	0	0	2552	2584
2C	300	0	45	3934	3976
			Branches (10) and (12)		Branch (8)
3A1 Outer	100	0	0.4	0	149
3B1 Walls	200	0	11.6	0	570
3C1 Intact	300	0	4.0	0	1001
					Branches (10) and (11)
3A2 Outer	100	0	289	0	300
3B2 Walls	200	0	928	0	970
3C2 Removed	300	0	1428	0	1515
			Branch (13)		Branch (27)
4A	100	0	0	0	0
4B	200	0	2344	0	57
4C	300	0	4004	0	810
5A	100	0	1281	0	1026
5B	200	0	2515	0	1843
5C	300	0	3657	0	2544

[a] See Fig. 4 for branch specifications and ref. 5 for detailed analyses.

[b] Air potentially contaminated with radioactive materials.

[c] Combined potentially contaminated air and uncontaminated air.

ORNL DWG 79-20872

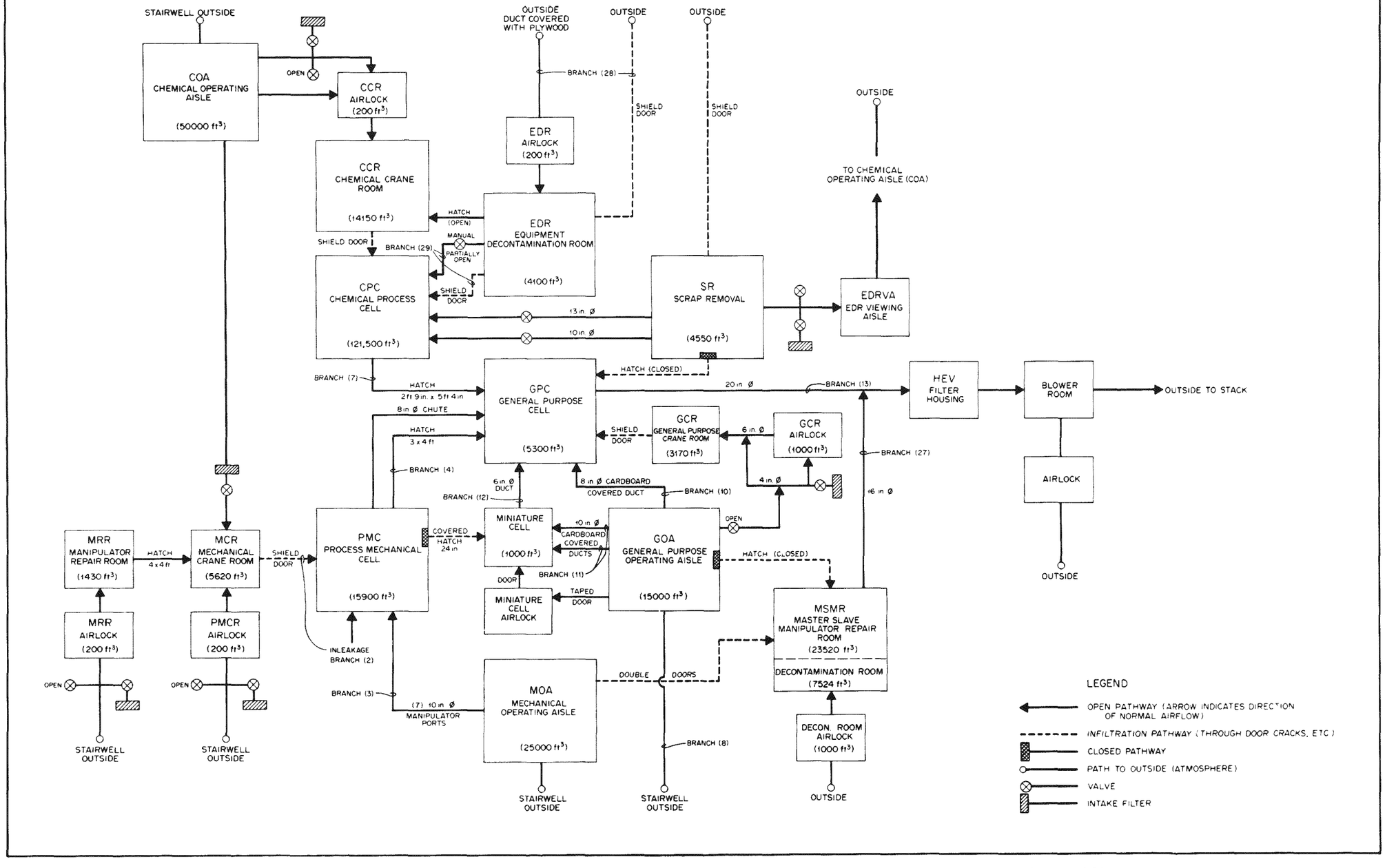

Fig. 7. Block diagram of NFS head-end cells, including air-flow branches of potential significance in releases of radioactive materials.

been used: (1) a method based on defining a spatial shape from which air within a cell is derived combined with the use of the maximum near-floor wind speeds calculated from the TVENT/SOLA-ICE combination; (2) a method based on evaluating fractional reentrainment within differential surface areas using the varying near-floor wind speeds calculated from the TVENT/SOLA-ICE combination. In either case, the degree to which reentrained particulate matter is discharged from a cell depends on the length of the path from the surface (floor or table) on which it is contained to a port that opens onto an operating aisle.

All cases in Table 11, except Cases 1A1 - 1C1 and 1A2 - 1C2, will be shown by simple arguments in Sect. 4.2.1 to involve no calculable discharge of radioactive particulate materials. Cases 2A - 2C involve discharge of air from the CPC. This is a large cell with a volume[7] of 88,000 ft^3; actual discharge of air would occur from an elevated port at the south end of the cell. Only in Case 2C does any air flow from the GPC to the CPC (Table 11) through the hatch at the north end of the CPC. In addition to there being significantly lower radiation readings in the CPC than in the GPC or PMC,[2] nearly all radioactive materials in the CPC are believed to be contained within process equipment. Thus, there are several factors that imply there will be no calculable quantities of particulate matter in air discharged from the CPC.

4.2.1 Assumed air-space shape

TVENT calculations yield values of air volumes discharged from cells during a strike by a tornado of specified maximum wind speed.[5] This air will always contain small quantities of radon from the decay chains of uranium and plutonium isotopes in fuel still in the head-end cells. However, the discharged air may not contain any particulate matter. In the absence of a three-dimensional model of air flow into and out of the PMC and GPC, cases requiring further analysis were identified on the basis of assuming a shape for the air space prior to its discharge through manipulator ports. A volumetric shape is used to determine whether there is, or is not, an intersection with surfaces on which particulate matter is contained. The concept is shown for a quarter sphere in the northwest corner of the PMC in Fig. 8 and in more detail in Fig. 9. A quarter-spherical volume of radius 10 ft (the distance of manipulator ports in the PMC and GPC above the floor) is about 1050 ft^3; a hemispherical volume of this radius is 2100 ft^3. Any cases involving smaller discharges, when these geometries can be assumed, are deleted from further consideration as containing no calculable amounts of particulate radioactivity.

An analysis of the problem of steady irrotational flow of air through an orifice provides a rationale for the choice of hemispherical or quarter-spherical volumetric shapes. This problem has been discussed by Morse and Feshback.[24] In the context of this report, a single open manipulator port (~10 in. in diameter), in the middle of a very thin wall with dimensions of 20 by 50 ft would, to a close approximation, be an orifice.

ORNL DWG 79-997

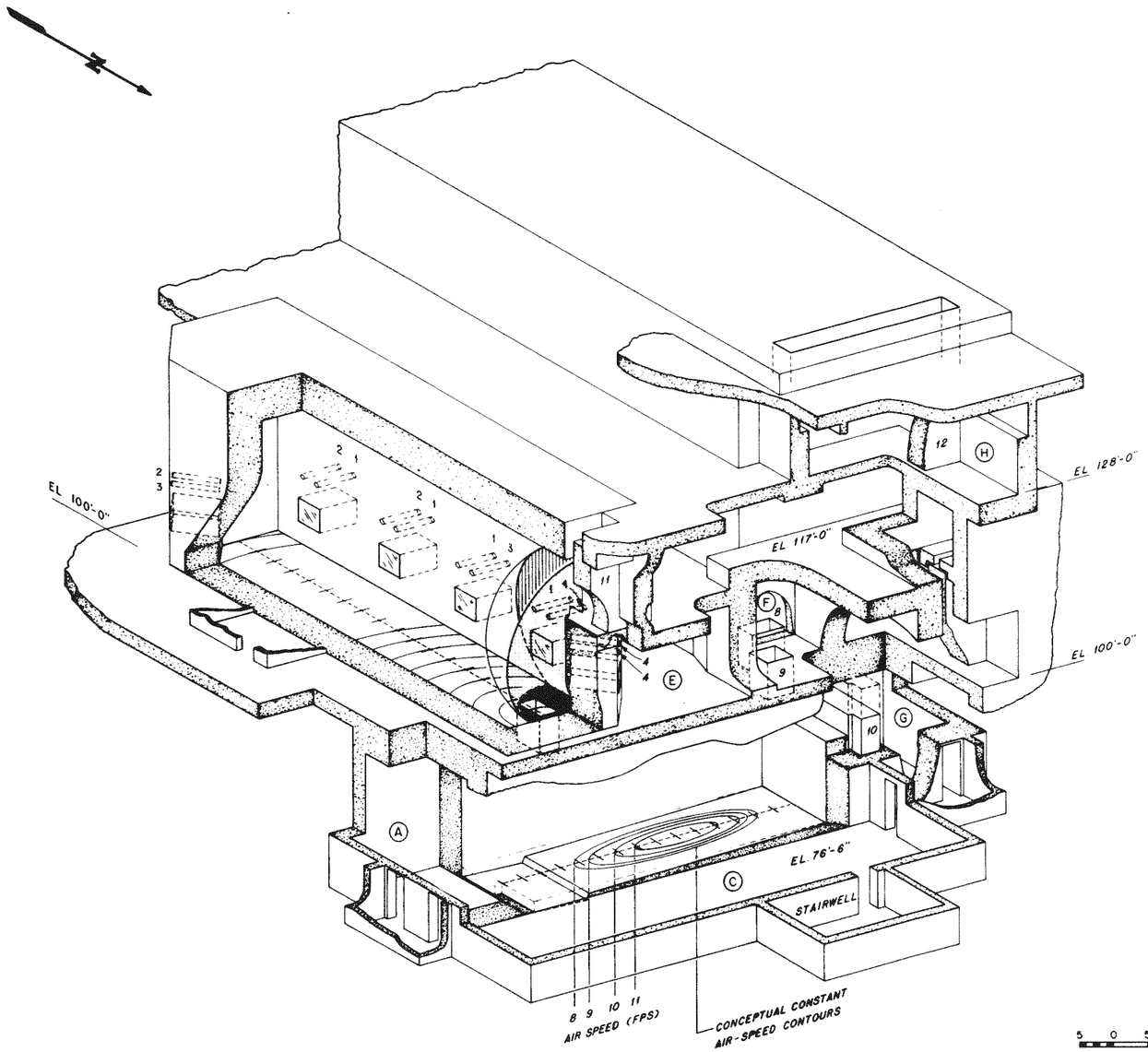

LEGEND

A MINIATURE CELL
B- GENERAL PURPOSE CELL (GPC)
C- GPC OPERATING AISLE
D- PROCESS MECHANICAL CELL (PMC)
E- PMC OPERATING AISLE
F- CHEMICAL PROCESSING CELL (CPC)
G- GPC CRANE REPAIR ROOM
H- CPC CRANE REPAIR ROOM

1- MANIPULATOR OPENING (MANIPULATOR IN PLACE)
2- MANIPULATOR OPENING (PLYWOOD COVER)
3- MANIPULATOR OPENING (HINGED, LOCKABLE COVER)
4- MANIPULATOR (TAPED-ON CARDBOARD COVER)
5- DUCT BETWEEN GPC AND MINIATURE CELL (OPEN)
6- TRANSFER PORT (OPEN)
7- HATCH - PMC TO GPC (OPEN)
8- HATCH - GPC TO CPC (OPEN)
9- HATCH - GPC TO SCRAP REMOVAL AREA (HATCH IS PLUGGED)
10- VERTICALLY MOVING DOOR - GPC TO GPC CRANE REPAIR AREA
11- VERTICALLY MOVING DOOR - PMC TO PMC CRANE REPAIR AREA
12- VERTICALLY MOVING DOOR - CPC TO CPC CRANE REPAIR AREA
13- VENTILATION EXHAUST DUCT (OPEN)
14- CO_2 TRANSFER OPENING (CO_2 TRANSFER HOSE TAPED INTO OPENING)

Fig. 8. Diametric cutaway of the head-end cells of the NFS fuel reprocessing plant showing estimated air-speed contours in the GPC and the quarter-spherical geometry of air discharged from the PMC.

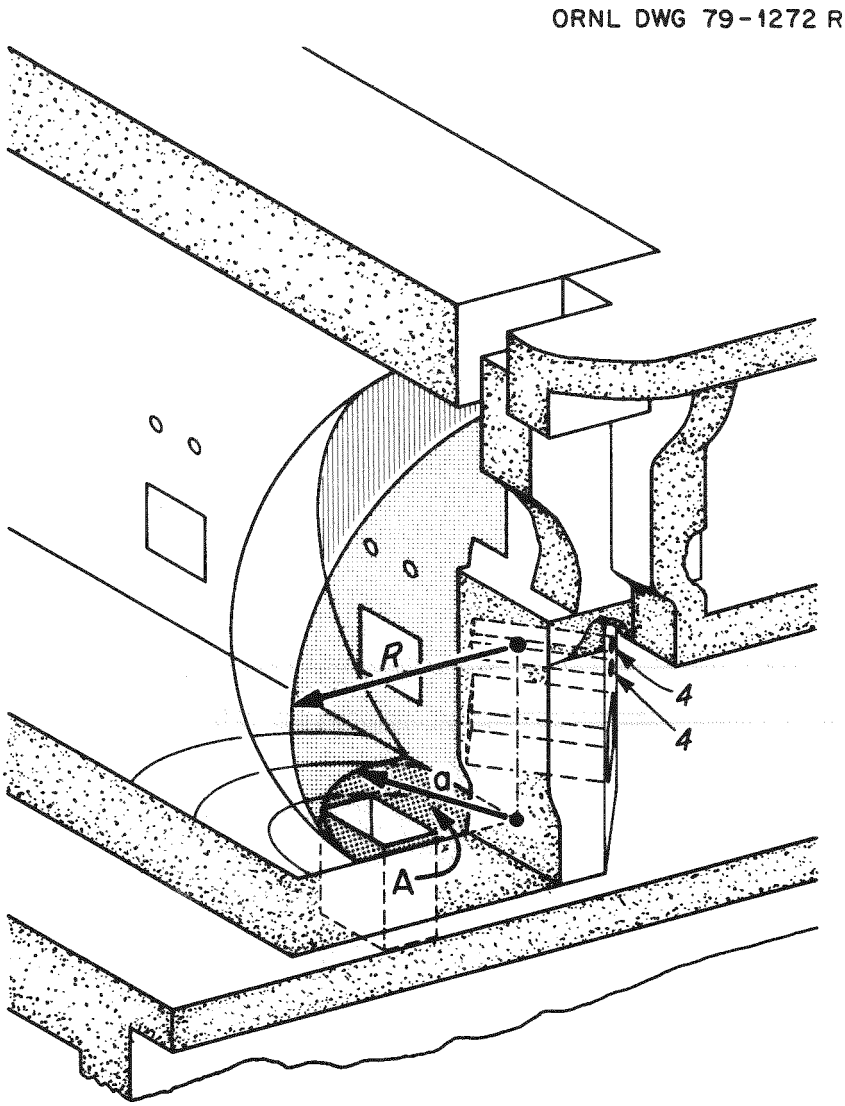

Fig. 9. Definition of quarter-spherical geometry used in calculating releases from the Process Mechanical Cell.

Equipotential surfaces of air flow under these idealized conditions are those of an oblate spheroid centered at the orifice, with the minor axis normal to the wall. The ratio of major to minor axes of the oblate spheroid is $\sqrt{R^2 + (d/2)^2}/R$, where d is the orifice diameter and R is the radius, on the wall, of the spheroid. Thus, for values of $R >> d/2$, the major axis is only slightly larger than the minor axis and the spheroid differs only slightly from spherical. For example, a 10-in.-diam hole centered in a large wall would have an oblate-spheroidal axis ratio of 1.0009 for a value of R equal to 10 ft. As mentioned above, a hemisphere, and also the hemioblate spheroid, of R = 10 ft would have a volume of about 2100 ft^3.

Idealized orifice flow of air from PMC or GPC into operating aisles through manipulator ports would be distorted by several factors, primarily: (1) the cell walls are thick; (2) in the PMC there are seven, not just one, ports that would become open in the case of a tornado; (3) there would be flow of air from GPC to PMC; and (4) three of the seven ports of concern in the PMC are in or near the northwest corner of the cell, not in the middle of a wall.

Within the context of the definitions of this model, Cases 3A1 - 3C1 and 3A2 - 3C2 involve discharge of air from the GPC through a port to the GPC operating aisle. The port is 10 ft above the floor of the GPC; any air flowing through this port would originate from an approximately hemispherical volume with its center at the port. As noted above, any hemispherical volume smaller than 2100 ft^3 would not contain particulate matter from the floor of the GPC in this case. The largest volumetric discharge from the GPC to the operating aisle is 1428 ft^3 in Case 3C2. 1428 ft^3 in Case 3C2. The radius of a hemisphere of this volume is only 8.8 ft. Case 3C2 and Cases 3A1, 3B1, 3C1, 3A2, and 3B2 (Table 11) are therefore eliminated from further analysis.

The ventilation exhaust in the GPC is 19.5 ft above the floor; a quarter-spherical volume of this radius exceeds 7700 ft^3. Since this volume exceeds all volumetric discharges from the GPC (Table 11) in Cases 4A - 4C and 5A - 5C, none of these require further analysis.

Three of the 7 ports in the PMC that are covered only with tape or cardboard, both of which would be blown out by a tornado, are located in the northwest corner, Fig. 8. Air and particulate matter could be discharged from each of these seven; however, we first use the conservative assumption, for the purpose of identifying the possible need for further analysis of Cases 1A1 - 1C1 and 1A2 - 1C2, that all discharges will be from the three in the northwest corner. In all of these cases the shape of the space from which air will originate is assumed to be a quarter sphere with its vertical diameter located in the northwest corner of the PMC, and its center at the manipulator ports, as shown in Fig. 8. Cases 1B1, 1C1, 1B2, and 1C2, with air discharges of 1142, 1922, 2222, and 3913 ft^3, respectively (Table 11), require further analysis on the basis of the criterion given above. However, we will include Cases 1A1 and 1A2 in subsequent discussion.

Air velocities near the floor of the PMC change greatly as a result of tornado touchdown, as shown in Fig. 10 for Case 1C1. Prior to touchdown, these velocities are <1 fps except at the north end of the cell, where they rise to about 2.7 fps. After tornado strike the air speeds near the floor at the north end of the PMC rise rapidly, first downward, to about 10 fps in Case 1B1 and about 14 fps in Case 1C1, then upward to about 8 and 9 fps, respectively. The change in direction of airflow corresponds to movement of air from the GPC to PMC. The duration of the wind disturbances is more important in the case of the PMC than the GPC because of the increasing cell area (Fig. 10) affected. The time scale and the air velocities, as determined from TVENT calculations, at the boundaries of the PMC are shown in Fig. 11 for Case 1C1. From Fig. 7 it may be seen that air normally enters the PMC at manipulator ports [Branch (3)] and inleakage locations [Branch (2)] and exhausts through the hatch to the GPC [Branch (4)]. However, within a few tenths of a second after the tornado strike, the air flow directions reverse and remain reversed until 10 to 11 s after touchdown in Cases 1B1 and 1C1. During this time an increasing portion of the PMC floor (measured from north to south, or grid number 19 to 1, Figs. 8 and 10) is subjected to higher speed winds, as presented in Table 12 for Case 1C1. The maximum speed along the floor is about 15 fps (460 cm/s). According to Table 10 or Fig. 4, the maximum sized particle of UO_2 that will move and become entrained, due to wind of this speed, is about 250 μm; according to Fig. 12, this corresponds to the potential reentrainment of 11 to 50% of the particulate matter on the segment of floor area of the PMC over which this wind speed applies, if this matter has the particle-size distribution of sheared fuel discussed in ref. 8.

Calculations with the TVENT code[5] show that air discharged from the PMC will flow mainly through manipulator ports that are covered with cardboard, plywood, or tape (ports labeled 2 or 4 in Fig. 8). The most conservative assessment of discharges of radioactive materials from the PMC is based on the assumptions that all of the vented air flows through the three ports in the northwest corner of the PMC and that the wind speed is the maximum 15 mph over all the intercepted surface. This, and the further assumption that the vented air is from the nearly quarter spherical volume shown in Figs. 8 and 9 was combined with TVENT data to calculate particulate discharges described below.

Figure 9 defines several parameters needed in these calculations, as follows:

R = the radius of the quarter-spherical segment;

a = the radius of the quarter-circular floor segment subtended by the quarter-spherical segment;

A = the floor surface area subtended by the quarter-spherical segment;

V = the volume of air vented from the PMC and assumed to be vented through the manipulator ports in the northwest corner of the PMC.

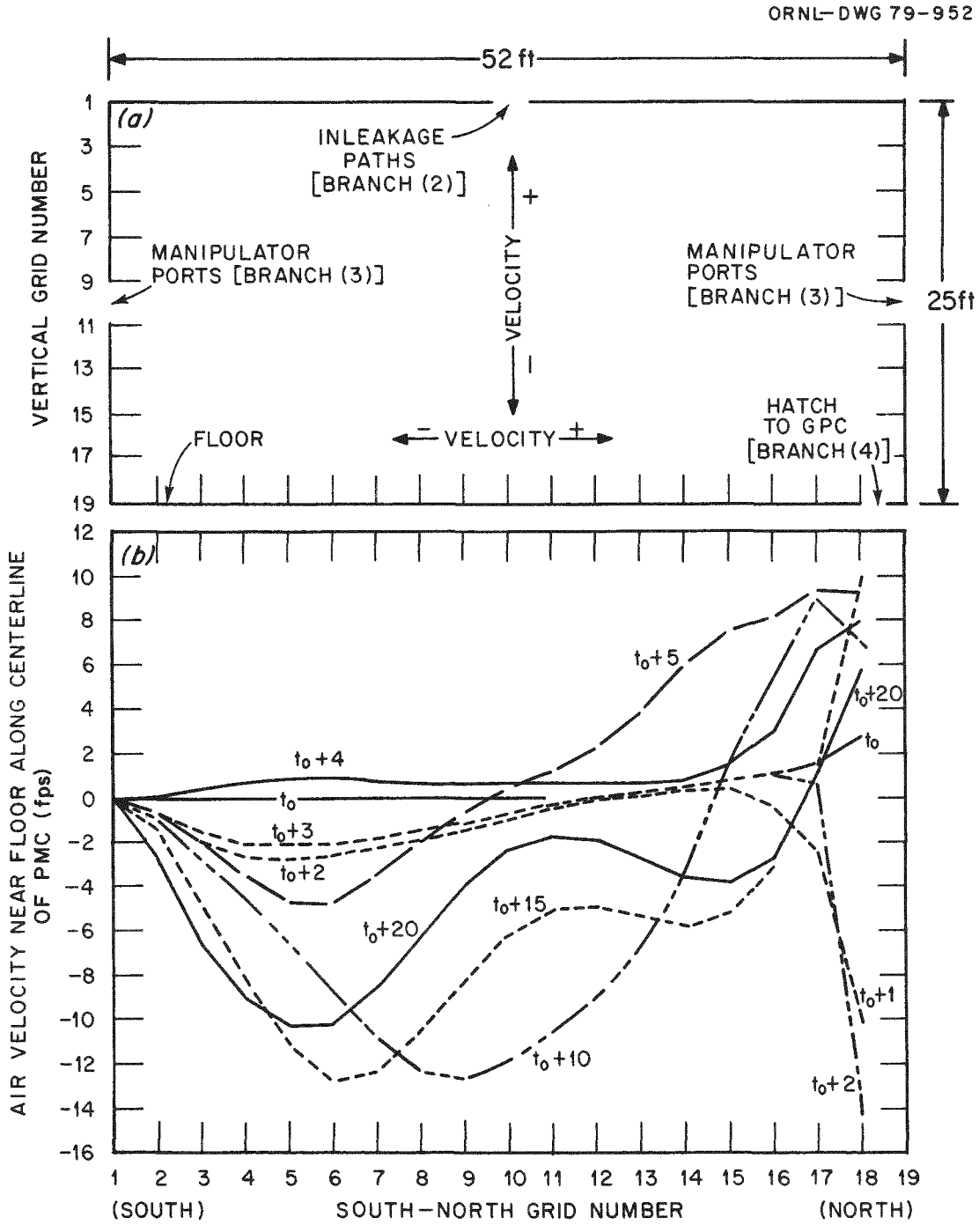

Fig. 10. (a) SOLA-ICE calculational grid and (b) air velocities near the floor on the south-north centerline of the PMC for normal ventilation (at t_o) and at successive times after touchdown of a 300-mph tornado (Case 1C1).

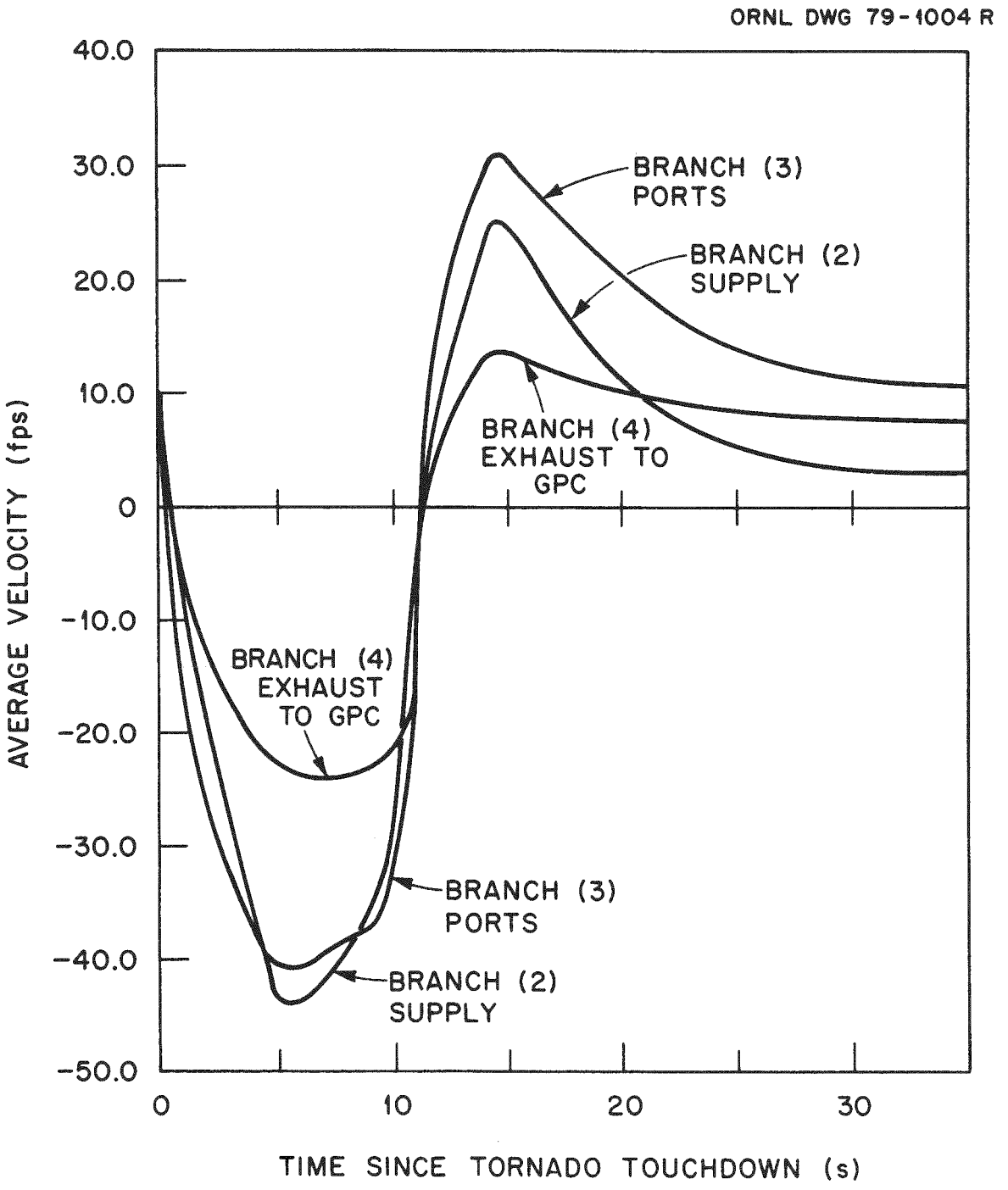

Fig. 11. Process mechanical cell boundary air velocities generated by the TVENT code for a 300-mph tornado with walls and doors intact (Case 1C1).

Table 12. Air velocities in PMC for Case 1C1 (300-mph tornado)[a]

Grid number	Air velocity (fps) in excess of 1 fps at tornado touchdown											
	0 s	1 s	2 s	3 s	4 s	5 s	6 s	7 s	8 s	9 s	10 s	11 s
2												
3		- 1.90	- 2.10	- 1.55		- 2.00	- 1.08	- 1.07	- 1.66	- 2.48	- 2.75	- 2.22
4		- 2.41	- 2.63	- 1.99		- 3.48	- 2.01	- 1.98	- 3.28	- 4.61	- 4.55	- 3.77
5		- 2.49	- 2.69	- 2.07		- 4.63	- 3.21	- 3.31	- 5.57	- 6.89	- 6.46	- 5.93
6		- 2.35	- 2.51	- 1.97		- 4.67	- 4.78	- 5.45	- 8.36	- 9.19	- 8.67	- 8.57
7		- 2.09	- 2.22	- 1.77		- 3.45	- 6.72	- 8.73	-11.25	-11.41	-10.86	-10.97
8		- 1.75	- 1.87	- 1.48		- 1.80	- 8.70	-12.69	-13.81	-13.13	-12.39	-12.28
9		- 1.33	- 1.44	- 1.12			- 9.53	-15.55	-15.28	-13.77	-12.71	-12.13
10							- 6.81	-14.27	-14.50	-12.98	-11.86	-11.00
11						1.25	2.00	- 6.29	-10.54	-10.99	-10.46	- 9.79
12						2.31	6.24	6.65	- 3.29	- 7.75	- 8.87	- 9.01
13						3.98	8.03	12.79	6.69	- 2.70	- 6.70	- 8.35
14						6.02	8.52	13.68	12.19	4.17	- 3.38	- 7.04
15					1.52	7.59	8.72	12.44	14.62	8.79	1.60	- 4.31
16				1.13	3.05	8.18	8.60	10.59	14.14	11.51	5.54	1.11
17	1.59	- 2.56		1.22	6.63	9.38	9.04	9.61	12.50	12.63	8.99	5.05
18	2.74	-10.25	-14.32	9.84	8.00	9.22	8.22	7.65	7.73	7.84	7.02	6.32
19												

[a]All blank spaces correspond to an absolute velocity (air speed) <1 fps.

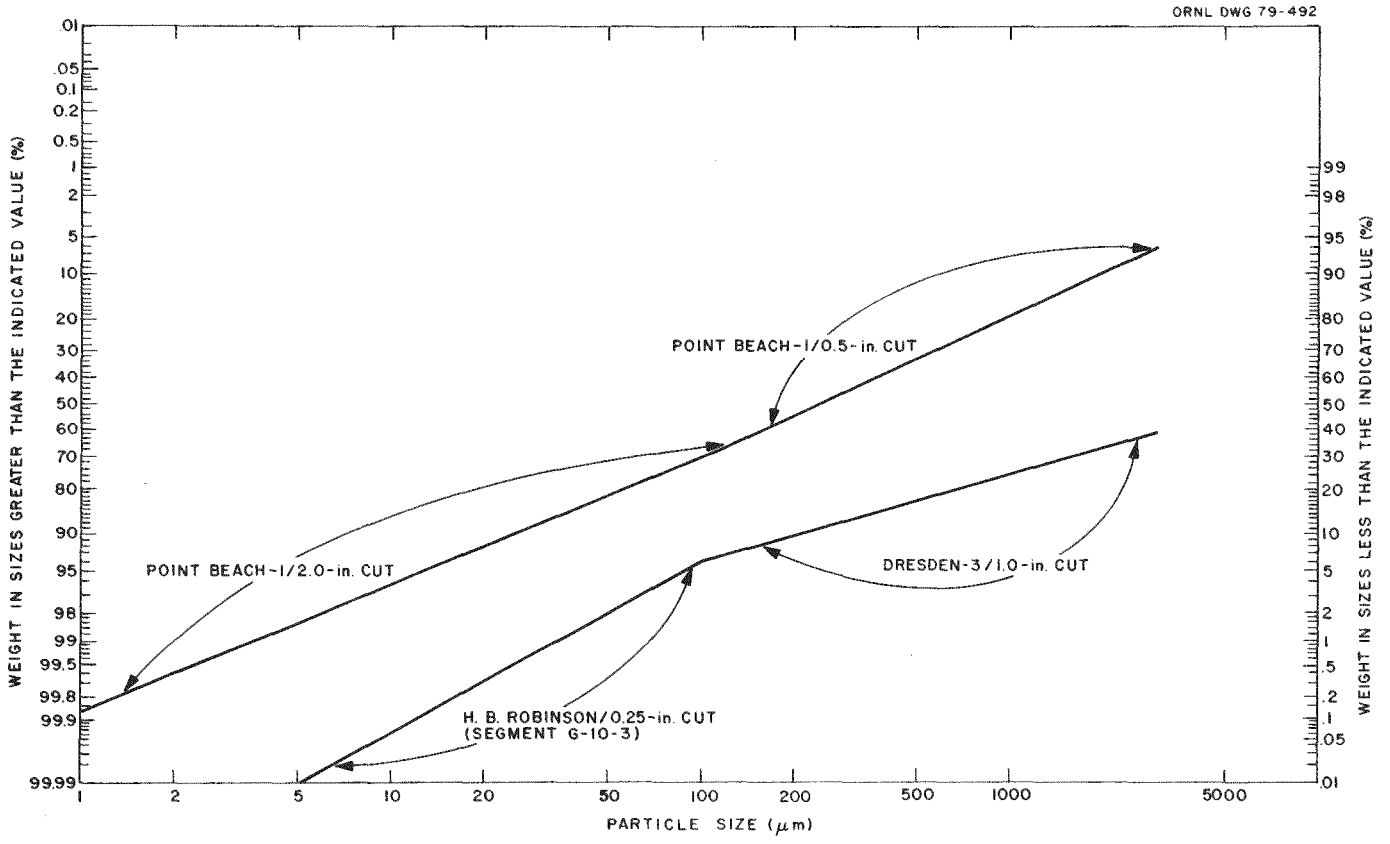

Fig. 12. Maximum and minimum quantities of irradiated fuel of size less than (or greater than) a specified value.

When there is intersection of a quarter sphere with the floor we must consider three possible relationships between R and V for ports 10 ft above the floor:

$10 < R \leq 12$ (the width of the cell), then

$$V = (\pi/12)[4R^3 - (R - 10)^2(2R + 10)]; \quad (9)$$

$12 < R \leq 15$ (the height of the cell above the ports), then

$$V = (\pi/12)[4R^3 - (R - 10)^2(2R + 10) - (R - 12)^2(2R + 12)]; \quad (10)$$

$15 < R$, then

$$V = (\pi/12)[4R^3 - (R - 10)^2(2R + 10) - (R - 12)^2(2R + 12) - (R - 15)^2(2R + 15)]. \quad (11)$$

If the volume of vented air is such that R is <10 ft then no particulate matter will be vented. As noted above, this volume is ~1050 ft^3.

Table 13 summarizes geometry and mass discharges from the PMC on the basis of the building walls and local doors remaining intact or being destroyed. The upper section of this table is based on the very conservative assumption that all air leaves the PMC only through the 3 ports in the northwest corner; the lower part of the table is based on the more realistic assumption that only 3/7 of the air will be so discharged since only 3 of the 7 potentially uncovered ports are in that location. It should be noted that the appropriate assumed shapes of air prior to discharge from the other 4 ports, marked 2 in Fig. 8, would be hemispheres. The radius of each of these, corresponding to 1/7 of the volumes listed in Table 13, would be significantly less than the 10-ft distance to the floor. Even in Case 1C2 (building walls and doors destroyed), the hemispherical radius is only 6.1 ft. Cases in Table 13 were evaluated on the basis of the following product:

$$(PMC)_{dis} = (A-A_h)\ W\ f_1\ f_2. \quad (12)$$

A and V are defined above. Other parameters are as follows:

A_h = the hatch area correction, m^2;

W = weight of UO_2 per unit area of PMC floor, 5 to 15 kg/m^2;

f_1 = fraction of available UO_2 (namely that dislodged from the cladding) that would become resuspended at the maximum near-floor wind speed of 15 mph, 0.1 to 0.5;

f_2 = fraction of fuel dislodged from the cladding, 0.5 to 1, as indicated in ref. 8.

An alternate shape, that corresponds to the SOLA-ICE model (but which differs somewhat from reality) is a truncated half-cone, suggested by the air-flow patterns shown in Fig. 6.10, particularly at 10 s after touchdown (20 s after time zero of the calculations), of Holloway and Andrae.

Table 13. Geometric parameters and discharges of particulate matter from the PMC to operating aisles for quarter-spherical geometry

	Building walls and local doors remain intact		Building walls and local doors are destroyed	
	Case 1B1 (200-mph tornado)	Case 1C1 (300-mph tornado)	Case 1B2 (200-mph tornado)	Case 1C2 (300-mph tornado)
Air volume, V, discharged from PMC to operating aisles, ft^3	1273	1983	1947	3057
	Parameters based on assuming all air is discharged via ports in northwest corner			
Radius, R, of quarter-spherical segment, ft	10.68[a]	12.49[b]	12.41[b]	14.77[b]
Radius, a, of intersected floor segment, ft	3.76[c]	7.48[c]	7.35[c]	10.87[c]
Intersected floor area, A, ft^2	11.1	44.0	42.4	92.8
m^2	1.0	4.1	3.9	8.6
Intersected hatch area, A_h, ft^2	0.	9.0	8.3	12.
m^2	0.	0.8	0.8	1.1
Quantity of particulate matter discharged, kg	0.25 - 7.5	0.8 - 25	0.8 - 23	2 - 55
	Parameters based on assuming 3/7 of air is discharged via ports in northwest corner			
Radius, R, of quarter-spherical segment, ft	8.16[a]	9.34[a]	9.29[a]	10.79[a]
Radius, a, of intersected floor segment, ft	0.	0.	0.	4.05[c]
Intersected floor area, A, ft^2	0.	0.	0.	12.9
m^2	0.	0.	0.	1.2
Intersected hatch area, A_h, ft^2	0.	0.	0.	0.
m^2	0.	0.	0.	0.
Quantity of particulate matter discharged, kg	0.	0.	0.	0.3 - 9

[a]Calculated from Eq. (9).

[b]Calculated from Eq. (10).

[c]Calculated as a $(R^2 - 100)^{1/2}$.

This half-cone is actually limited in the east-west direction to 12 ft, the width of the PMC, as shown in Fig. 13. The following definitions are used:

y_o = half-width of the cell, 6 ft;

R_1 = radius of the base of the half-cone, ft;

H = height of the half-cone, ft;

V = volume of half-cone, ft^3.

When the radius, R_1, of the half-cone does not exceed y_o, then

$$V = \pi R_1^2 H/6 \quad (R_1 \leq y_o) \tag{13}$$

However, this case is significant only for discharges of small air volumes and small quantities of particulate matter from the PMC. When R_1 exceeds y_o, then

$$V = (R_1^2 H/3)\{\sin^{-1}(y_o/R_1) - (\pi/2)(y_o/R_1)^3 + 2(y_o/R_1)[\sqrt{1-(y_o/R_1)^2} - 0.5\,(y_o/R_1)^2 \ln[(1 + \sqrt{1 - (y_o/R_1)^2}/(y_o/R_1)] + \pi H(y_o/R_1)\, y_o^2/6 \quad (R_1 > y_o) \tag{14}$$

In Eq. (14) the last term is the volume of that portion of the half-cone that lies entirely within the width of the cell (although it may be higher than the 25-ft height of the PMC), while all other terms comprise the volume of the lower portion of the half-cone that is cut by the two north-south walls of the PMC.

Figure 14 contains plots of the base area of a truncated half-cone as a function of the volume and height. Only the volume contained in the lower 15 ft of the truncated cone is included to correspond to discharge of air only from the lower 15 ft of the PMC. It is apparent that the floor area corresponding to a specified air volume is another parameter that must be specified as a range, rather than a single value. Such ranges are listed in Table 14.

From Eq. (13), the volume of a half-cone lying entirely in the PMC and with R_1 = 6 ft and H = 10 ft, is V = 188 ft^3. A half-cone with these parameters just touches the floor and corresponds to the largest volumetric discharge that will not contain particulate matter. This calculation shows that Cases 1A1 and 1A2 (Table 11) must be considered further, at least when it is assumed that all air leaving the PMC flows through the ports in the northwest corner of the cell. When the more realistic assumption is made, that only 3/7 of the total volume discharged from the PMC will leave via ports in the northwest corner, Case 1A1 (building walls and doors intact) ceases to be of concern; however, particulate matter would be discharged in Case 1A2.

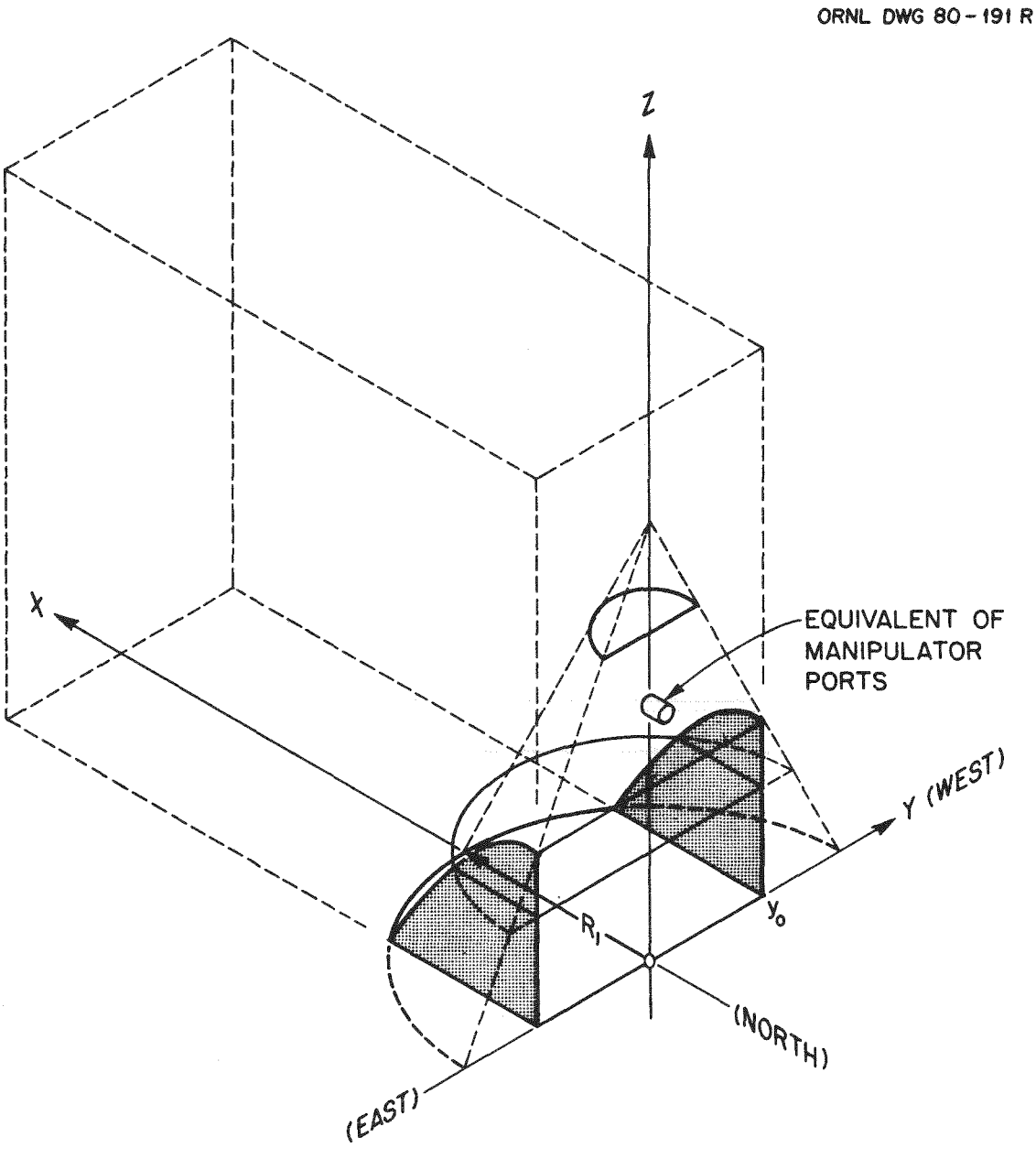

Fig. 13. Geometry of a truncated half-cone in the north end of the PMC.

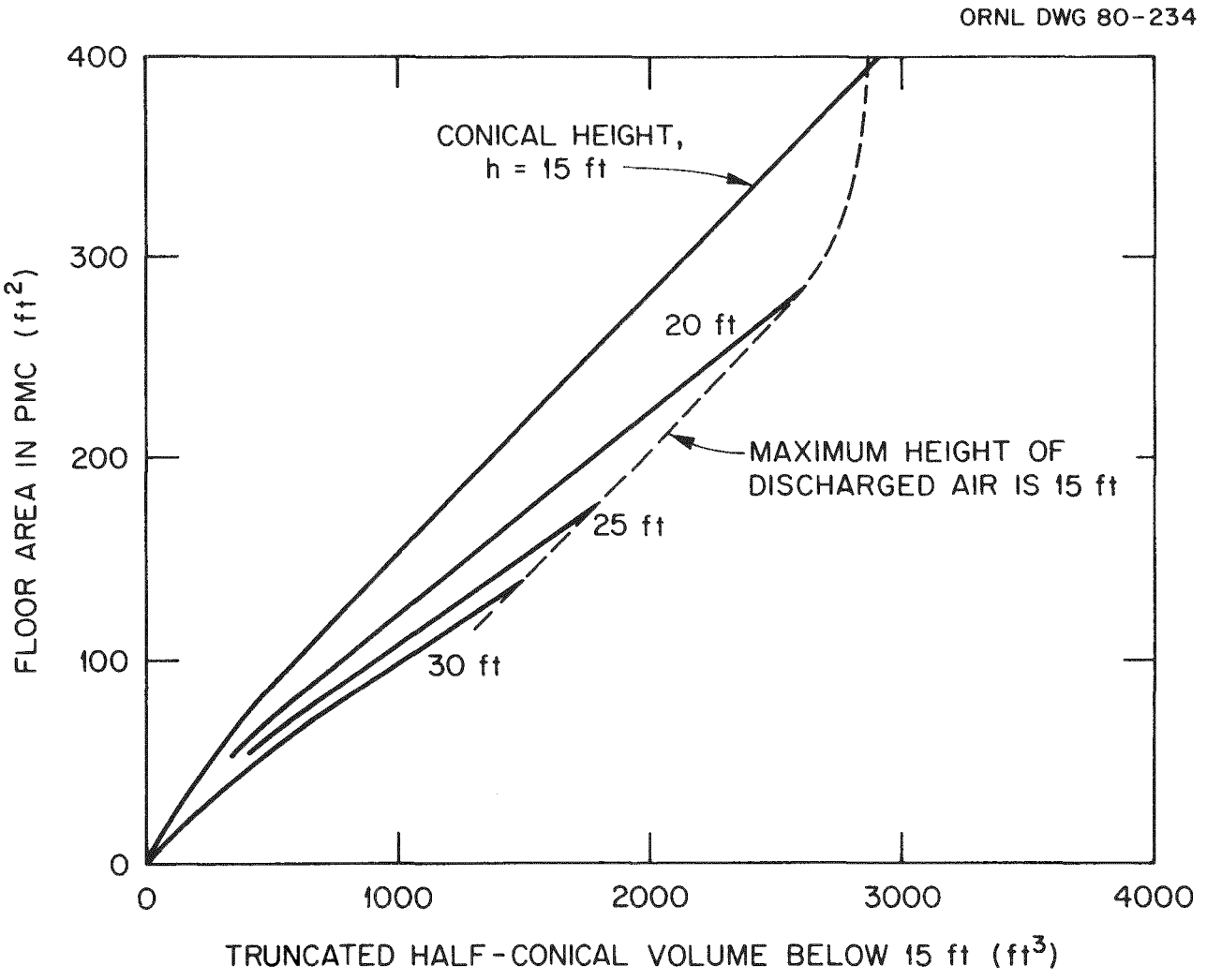

Fig. 14. Variation of intercepted floor area with volume of truncated half-cone and conical height.

Table 14. Geometric parameters and discharges of particulate matter from the PMC to operating aisles for truncated half-conical geometry

	Building walls and local doors remain intact			Building walls and local doors are destroyed		
	Case 1A1 (100-mph tornado)	Case 1B1 (200-mph tornado)	Case 1C1 (300-mph tornado)	Case 1A2 (100-mph tornado)	Case 1B2 (200-mph tornado)	Case 1C2 (300-mph tornado)
Air volume, V, discharged from PMC to operating aisles, ft^3	362	1273	1983	484	1947	3057
	Parameters based on assuming all air is discharged via ports in northwest corner					
Intersected floor area, A, ft^2	40 - 70[a]	110 - 180[a]	200 - 275[a]	50 - 80[a]	200 -275[a]	(300 - 400)[a]
m^2	3.7 - 6.5	10 - 17	19 - 26	4.6 - 7.4	19 - 26	28 - 37
Intersected hatch area, A_n, ft^2	12	12	12	12	12	12
m^2	1.1	1.1	1.1	1.1	1.1	1.1
Radius, R_1, of base of truncated half-conical segment, ft	<6 - 7[b]	10.5 - 16[b]	19 - 23.5[b]	<6 - 8[b]	19 - 23.5[b]	~38[c]
Quantity of particulate matter discharged, kg	0.6 - 40	2 - 120	4 - 190	0.9 - 50	4 - 190	7 - 270
	Parameters based on assuming 3/7 of air is discharged via ports in northwest corner					
Intersected floor area, A, ft^2	0.	60 - 90[a]	90 - 130[a]	41[d]	90 - 130[a]	130 - 210[a]
m^2	0.	5.6 - 8.4	8.4 - 12	3.9	8.4 - 12	12 - 20
Intersected hatch area, A_h, ft^2	0.	12	12	12	12	12
m^2	0.	1.1	1.1	1.1	1.1	1.1
Radius, R_1, of base of truncated half-conical segment, ft	-	6.5 - 8.5[b]	8 - 11.5[b]	5.1	8 - 11.5[b]	11.5 - 17.5
Quantity of particulate matter discharged, kg	0.	1.1 - 55	1.8 - 80	0.7 - 21	1.8 - 80	3 - 140

[a] From Fig. 14.

[b] From Eq. (14).

[c] Extrapolation of calculations with Eq. (14).

[d] From Eq. (13) with H = 15 ft.

A comparison of discharges calculated for quarter-spherical and truncated half-cones, Tables 13 and 14, shows that the latter leads to higher calculated releases. Qualitatively, significant quantities of radioactive material will be released from the PMC in Cases 1B1, 1C1, 1B2, and 1C2 if it is assumed that all air leaves via the ports in the northwest corner of that cell. When the more realistic assumption that only 3/7 of the air will leave via those ports, then releases of particulate matter will probably not occur in Cases 1A1 or 1A2 but nearly certainly will occur in Cases 1B1, 1C1, 1B2, and 1C2, particularly in the latter two wherein building walls and local doors are destroyed.

4.2.2 Differential area/wind speed analysis

More detailed analyses of reentrainment of particles from horizontal surfaces can be performed by use of near-floor wind speeds obtained from the SOLA-ICE program. In this subsection we use point values of near-floor wind speeds rather than just the maximum in Subsect. 4.2.1.

Data from SOLA-ICE calculations for the GPC are shown in Figs. 15 and 16 for normal ventilation and for Cases 1B1 (200-mph tornado) and 1C1 (300-mph tornado) wherein building walls remain intact. Normal near-floor ventilation air speeds are of particular interest because they attain values up to 9 fps (270 cm/s), corresponding to the probable reentrainment of particles sized up to 150 μm. Thus, we would expect there to be essentially no particulate matter of sizes less than ~100 μm near the center of the GPC floor. Smaller-sized particles presumably were blown to the outer areas of this floor and may have been the cause of the need to provide additional gamma-ray shielding around the ventilation exhaust at ceiling level in the GPC operating aisle. As discussed in Appendix A, particles on smear samples taken on or close to walls of the GPC are considerably smaller than those produced by shearing single rods of irradiated fuel.[8]

The highest air speeds near the floor are attained in Case 1C1 at 3s after grounding of the tornado. Interpolated grid values for this case were read from Fig. 15 and replotted as the ends of conceptual, elliptical, constant air-speed profiles shown in Fig. 8. In order to approximate the fraction of particulate matter that would become airborne from a floor over which the air velocity was varying, we performed a finite-difference integration using the specified velocity profiles, areas within these, and the differential areas between successive profiles (Appendix B). Derived quantities, as well as final estimates of the fractional reentrainment, are given in Tables 15-17 for normal ventilation and for 200- and 300-mph tornados at $t_o + 2$ and $t_o + 3$, respectively. (t_o is the time the tornado touches ground.) The size of particle that would have a threshold friction speed or terminal settling speed corresponding to the mid-point velocity of successive velocity contours was then obtained from Table 10 or Fig. 4. Finally, from the upper and lower lines of Fig. 12, or from more detailed calculations shown in Table 10, we calculated maximum and minimum fractions of the UO_2 mass that are in the form of particles of size smaller than that calculated. These quantities were then used to obtain estimates of the minimum and maximum fractional reentrainments based on a model of uniform dispersion of particulate matter over the floor of the GPC.

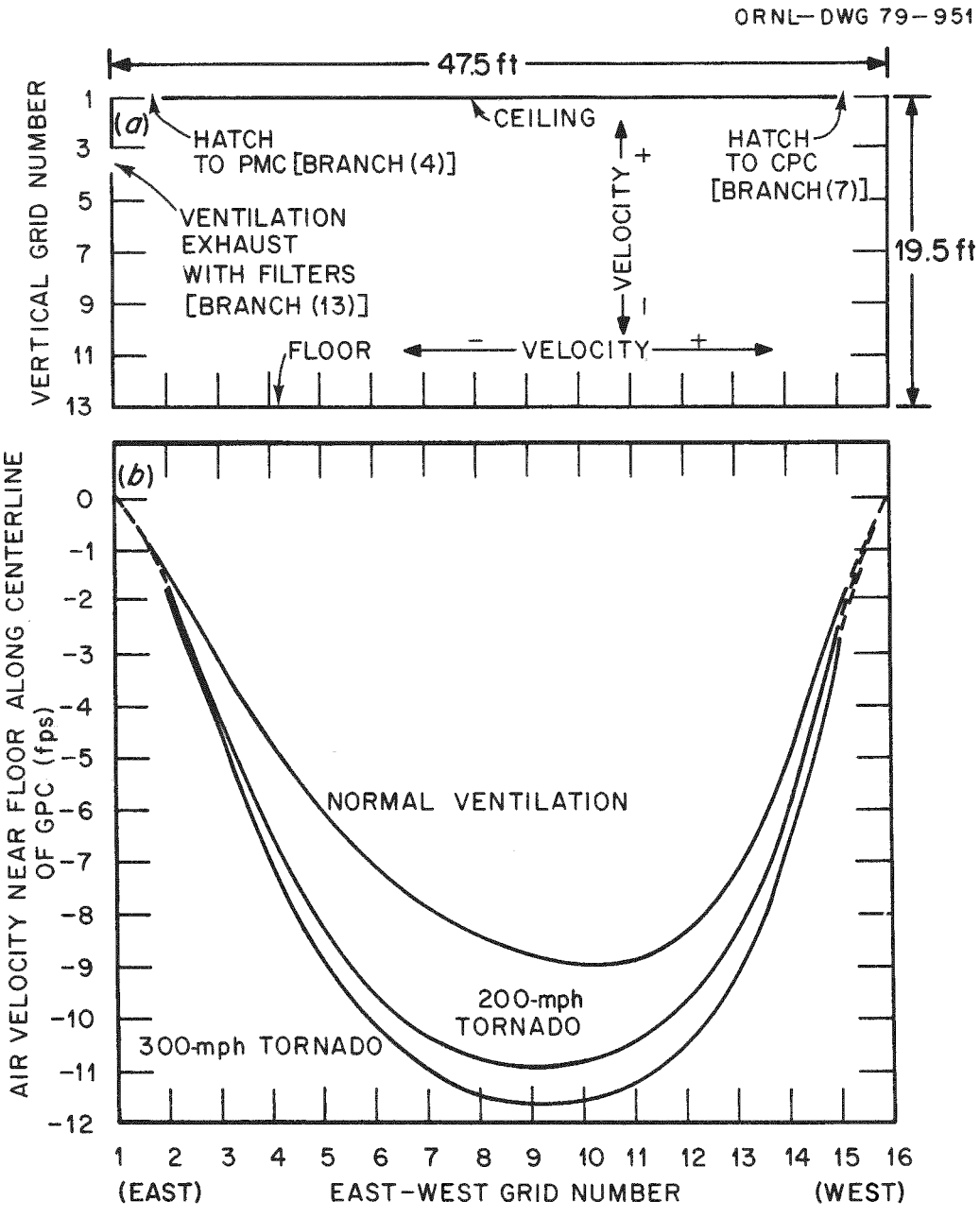

Fig. 15. (a) SOLA-ICE calculational grid, and (b) air velocities near the floor on east-west centerline of GPC for normal ventilation and at 2 s after tornado touchdown (Cases 1B1 and 1C1).

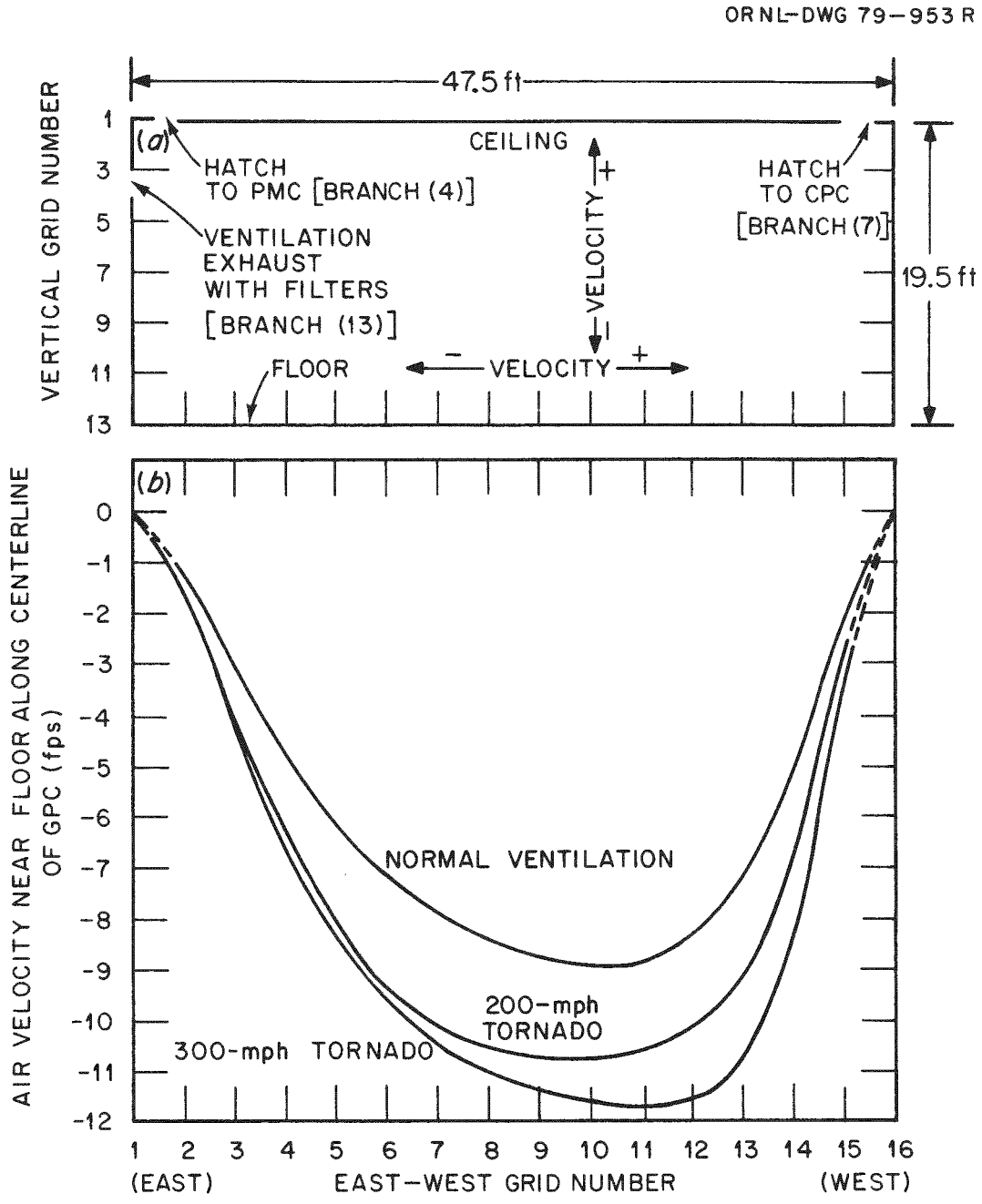

Fig. 16. (a) SOLA-ICE calculational grid, and (b) air velocities near the floor on east-west centerline of GPC for normal ventilation and at 3 s after tornado touchdown (Cases 1B1 and 1C1).

Table 15. Resuspension of UO_2 under normal ventilation flows in the GPC at NFS[a]

Air velocity near floor of General Purpose Cell (GPC)		Floor length over which air velocity equals or exceeds stated value	Floor area within elliptical contour		Differential area A_i	Fraction of GPC area within differential area	Maximum size of particle becoming airborne	Fraction of UO_2 mass of size ≤ stated value[d]	
								$^1f_{1i}$	$^2f_{1i}$
(ft/s)	(m/s)	(Grid Units)[b]	(ft^2)	(m^2)	(m^2)		(μm)[c]	(min)	(max)
0.	0.	15.0	397	36.9					
1	0.30				10.87	0.231	30	0.0072	0.115
2	0.61	12.6	280	26.1					
3	0.91				6.56	0.139	65	0.030	0.22
4	1.22	10.9	210	19.5					
5	1.52				7.08	0.151	95	0.053	0.28
6	1.83	8.7	134	12.4					
7	2.13				7.98	0.170	125	0.07	0.34
8	2.44	5.2	48	4.4					
8.5	2.59				4.44	0.094	145	0.078	0.37
9	2.74	0.0	0.	0.					

[a]The minimum and maximum area-weighted fractional resuspension values, $f_1(\text{min})$ and $f_1(\text{max})$ of Eq. (12), are calculated as $f_1(\text{min}) = \Sigma A_i {}^1f_{1i}/\Sigma A_i$ and $f_1(\text{max}) = \Sigma A_i {}^2f_{1i}/\Sigma A_i$. For this case, $f_1(\text{min}) = 0.033$ and $f_1(\text{max}) = 0.192$.

[b]Taken from Fig. 14(b) or 15(b).

[c]Taken from Fig. 4 at velocities corresponding to those in column 2.

[d]Taken from Fig. 12 or Table 10.

Table 16. Resuspension of UO_2 at 2 s after onset of tornado conditions 1B1 (200 mph) at NFS[a]

Air velocity near floor of General Purpose Cell (GPC)		Floor length over which air velocity equals or exceeds stated value	Floor area within elliptical contour		Differential area A_i	Fraction of GPC area within differential area	Maximum size of particle becoming airborne	Fraction of UO_2 mass of size ≤ stated value[d]	
								$^1f_{1i}$	$^2f_{1i}$
(ft/s)	(m/s)	(Grid Units)[b]	(ft^2)	(m^2)	(m^2)		(μm)[c]	(min)	(max)
0.	0.	15.0	397	36.9					
1	0.30				9.19	0.195	30	0.0072	0.115
2	0.61	13.0	298	27.7					
3	0.91				5.27	0.112	65	0.030	0.22
4	1.22	11.7	242	22.5					
5	1.52				5.39	0.115	95	0.053	0.28
6	1.83	10.2	184	17.1					
7	2.13				5.49	0.117	125	0.07	0.34
8	2.44	8.4	125	11.6					
9	2.74				7.31	0.156	150	0.08	0.37
10	3.05	5.1	46	4.3					

[a]The minimum and maximum area-weighted fractional resuspension values, $f_1(\text{min})$ and $f_1(\text{max})$ of Eq. (12), are calculated as $f_1(\text{min}) = \Sigma A_i {}^1f_{1i}/\Sigma A_i$ and $f_1(\text{max}) = \Sigma A_i {}^2f_{1i}/\Sigma A_i$. For this case $f_1(\text{min}) = 0.039$ and $f_1(\text{max}) = 0.210$.

[b]Taken from Fig. 14(b) corresponding to 2 s after tornado touchdown (the time of maximum floor velocities).

[c]Taken from Fig. 4 at velocities corresponding to those in column 2.

[d]Taken from Fig. 12 or Table 10.

Table 17. Resuspension of UO_2 at 3 s after onset of tornado condition 1C1 (300 mph) at NFS[a]

Air velocity near floor of General Purpose Cell (GPC)		Floor length over which air velocity equals or exceeds stated value	Floor area within elliptical contour		Differential area A_i	Fraction of GPC area within differential area	Maximum size of particle becoming airborne	Fraction of UO_2 mass of size ≤ stated value[d]	
								$^1f_{1i}$	$^2f_{1i}$
(ft/s)	(m/s)	(Grid Units)[b]	(ft^2)	(m^2)	(m^2)		(μm)[c]	(min)	(max)
0	0	15.0	397	36.9					
1	0.30				8.33	0.177	30	0.0072	0.115
2	0.61	13.2	308	28.6					
3	0.91				4.96	0.106	65	0.030	0.22
4	1.22	12.0	254	23.6					
5	1.52				4.49	0.096	95	0.053	0.28
6	1.83	10.8	206	19.1					
7	2.13				4.95	0.105	125	0.07	0.34
8	2.44	9.3	153	14.2					
9	2.74				6.15	0.131	150	0.08	0.37
10	3.05	7.0	87	8.0					
10.75	3.28				6.93	0.147	180	0.09	0.42
11.5	3.51	2.6	12	1.1					

[a]The minimum and maximum area-weighted fractional resuspension values, $f_1(\text{min})$ and $f_1(\text{max})$ of Eq. (12), are calculated as $f_1(\text{min}) = \Sigma A_i {}^1f_{1i}/\Sigma A_i$ and $f_1(\text{max}) = \Sigma A_i {}^2f_{1i}/\Sigma A_i$. For this case $f_1(\text{min}) = 0.043$ and $f_1(\text{max}) = 0.226$.

[b]Taken from Fig. 15(b) corresponding to 3 s after tornado touchdown (the time of maximum floor velocities).

[c]Taken from Fig. 4 at velocities corresponding to those in column 2.

[d]Taken from Fig. 12 or Table 10.

Air velocities in the first two columns of Tables 15-17 pertain to cases in which the building walls and local doors remain intact. Minimum and maximum quantities of UO_2 that will be reentrained, given in footnote a of each of these tables, also refer to this same structural integrity. These fractional ranges are 0.03 to 0.19, 0.04 to 0.21, and 0.04 to 0.22 of the available UO_2 for normal ventilation, 200-mph tornado, and 300-mph tornado, respectively. The significance of these ranges is that they are smaller, as would be expected, than values of 0.1 to 0.5 obtained by assuming that the maximum wind speed of 15 mph applies to all of the GPC floor. Specifically, the ranges of fractional reentrainment are 2 to 3 times smaller than the maximum range.

More detailed calculations were made of reentrainment in the PMC. The grid used in these calculations is shown in Fig. 8; the correlation between floor area and north-to-south distance from the north end of the PMC (for half-cones truncated at a 12-ft width and a 15-ft height) is shown in Fig. 17. SOLA-ICE calculations are listed for Case 1C1 (walls and doors intact) in Table 12. Similar calculations are presented by Holloway and Andrae[5] for 100- and 200-mph tornados. The 200-mph tornado produces the highest near-floor wind speeds at about 15 s after tornado strike. These wind speeds were combined with data from other figures and tables in this report to calculate more realistic values, shown in Tables 18 and 19, of reentrainment than that given by the assumption of $f_1 = 0.1$ to 0.5 of Sect. 4.2.1. In Case 1B1, Table 18, the area-weighted fractional reentrainment is 0.036 to 0.23. The lower end of this range, 0.036, is only about a third of the value 0.1 used in calculations of Table 14, while the upper end of the range, 0.23, is less than half that used in Table 14. Similar calculations of fractional reentrainment for Case 1C1 show that use of the range 0.1 to 0.5 in Table 14 did not greatly exceed the range 0.081 to 0.39 shown in Table 19.

4.3 Source Term for Radioactive Airborne Releases

Calculations in Sect. 4.2 on weights of radioactive materials resuspended as a result of tornado strikes can be used to calculate source terms for airborne releases of these materials. As stated in Sect. 4.2, Tables 13 and 14 overestimate the quantities of particulate matter that become resuspended. In particular, a relatively large factor of conservatism is contained within the assumption that all air discharged from the PMC originated in that cell. Actually, much, perhaps 50 to 90%, of the air came through the hatch (Figs. 8 and 9) into the PMC from elevated spaces in the GPC where there would be no particulate matter.

The most realistic, yet conservative, estimates of resuspension are contained in the lower portion of Table 14. Specifically the values to be considered, with walls and local doors intact, are: (1) no releases in Case 1A1, (2) 1.1 to 55 kg released in Case 1B1, and (3) 1.8 to 80 kg released in Case 1C1. However, these need to be corrected on the basis of more realistic values of fractional entrainment [f_1 of Eq. (12)]. These are given as 0.036 to 0.23 for Case 1B1 in Table 18 and 0.081 to 0.39 for Case 1C1 in Table 19. By contrast, a range 0.1 to 0.5 was used to calculate

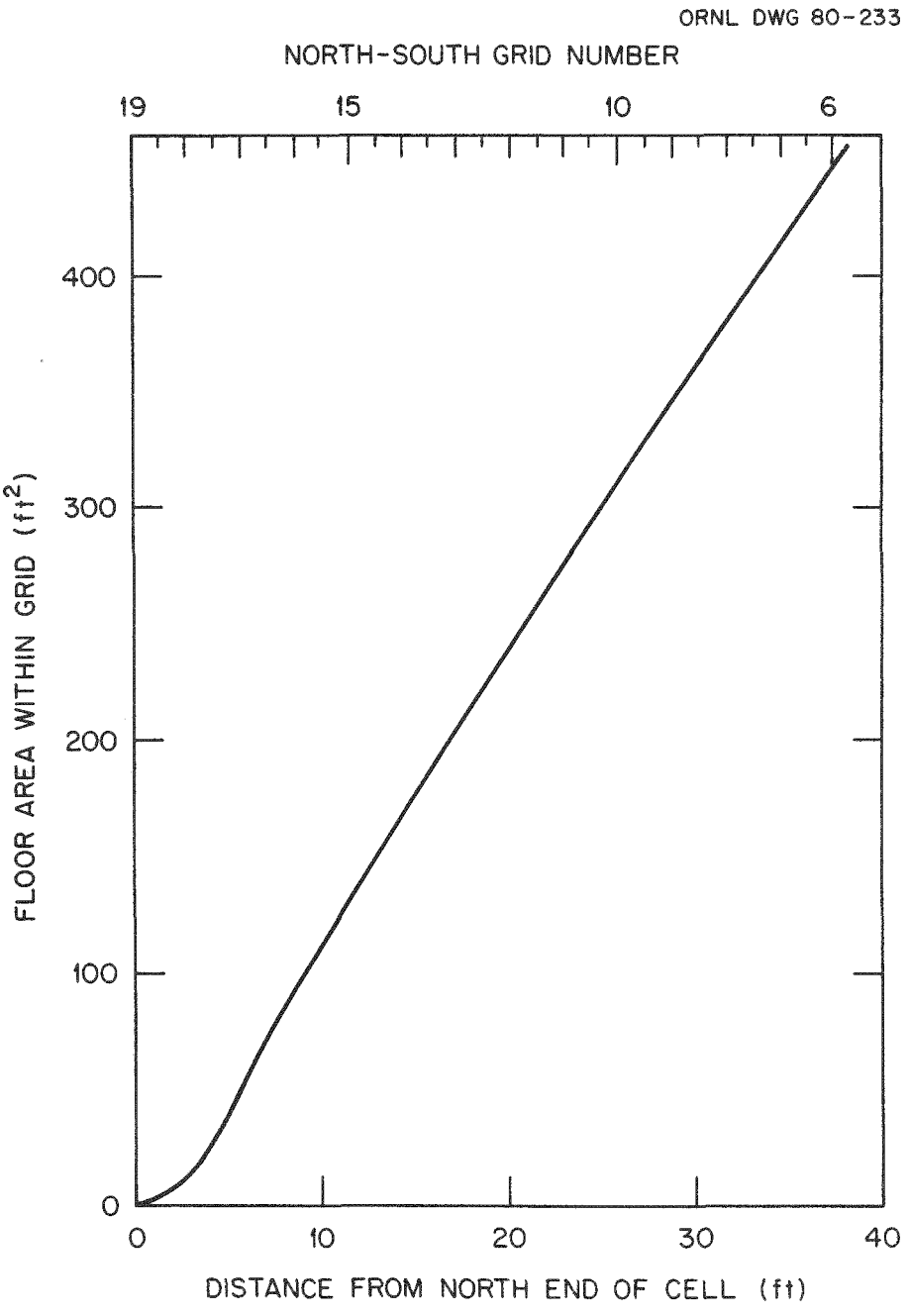

Fig. 17. Variation of PMC floor area with distance from north end of cell.

Table 18. Resuspension of UO_2 in Case 1B1 (200-mph wind) with building walls and doors intact[a]

Grid No. (i)	Area within grid[b] (ft^2)	Differential area		Maximum near-floor air speed (at t_o + 5 s)		Max size of reentrained particle (μm)[d]	Fraction of particles reentrained[e]	
		(ft^2)	A_i (m^2)	(fps)[c]	(cm/s)		$^1f_{1i}$ (min)	$^2f_{1i}$ (max)
19	0			0				
		13	1.2		125	82	0.043	0.26
18	13			8.13				
		39	3.6		245	140	0.076	0.36
17	52			7.95				
		42	3.9		215	125	0.070	0.34
16	94			6.31				
		37	3.4		175	105	0.052	0.305
15	131			5.06				
		37	3.4		130	85	0.046	0.265
14	168			3.39				
		37	3.4		80	60	0.027	0.21
13	205			2.01				
		36	3.3		50	45	0.016	0.165
12	241			1.22				
		35	3.3		30	33	0.009	0.125
11	276			0.83				
		35	3.3		20	33	0.009	0.125
10	311			0.53				
		35	3.3		10	33	0.009	0.125
9	346			0.22				
		35	3.3		0	0	0.	0.
8	381			(-0.28)[f]				

[a]The minimum and maximum area-weighted fractional resuspension values, f_1(min) and f_1(max) of Eq. (12), are calculated as $f_1(\text{min}) = \Sigma A_i {}^1f_{1i}/\Sigma A_i$ and $f_1(\text{max}) = \Sigma A_i {}^2f_{1i}/\Sigma A_i$. For this case f_1(min) = 0.036 and f_1(max) = 0.23.

[b]From Fig. 16.

[c]From SOLA-ICE calculations similar to those in Table 12. The maximum wind speeds occur at t_o + 5 s in this case.

[d]From Fig. 4.

[e]From Table 10 and Fig. 12.

[f]Negative values, corresponding to downflow of air, were not used in calculating values listed in note a.

Table 19. Resuspension of UO_2 in Case 1C1 (300-mph wind) with building walls and doors intact[a]

Grid No. (i)	Area within grid[b] (ft^2)	Differential area		Maximum near-floor air speed (at t_o + 8 sec)		Max size of reentrained particle (μm)[d]	Fraction of particles reentrained[e]	
		(ft^2)	A_i (m^2)	(fps)[c]	(cm/s)		$^1f_{1i}$ (min)	$^2f_{1i}$ (max)
19	0	13	1.2	0.	120	80	0.041	0.23
18	13	39	3.6	7.73	310	170	0.083	0.405
17	52	42	3.9	12.50	405	220	0.102	0.47
16	94	37	3.4	14.14	440	235	0.108	0.485
15	131	37	3.4	14.62	410	220	0.102	0.47
14	168	37	3.4	12.19	290	160	0.082	0.395
13	205	36	3.3	6.69	50	44	0.015	0.16
12	241	35	3.3	(-3.29)[f]	0	0	0.	0.
11	276			(-10.54)[f]				

[a]The minimum and maximum area-weighted fractional resuspension values, f_1(min) and f_1(max) of Eq. (12), are calculated as $f_1(\text{min})$ and $\Sigma A_i {}^1f_{1i}/\Sigma A_i$ and $f_1(\text{max}) = \Sigma A_i {}^2f_{1i}/\Sigma A_i$. For this case $f_1(\text{min}) = {}^1 0.081$ and $f_1(\text{max}) = 0.39$.

[b]From Fig. 16.

[c]From Table 12.

[d]From Fig. 4.

[e]From Table 10 and Fig. 12.

[f]Negative values, corresponding to downflow of air, were not used in calculating values listed in note a.

values in Table 14. Using these changes in f_1, the source terms in Table 20 were calculated. These values are conservative due to still another assumption, namely that none of the particles settle back onto horizontal surfaces in the PMC; instead, they are all discharged into operating aisles.

If the building walls and doors remain intact, much of the material vented from the PMC into operating aisles will probably settle in those aisles. If, however, building walls and doors are destroyed in 200- or 300-mph tornadoes, then releases in excess of those listed in Table 20 may reach the atmosphere and be widely dispersed.

Particle-size distributions of solids discharged from the PMC, as in Cases 1B1 and 1C1, can be calculated within the accuracies of the various other assumptions by interpolating in Table 10 and using areas and fractional discharges listed in Tables 18 or 19 (or 15-17). Referring to Table 18, we see that the maximum-sized particles that can be reentrained between grids 19 and 18 are sized 82 μm. The particle-size distribution of particles between these grids for minimum reentrainment is obtained by dividing values in the penultimate column of Table 10 by the value $^1f_{1i}$ (=0.043) from Table 18; the distribution for maximum reentrainment for this same differential area is obtained by dividing values in the last column of Table 10 by the value $^2f_{1i}$ (=0.26) from Table 18. The operations are performed only for particles sized up to 82 μm for this segment. By repeating these calculations for each differential area up to the maximum size of particle that can be reentrained in that area, a distribution of sizes of all material discharged from the PMC can be obtained. In Case 1B1 all discharged particles will be smaller than 140 μm while in Case 1C1 all particles will be <235 μm.

As described in Sect 3.1, the average decay time of fuel particles in the PMC and GPC prior to November 1978, was ~10 years. Particle agglomeration undoubtedly occurred during this time as shown by the figures in the appendix. However, such agglomeration is apparently not important in this case since agglomerates on three wipe samples taken in the GPC attain a maximum size of about 40 to 50 μm. They, and the smaller particles which form them, would have been moved (had their critical friction speeds exceeded) and reentrained at the near-floor air speeds induced by tornadoes considered in this report. As noted in Table 10, the critical friction speed of a 50-μm particle is, with adhesion, <35 cm/s; near-floor air speeds considered in this report range up to 450 cm/s (15 fps). We cannot, of course, be certain that particles on the three wipe samples taken in the GPC are representative of all material in this cell or in the PMC.

Table 20. Radioactive materials in particulate matter potentially discharged from the PMC: condition — building walls and local doors remain intact[a]

	ORIGEN yield (11 years' decay) (Ci/MTU)	Quantities of radioactivity (Ci)	
		Case 1B1	Case 1C1
Quantity of particulate matter discharged, kg		0.4 - 25	1.5 - 65
^{90}Sr	3.2E+4	1.E+1 - 8.E+2	5.E+1 - 2.E+3
^{90}Y	3.2E+4	1.E+1 - 8.E+2	5.E+1 - 2.E+3
^{99}Tc	6.8E+0	3.E-3 - 2.E-1	1.E-2 - 4.E-1
^{106}Ru	1.3E+2	5.E-2 - 3.E+0	2.E-1 - 8.E+0
^{113m}Cd	1.2E+1	5.E-3 - 3.E-1	2.E-2 - 8.E-1
^{125}Sb	4.6E+2	2.E-1 - 1.E+1	7.E-1 - 3.E+1
^{125m}Te	1.1E+2	4.E-2 - 3.E+0	2.E-1 - 7.E+0
^{134}Cs	1.0E+3	4.E-1 - 3.E+1	1.E+0 - 6.E+1
^{137}Cs	4.0E+4	2.E+1 - 1.E+3	6.E+1 - 3.E+3
^{137m}Ba	3.8E+4	2.E+1 - 1.E+3	6.E+1 - 2.E+3
^{144}Ce	5.0E+1	2.E-2 - 1.E+0	7.E-2 - 3.E+0
^{144}Pr	5.0E+1	2.E-2 - 1.E+0	7.E-2 - 3.E+0
^{151}Sm	2.4E+2	1.E-1 - 6.E+0	4.E-1 - 2.E+1
^{152}Eu	2.7E+0	1.E-3 - 7.E-2	4.E-3 - 2.E-1
^{154}Eu	9.9E+2	4.E-1 - 2.E+1	1.E+0 - 6.E+1
^{155}Eu	4.1E+2	2.E-1 - 1.E+1	6.E-1 - 3.E+1
Total fission products	1.5E+5	6.E+1 - 4.E+3	2.E+2 - 1.E+4
^{239}Np	1.1E+0	4.E-4 - 3.E-2	2.E-3 - 7.E-2
^{238}Pu	3.7E+2	1.E-1 - 9.E+0	5.E-1 - 2.E+1
^{239}Pu	2.6E+2	1.E-1 - 7.E+0	4.E-1 - 2.E+1
^{240}Pu	2.5E+2	1.E-1 - 6.E+0	4.E-1 - 2.E+1
^{241}Pu	3.1E+4	1.E+1 - 8.E+2	5.E+1 - 2.E+3
^{241}Am	7.4E+2	3.E-1 - 2.E+1	1.E+0 - 5.E+1
^{243}Am	1.1E+0	4.E-4 - 3.E-2	2.E-3 - 7.E-2
^{244}Cm	2.6E+1	1.E-2 - 7.E-1	4.E-2 - 2.E+0
Total actinides	3.2E+4	1.E+1 - 8.E+2	5.E+1 - 2.E+3

[a]No material is discharged in Case 1A1 (100-mph tornado).

APPENDIXES

5.1 Appendix A: Analysis of Samples from the General Purpose Cell

On June 4, 1979, members of the staff of NFS, at the request of A. T. Clark of NRC, recovered three pieces of cladding hulls and took three smears of surfaces from the GPC. These samples were transferred to a hot cell in the analytical chemistry area and placed in individual polyethylene bags. The bags were then placed in a stainless steel container that constitutes the inner vessel of a General Electric Model 8400 radioactive materials shipping container. This was subsequently shipped to the Oak Ridge National Laboratory for various analyses.

According to A. C. Pierce of NFS, the three unflattened cladding samples were obtained as follows: hull A, from the GPC floor in front of the east window; hull B, from the center of the cell; hull C, from an unknown location, previously stored in analytical cells (see Fig. 2). Smears were taken from the following locations: smear 1, a 6-in. swipe from inside the dumping station; smear 2, an 8-in. swipe from the top surface of the basket cooler in front of the middle window; and smear 3, an 8-in. swipe from the vertical wall in front of the east window.

Two types of analyses of the samples were performed: first, the obtaining of gamma-ray spectra from a 4096-channel analyzer; second, the obtaining of photomicrographs of the three wipe papers.

5.1.1 Radioactivity from gamma-ray analyses

Results of the gamma-ray scans are summarized in Table A-1. This summary also contains a $^{134}Cs/^{137}Cs$ age, which was read from Fig. A-1. This figure is based on ORIGEN calculations described in Sect. 3.1. The data of Table A-1 are expressed in Table A-2 after normalization with respect to ^{137}Cs activity in the fuel. Also included in Table A-2 are values of these ratios for cladding and fuel activity ratios calculated from ORIGEN.

The presence of the fission products ^{125}Sb, ^{134}Cs, ^{137}Cs, ^{154}Eu, and ^{155}Eu on smear and cladding samples clearly implies that irradiated fuel is present on all of them. However, only the $^{134}Cs/^{137}Cs$ ages and the ratios $^{154}Eu/^{137}Cs$ are in good agreement with values expected from ORIGEN calculations.

Radioactivity contamination, at ORNL or NFS, is indicated from the ratios for ^{51}Cr, ^{54}Mn, and ^{95}Zr, all with half-lives less than 1 year, given in Table A-2. Each of these nuclides should be present in quantities below analytical limits, as is the case with ^{51}Cr on smears 2 and 3, Table A-1. Contamination is further implied by the presence of any radioactivity on the stainless steel container. The $^{60}Co/^{137}Cs$ value for cladding sample A in Table A-2 implies contamination. Values of this ratio for the other samples are also of uncertain significance since ^{60}Co (cladding)/^{137}Cs (fuel), given as 2.3E-2 in the last column of Table A-2, corresponds to the ratio expected for a cladding sample (from a PWR) that is essentially full of reference fuel or, in the case of smear samples, that contains hardware and fuel in the ratio 260 kg of hardware per Mg U.

Table A-1. Gamma-ray analyses of samples from NFS and the $^{134}Cs/^{137}Cs$ age.

Nuclide	Stainless steel container (dps on 6/27/79)	Smear (μCi on 7/10/79)			Cladding (μCi on 7/10/79)		
		1	2	3	A	B	C
^{51}Cr	-	2.7E-1	≤4.2	≤6. E-1	-	9.02	5.82
^{54}Mn	-	-	-	-	6.08E+1	-	-
^{60}Co	1.6 E+3	2.7	1.0	1.3 E-1	1.32E+4	1.34E+2	3.23E+1
^{95}Zr	-	7. E-2	8.1 E-1	8. E-2	-	2.6	5.4 E-1
^{106}Ru	2.0 E+3	-	-	-	-	-	-
^{125}Sb	2.3 E+3	6.22	3.85	-	-	3.42E+2	1.33E+2
^{134}Cs	4.8 E+3	2.0	2.2 E+1	1.86	9.2 E+1	4.0 E+1	9.08
^{137}Cs	1.01E+5	5.1E+1	3.88E+2	4.89E+1	1.26E+3	1.48E+3	4.47E+2
^{152}Eu	-	-	-	-	-	-	≤5. E-1
^{154}Eu	3.3 E+3	9.7E-1	1.16E+1	1.23	3.5 E+1	3.7 E+1	6.5
^{155}Eu	3.3 E+2	2.7E-1	2.6	3.3 E-1	-	5.8	1.73
$^{134}Cs/^{137}Cs$	4.8 E-2	3.9E-2	5.7 E-2	3.8 E-2	7.3 E-02	2.7 E-2	2.0 E-2
Cesium age, year	12	13	11.5	13	11	14	15

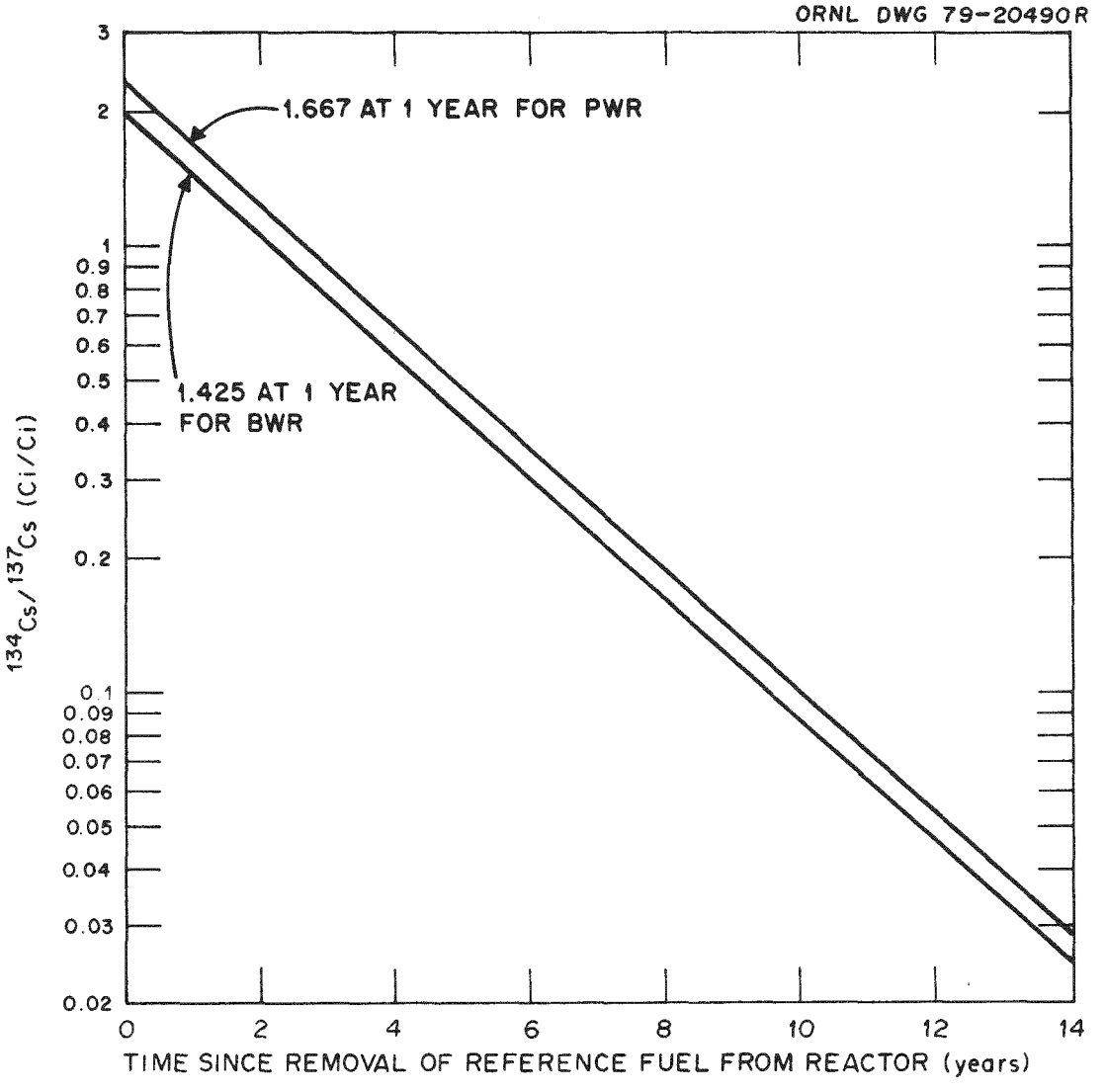

Fig. A-1. Variation of $^{134}Cs/^{137}Cs$ activity age with decay time.

Table A-2. Activity ratios compared with ORIGEN calculations

Nuclide	Half-life	Nuclide activity/^{137}Cs activity (Ci/Ci)								
		Stainless steel container	Smear samples			Cladding samples			ORIGEN calculations (11-year decay of reference fuels[a])	
			1	2	3	A	B	C	Fiss. Prod.	Activ. Prod.
^{51}Cr	27.71 d	-	5.3E-3	<1.1E-2	<1.2E-2	-	6.1E-3	1.3E-2	0.	1.3E-44
^{54}Mn	312.5 d	-	-	-	-	4.8E-2	-	-	0.	2.0E-7
^{60}Co	5.272 y	1.6E-2	5.3E-2	2.6E-3	2.7E-3	1.0E+1	9.1E-2	7.2E-2	0.	2.3E-2
^{95}Zr	65.5 d	-	1.4E-3	2.1E-3	1.6E-3	-	1.8E-3	1.2E-3	4.5E-18	1.1E-19
^{106}Ru	369 d	2.0E-2	-	-	-	-	-	-	3.2E-3	1.1E-22
^{125}Sb	2.73 y	2.3E-2	1.2E-1	9.9E-3	-	-	2.3E-1	3.0E-1	1.1E-2	1.4E-3
^{134}Cs	2.06 y	4.8E-2	3.9E-2	5.7E-2	3.8E-2	7.3E-2	2.7E-2	2.0E-2	2.6E-2	1.0E-26
^{137}Cs	30.1 y	1.	1.	1.	1.	1.	1.	1.	1.	2.3E-44
^{152}Eu	13 y	-	-	-	-	-	-	<1.1E-3	6.7E-5	1.6E-15
^{154}Eu	8.6 y	3.3E-2	1.9E-2	3.0E-2	2.5E-2	2.8E-2	2.5E-2	1.5E-2	2.5E-2	1.2E-6
^{155}Eu	4.8 y	3.3E-3	7.6E-4	6.7E-3	6.7E-3	-	3.9E-3	3.9E-3	1.0E-2	2.4E-7

[a]The reference fuel is defined in Sect. 4. Both fission products and activation products refer to irradiation in a PWR and cladding composition for PWR fuels as given by Croff et al.[11]. These are 235 kg Zircaloy per Mg U, 12.8 kg Inconel per Mg U, 2.6 kg Nicrobraze 50 per Mg U, and 9.94 kg SS per Mg U.

5.1.2 Distribution of sizes of particles on wipe papers

Photomicrographs of particulate matter on the three wipe samples are shown in Figs. A-2 to A-5. Of these, Figs. A-2, A-4, and A-5 illustrate the central sections of smears 1, 2, and 3, respectively; Fig. A-3 contains photomicrographs of an outer segment of smear 1.

The frequency of occurrence of particles of size between two specified values was determined by use of Carl Zeiss Particle Size Analyzer, model TGZ 3, with photomicrographs of 600X magnification. Data from these frequency measurements were plotted in several ways in a search for a mathematical model of frequency distribution. Figure A-6 suggests that neither the number of particles nor their weight conform to the normal distribution function. However, Figs. A-7 and A-8 support a conclusion that the number frequency is lognormally distributed according to particle size. On the basis of these plots, the number frequency distribution of each of the four portions of the three wipe samples was analyzed in a manner similar to that used previously,[8] namely by use of the Marquardt program[25,26] for estimating the one linear and two nonlinear parameters of the lognormal distribution function. This function, discussed in detail by Aitchison and Brown,[27] is given as

$$d\Lambda(x) = B \frac{e^{-(\ln x - m)^2/(2s^2)}}{xs} dx, \qquad \text{(A-1)}$$

where

$d\Lambda(x)$ = probability that a particle will have a size (diameter) between x and x + dx,

$B = 1/(2\pi)^{1/2}$ if the lognormal distribution does apply and the photomicrographs are representative of particles on the smear sample,

$= 1/(2\pi)^{1/2}$ X (a constant), if the lognormal distribution does not truly apply, but the computer program is still able to fit the data to the model,

x = particle size,

s = estimated standard deviation of the natural logarithms of particle sizes,

m = estimated median of the natural logarithm of particle sizes.

Solid curves drawn through the data and extrapolated below a 1-μm particle size in Figs. A-7 and A-8 were calculated from the parameters obtained from a nonlinear least-squares analysis of the lognormal distribution function. This analysis is based on numerical integration of Eq. (A-1):

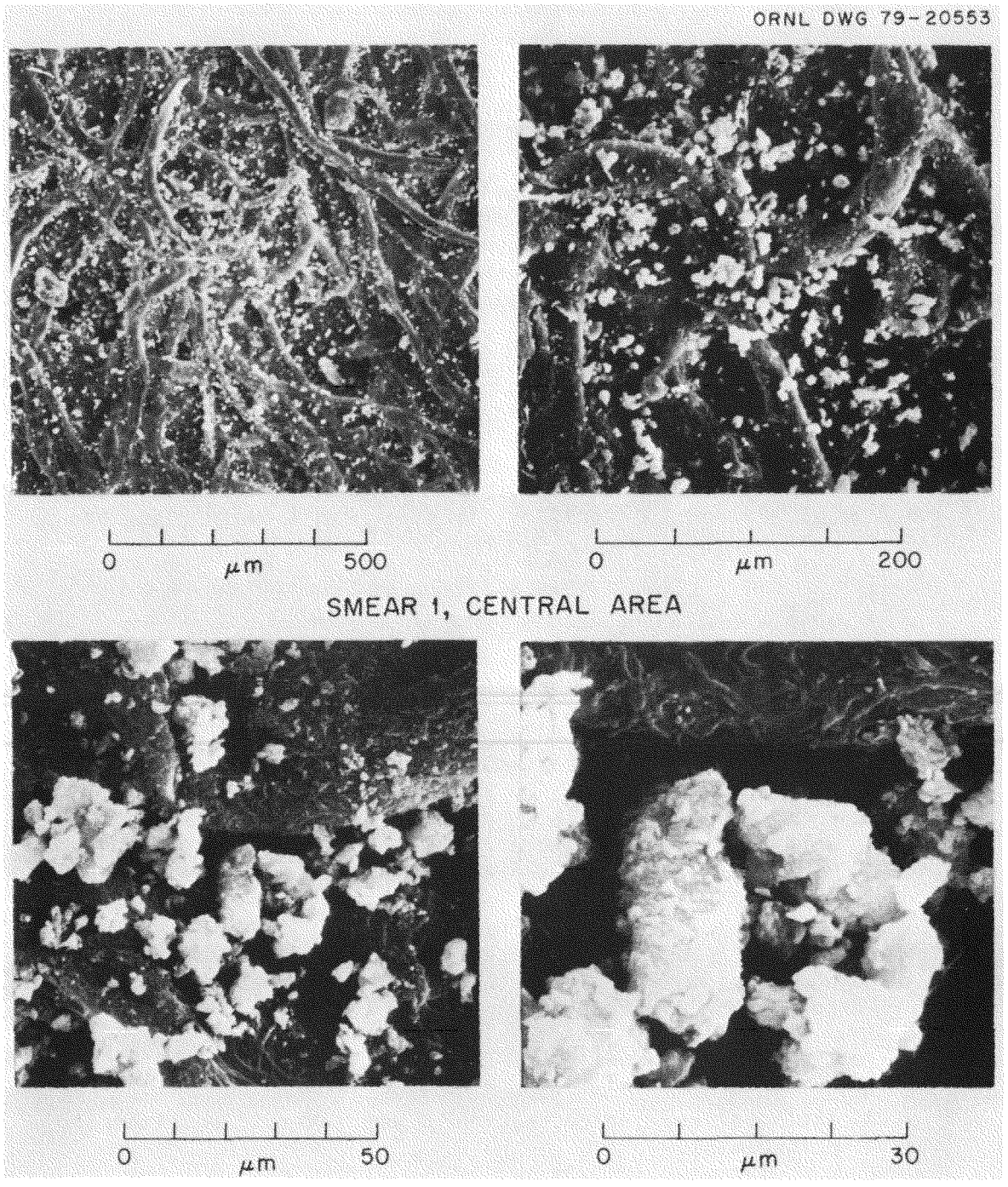

Fig. A-2. Photomicrographs of central area of smear 1.

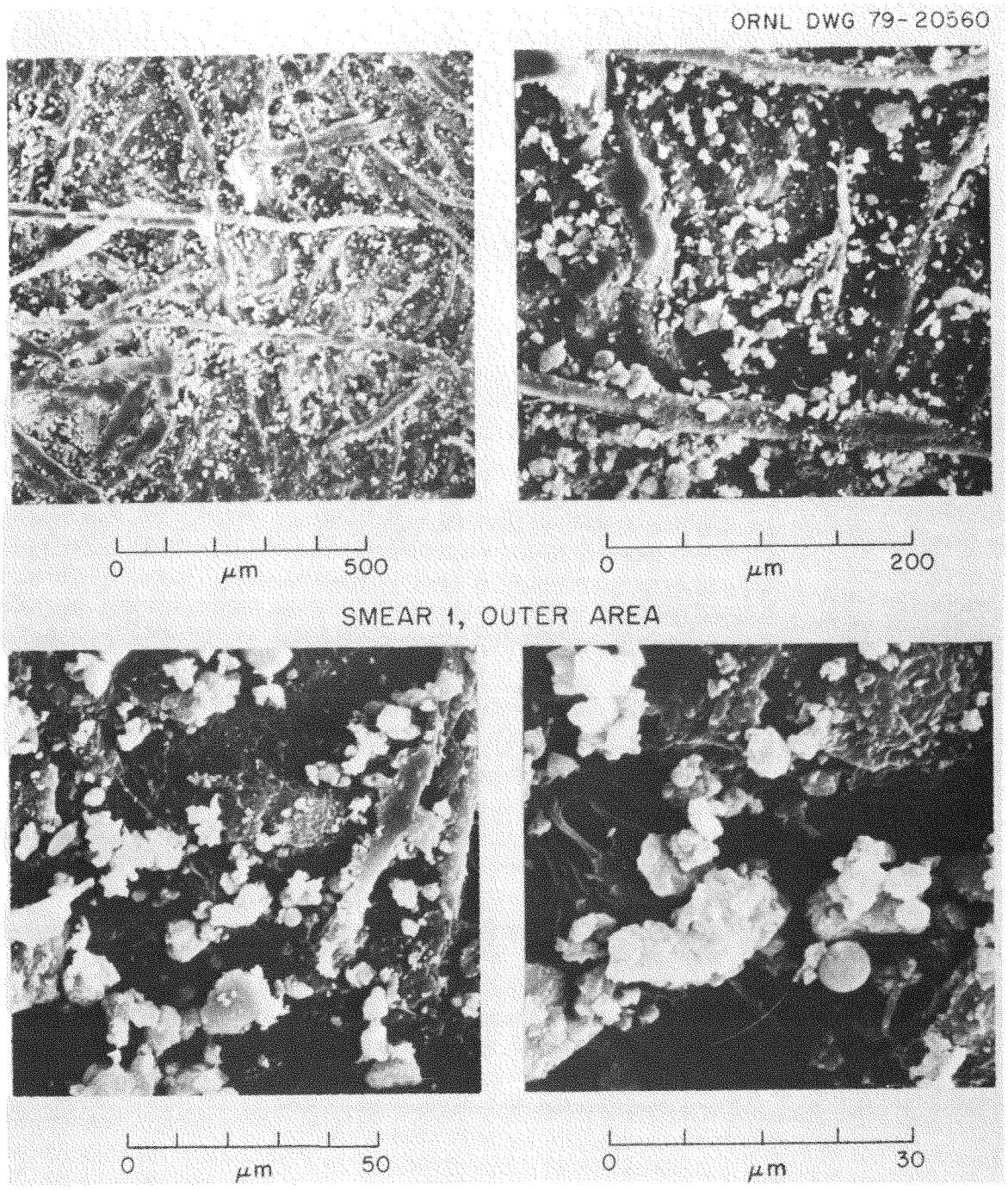

Fig. A-3. Photomicrographs of outer area of smear 1.

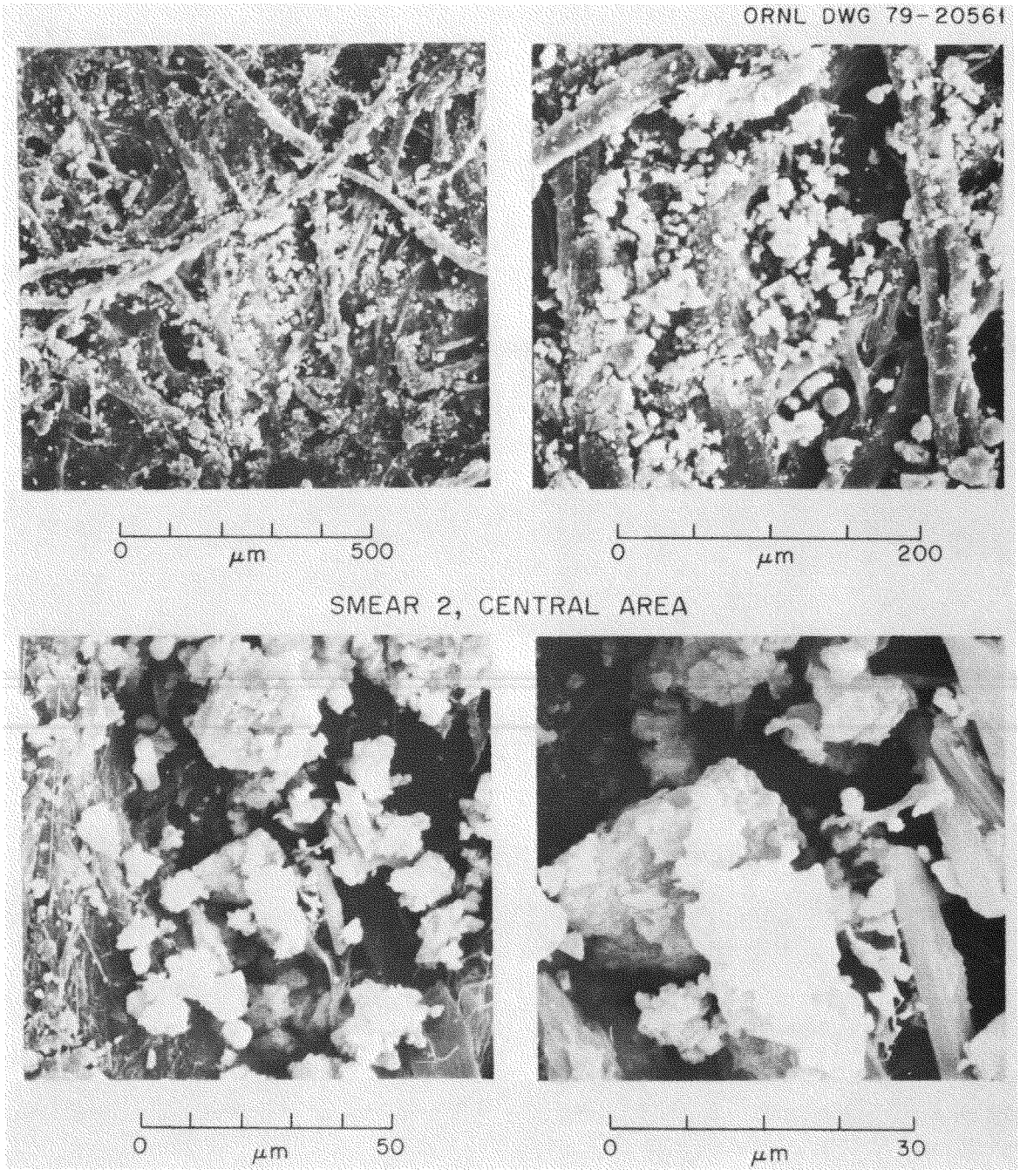

Fig. A-4. Photomicrographs of central area of smear 2.

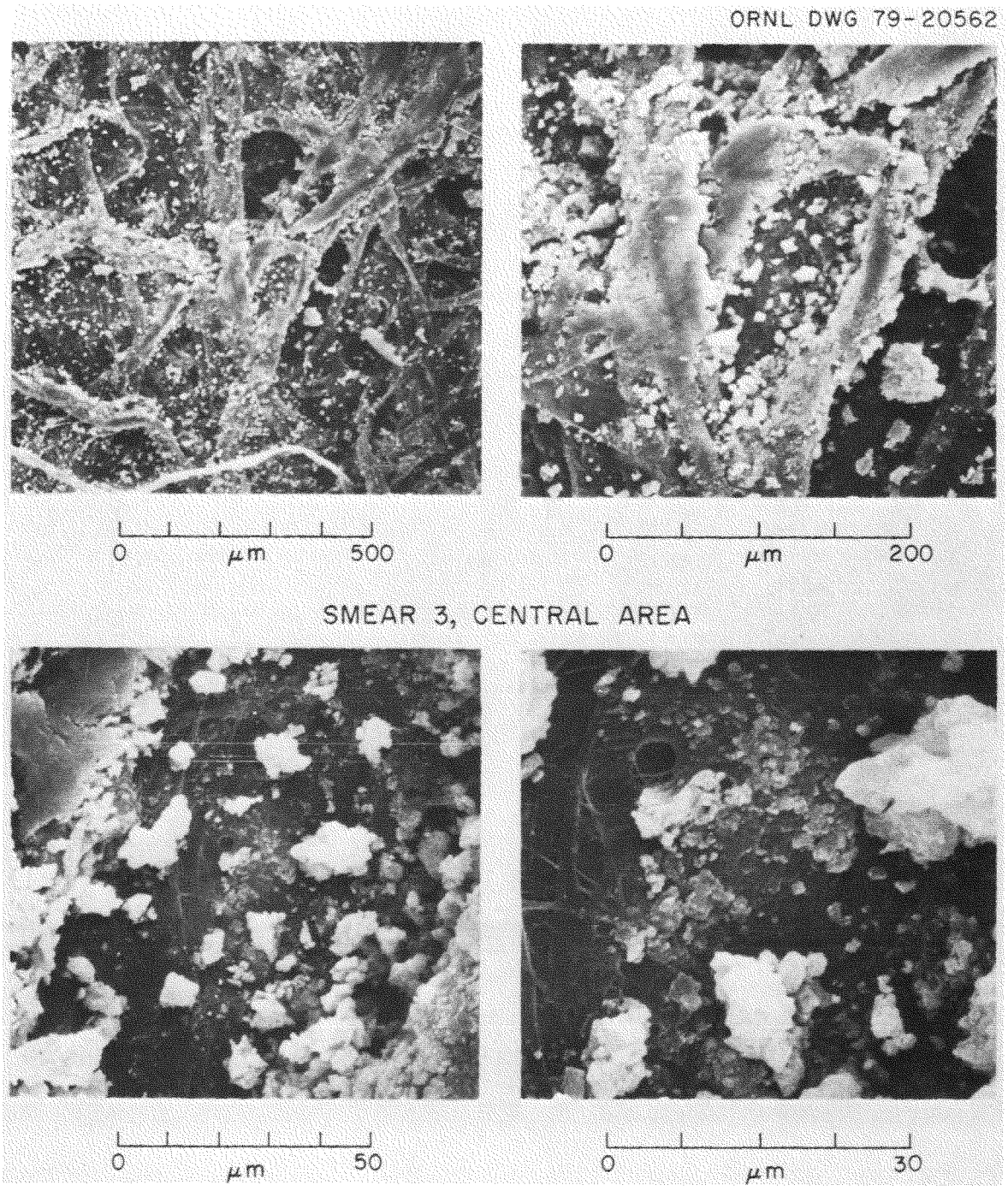

Fig. A-5. Photomicrographs of central area of smear 3.

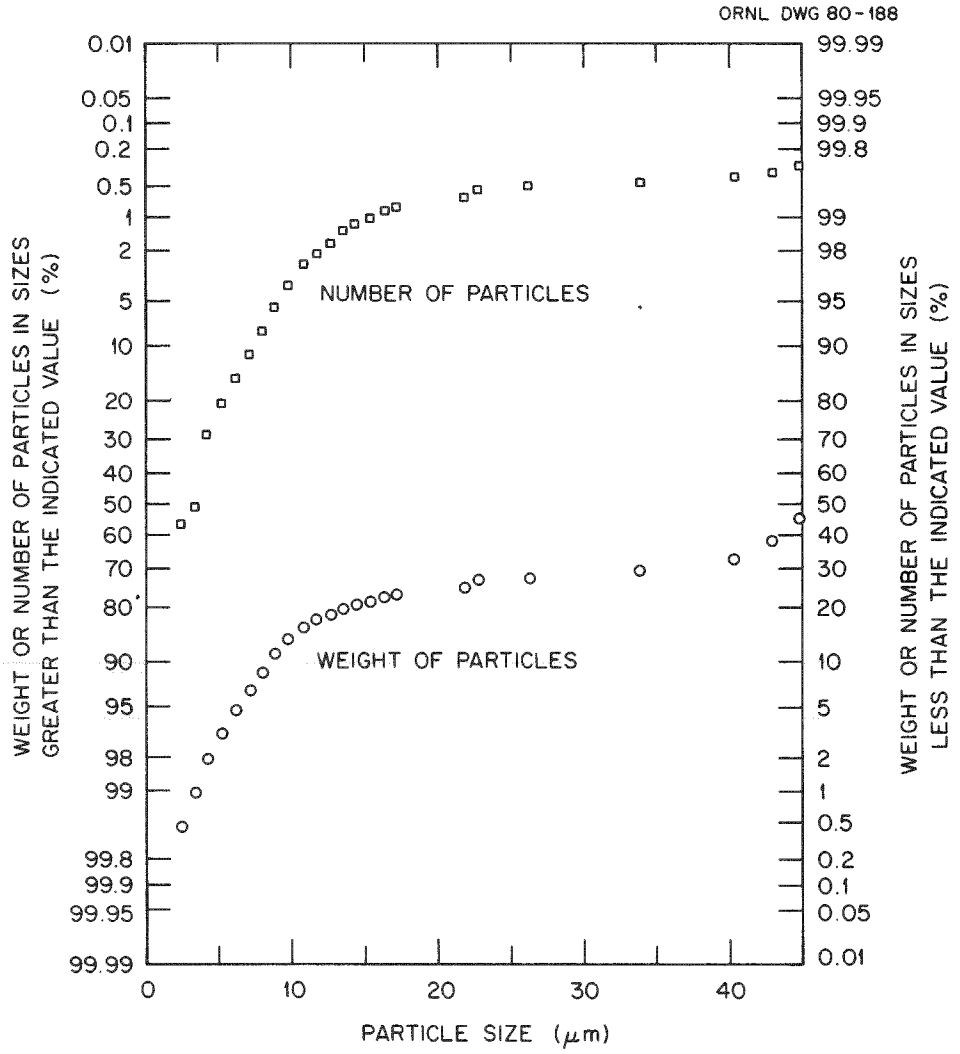

Fig. A-6. Normal distribution plots of number and weight of particles as a function of particle size. This distribution does not appear to apply.

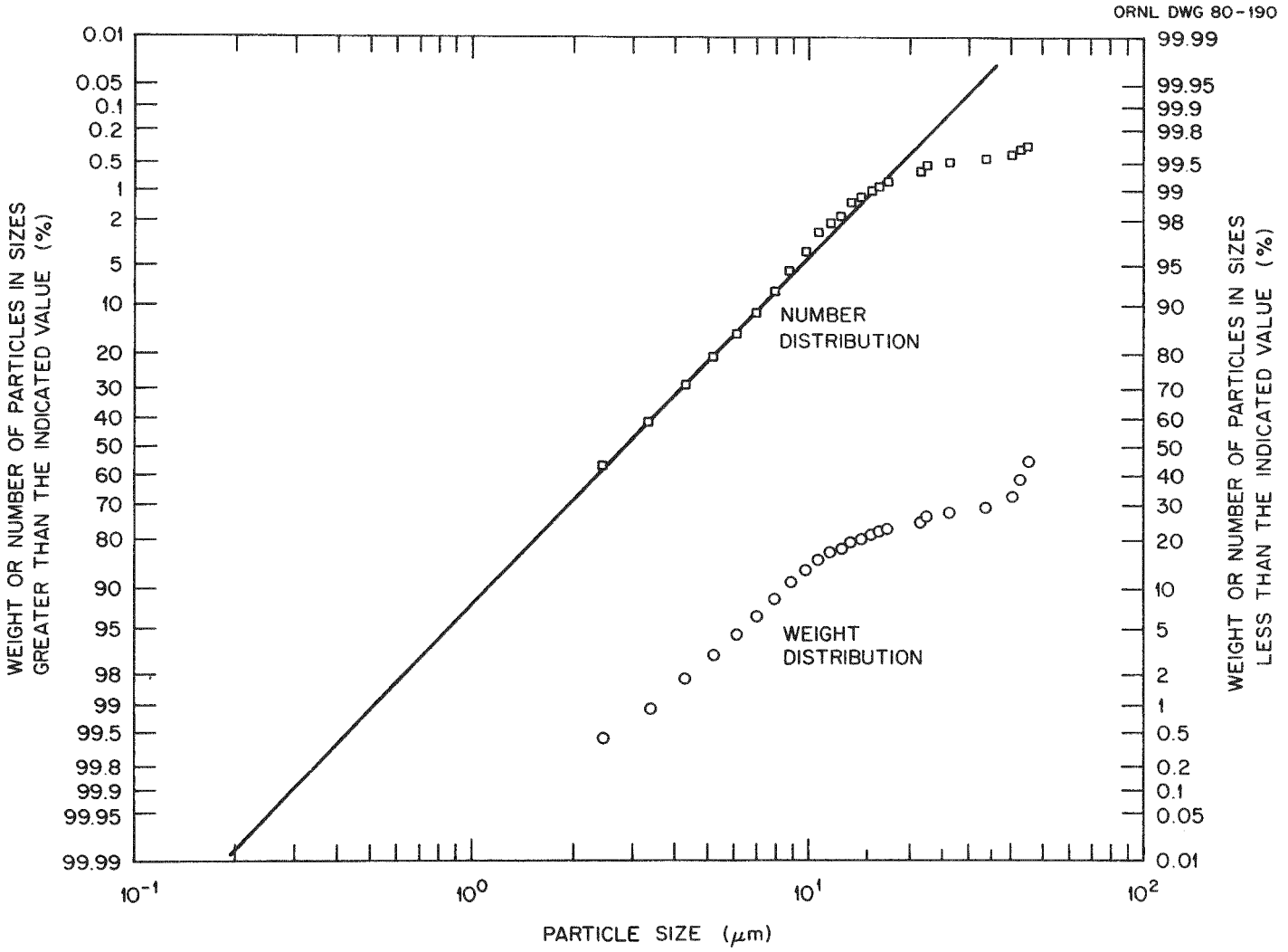

Fig. A-7. Lognormal distributions of number and weight of particles on the central section of smear 1 as a function of particle size. The number distribution describes the data very well.

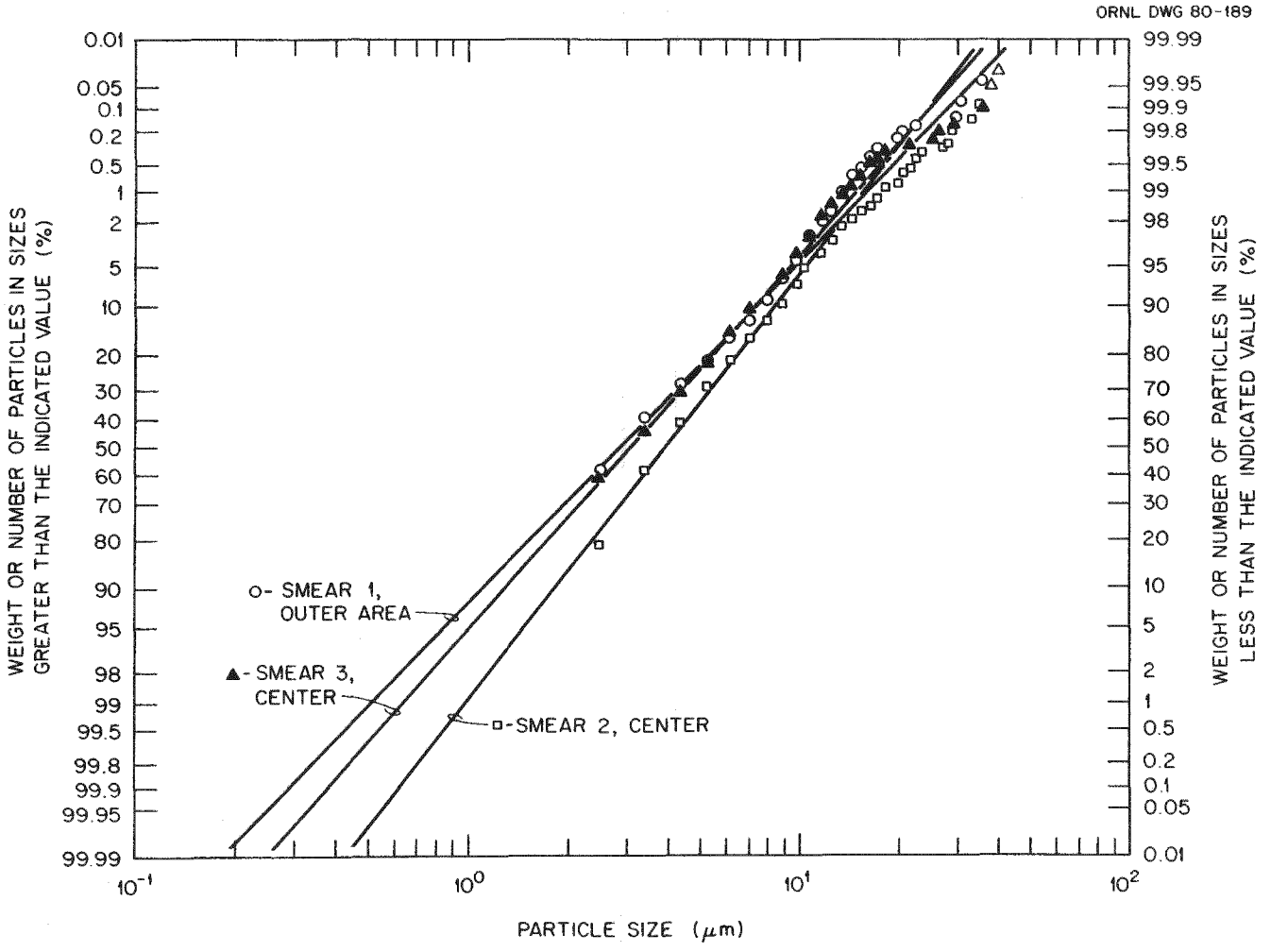

Fig. A-8. Lognormal distributions of number of particles as a function of particle size for three smear samples.

$$\Lambda(x) = \Lambda(x') + B \int_{x'}^{x} \frac{e^{-(\ln t - m)^2/(2s^2)}}{ts}\, dt, \qquad \text{(A-2)}$$

where

$$\Lambda(x') = B \int_{0}^{x'} \frac{e^{-(\ln t - m)^2/(2s^2)}}{ts}\, dt, \qquad \text{(A-3)}$$

and t is a dummy integration variable.

As noted previously,[8] splitting $\Lambda(x)$ into two terms, one of which, namely $\Lambda(x')$, is very small in comparison with the other, provides an easy method for avoiding the numerical difficulties of $-\infty$ due to ln t as $t \to 0$. In particular, $\Lambda(x')$ is in the order of 10^{-5} to 10^{-9} for x' in the range 0.1 to 0.01 μm; by contrast, the integral term of Eq. (2) is in the range 0.1 to 0.99, corresponding to 10 to 99% of the number distribution being in the form of particles between 1 and 50 μm. Once a set of parameters B, m, and s has been estimated, these can be used with graphical or numerical methods to improve the estimate of $\Lambda(x')$, where x' can be made a very small positive number.

Results of the particle-size distribution analyses, based on $B = 1/(2\pi)^{1/2}$, are presented in Table A-3. B was set to this value after it was first determined, with B as a parameter, that $B(2\pi)^{1/2} = 1.0$ within experimental error. It is apparent that particles on the wipe samples from the GPC at NFS are considerably smaller than particles produced by shearing irradiated or unirradiated light-water reactor (LWR) fuels.[8] Thus, mode, median, and mean particle sizes on the wipe samples are in the range 2, 3, and 4 μm, respectively; corresponding values of mode and median for particles from shearing LWR fuels were in the range 6 to 60 μm and 100 to 6000 μm, respectively.

Table A-3. Analysis of data on sizes of particles on wipe samples from the General Purpose Cell of the NFS West Vally Plant[a]

Sample designation	Parameter[b] m and $\hat{S}_m$	Parameter[b] s and $\hat{S}_s$	Standard deviation of fit	Mode[c] (μm)	Median[c] (μm)	Mean[c] (μm)
	Constant error in the fraction of particles of size smaller than specified[d]					
Smear 1 center	1.0447 0.0058	0.7352 0.0075	4.702E-3	1.66	2.84	3.73
Smear 1 outer area	1.0481 0.0093	0.7426 0.0119	7.487E-3	1.64	2.85	3.76
Smear 2 center	1.3576 0.0084	0.5952 0.0113	1.103E-2	2.73	3.89	4.64
Smear 3 center	1.1162 0.0031	0.6758 0.0041	2.942E-3	1.93	3.05	3.84
	Constant fractional error in the fraction of particles of size smaller than specified[e]					
Smear 1 center	1.0384 0.0037	0.7467 0.0065	5.844E-3	1.62	2.83	3.73
Smear 1 outer area	1.0506 0.0056	0.7377 0.0100	9.331E-3	1.66	2.86	3.75
Smear 2 center	1.3699 0.0072	0.5379 0.0099	2.230E-2	2.95	3.94	4.55
Smear 3 center	1.1144 0.0018	0.6799 0.0034	3.646E-3	1.92	3.05	3.84

[a] Based on the distribution of the number of particles of size smaller than a specified value.

[b] See Eq. (A-1) for definitions of m and s as used in this table. The symbol $\hat{S}$ is used to specify standard deviation of the parameter estimated from the data. Thus, $\hat{S}_m$ is the estimated standard deviation of m, $\hat{S}_s$ is the estimated standard deviation of s.

[c] Mode = $\exp(m - s^2)$; Median = $\exp(m)$; Mean = $\exp(m + s^2/2)$ (ref. 26).

[d] In this analysis the statistical weighting factor was 1.0.

[e] In this analysis the statistical weighting factor was (1.0/fraction of particles of size smaller than specified).

5.2 Appendix B: Calculation of Fractional Resuspension

Calculations of the fractions of UO_2 particles that will become resuspended for specific particle-size distribution, air-velocity distribution, and for elliptically shaped floor segments were performed by use of the computer program listed on the next two pages of this appendix. Input to this program consist of air speeds (ft/s), the maximum size (in micrometers) of particles that would remain entrained at the specified air speed, the minimum fractional and maximum fractional weights contained as particles of sizes less than the stated values (Table 10 or Fig. 4), and the floor lengths over which the air velocities exceed the stated values. These data are listed in columns 1, 8, 9, and 10, and 3, respectively, in Tables 15-17. As an example, the input for Case 1C1 (a 300-mph tornado with building walls intact) are given on page 78. Output from the program, including calculated floor areas and fractional floor areas within air-velocity contours, are given for this case on page 78. This corresponds to Table 17.

```
      DIMENSION AFT2(20), AM2(20)
      DIMENSION CON(10)
      DIMENSION DIFAM2(20)
      DIMENSION FAREA(20), FRMIN(20), FRMAX(20)
      DIMENSION GU(20)
      DIMENSION PSMAX(20)
      DIMENSION WINDSF(20), WINDSM(20), WNDSIF(20), WNDSIM(20)
      CON(1) = 3.14159 * (11. / 15.) * (46. / 15.) / 4.
      CON(2) = 0.3048
      CON(3) = 0.0929
      CON(4) = 46. * 11. * CON(3)
   41 TYPE 1031
      ACCEPT 901, NOF
      IF (NOF.EQ.0) CALL EXIT
      TYPE 1041
      ACCEPT 901, NO
      GO TO (51,61,71,81) NOF
   51 OPEN (UNIT=1, FILE='CASE1.DAT')
      GO TO 91
   61 OPEN (UNIT=1, FILE='CASE2.DAT')
      GO TO 91
   71 OPEN (UNIT=1, FILE='CASE3.DAT')
      GO TO 91
   81 OPEN (UNIT=1, FILE='CASE4.DAT')
   91 I = 0
  121 I = I + 1
      READ (1,911) WINDSF(I), GU(I)
      READ (1,921) WNDSIF(I), PSMAX(I), FRMIN(I), FRMAX(I)
      IF (WNDSIF(I).GE.0.0) GO TO 121
      NDP = I - 1
      NDP1 = I
      GO TO (151,161,171,181) NOF
  151 CLOSE (UNIT=1, FILE='CASE1.DAT')
      GO TO 191
  161 CLOSE (UNIT=1, FILE='CASE2.DAT')
      GO TO 191
  171 CLOSE (UNIT=1, FILE='CASE3.DAT')
      GO TO 191
  181 CLOSE (UNIT=1, FILE='CASE4.DAT')
  191 CONTINUE
      DO 201 I = 1,NDP1
        AFT2(I) = CON(1) * GU(I) * GU(I)
        AM2(I) = AFT2(I) * CON(3)
        WINDSM(I) = WINDSF(I) * CON(2)
  201 CONTINUE
      SUMMIN = 0.0
      SUMMAX = 0.0
      DO 251 I = 1,NDP
        DIFAM2(I) = AM2(I) - AM2(I+1)
        FAREA(I) = DIFAM2(I) / CON(4)
        WNDSIM(I) = WNDSIF(I) * CON(2)
        TEMP = AM2(I) / CON(4)
        IF (I .GT. 1) GO TO 231
        TERM1 = FRMIN(I)
        TERM2 = FRMAX(I)
        GO TO 241
```

```
231    TERM1 = FRMIN(I) - FRMIN(I-1)
       TERM2 = FRMAX(I) - FRMAX(I-1)
241    SUMMIN = SUMMIN + TEMP * TERM1
       SUMMAX = SUMMAX + TEMP * TERM2
251 CONTINUE
    WRITE (NO,1101)
    WRITE (NO,1111)
    WRITE (NO,1121)
    WRITE (NO,1131)
    WRITE (NO,1141)
    WRITE (NO,1151)
    WRITE (NO,1171)
    DO 401 I = 1,NDP
      WRITE (NO,1201) WINDSF(I), WINDSM(I), GU(I), AFT2(I), AM2(I)
      WRITE (NO,1211) WNDSIF(I), WNDSIM(I), DIFAM2(I), FAREA(I),
   1                  PSMAX(I), FRMIN(I), FRMAX(I)
401 CONTINUE
    WRITE (NO,1201) WINDSF(NDP1), WINDSM(NDP1), GU(NDP1), AFT2(NDP1),
   1                AM2(NDP1)
    WRITE (NO,1241)
    WRITE (NO,1251) SUMMIN, SUMMAX
    WRITE (NO,1301)
    GO TO 41
901 FORMAT (I1)
911 FORMAT (E10.0, 30X, E10.0)
921 FORMAT (7E10.0)
1031 FORMAT ('  PLEASE TYPE A FILE NUMBER TO SPECIFY WHETHER THE    '/
   1         '  TORNADO CONDITION FILE IS 1, 2, 3, OR 4             '/)
1041 FORMAT ('  PLEASE TYPE A UNIT NUMBER TO SPECIFY DESTINATION OF '/
   1         '  THE OUTPUT.                                         '/)
1101 FORMAT ('                        FLOOR                              FRACT
   1  MAX                          ' / )
1111 FORMAT ('     WIND  SPEED      LENGTH                              OF GPC
   1  SIZE   FRACTION OF           ' / )
1121 FORMAT ('     NEAR  FLOOR       OVER      FLOOR AREA               AREA
   1   OF    PARTICULATE           ' / )
1131 FORMAT ('     OF  GENERAL      WHICH        WITHIN                  IN
   1 PARTI   WEIGHT THAT           ' / )
1141 FORMAT ('       PURPOSE       SPEED IS    ELLIPTICAL    DIFF      DIFF
   1 AIR-      BECOMES            ' / )
1151 FORMAT ('     CELL  (GPC)     EXCEEDED     CONTOUR      AREA      AREA
   1 BORNE    AIRBORNE            ' / )
1171 FORMAT ('     FT/S     M/S    GRID UN.    FT**2  M**2    M**2
   1   M                          ' / )
1201 FORMAT (F8.2, F7.2, F9.1, F10.0, F6.1)
1211 FORMAT (F8.2, F7.2, 25X, F7.2, F8.3, F7.0, F7.2, ' -', F5.2)
1241 FORMAT (///)
1251 FORMAT ('  BASED ON UNIFORM DISTRIBUTION OF SOLIDS ON THE FLOOR,
   1    '/
   2         '  THE FRACTION OF SOLIDS THAT BECOMES AIRBORNE IS BETWEEN
   3    '/
   4         F7.3, ' AND', F6.3)
1301 FORMAT (1H1)
     RETURN
     END
```

Sample Input Data

0.0				15.
1.0	30.	0.0072	0.115	
2.0				13.2
3.0	65.	0.030	0.22	
4.0				12.0
5.0	95.	0.053	0.28	
6.0				10.8
7.0	125.	0.07	0.34	
8.0				9.3
9.0	150.	0.08	0.37	
10.0				7.0
10.75	180.	0.09	0.42	
11.5				2.6
-1.0				

Output Results

WIND SPEED NEAR FLOOR OF GENERAL PURPOSE CELL (GPC)		FLOOR LENGTH OVER WHICH SPEED IS EXCEEDED	FLOOR AREA WITHIN ELLIPTICAL CONTOUR		DIFF AREA	FRACT OF GPC AREA IN DIFF AREA	MAX SIZE OF PARTI AIR-BORNE	FRACTION OF PARTICULATE WEIGHT THAT BECOMES AIRBORNE
FT/S	M/S	GRID UN.	FT**2	M**2	M**2		μM	
0.00	0.00	15.0	397.	36.9				
1.00	0.30				8.33	0.177	30.	0.01 - 0.12
2.00	0.61	13.2	308.	28.6				
3.00	0.91				4.96	0.106	65.	0.03 - 0.22
4.00	1.22	12.0	254.	23.6				
5.00	1.52				4.49	0.096	95.	0.05 - 0.28
6.00	1.83	10.8	206.	19.1				
7.00	2.13				4.95	0.105	125.	0.07 - 0.34
8.00	2.44	9.3	153.	14.2				
9.00	2.74				6.15	0.131	150.	0.08 - 0.37
10.00	3.05	7.0	87.	8.0				
10.75	3.28				6.93	0.147	180.	0.09 - 0.42
11.50	3.51	2.6	12.	1.1				

BASED ON UNIFORM DISTRIBUTION OF SOLIDS ON THE FLOOR,
THE FRACTION OF SOLIDS THAT BECOMES AIRBORNE IS BETWEEN
0.043 AND 0.226

6. REFERENCES

1. U.S. Department of Energy, Western New York Nuclear Service Center Study, TID-28905-3 (December 1978).

2. U.S. Nuclear Regulatory Commission, Interim Safety Evaluation I. Nuclear Fuel Services, Inc., and New York State Energy Research and Authority, Western New York Nuclear Service Center, Docket No. 50-201 (August 1977).

3. R. W. Andrae, R. A. Martin, and W. S. Gregory, Analysis of Nuclear Facilities for Tornado-Induced Flow and Reentrainment, Los Alamos Scientific Laboratgory, NUREG/CR-0521 (LA-7571-MS, Informal report) (January 1979).

4. K. H. Duerre, R. W. Andrae, and W. S. Gregory, TVENT, A Computer Program for Analysis of Tornado-Induced Transients in Ventilation Systems, LA-7397-M (July 1978).

5. L. J. Holloway and R. W. Andrae, Potential Radiological Impact of Tornadoes on the Safety of Nuclear Fuel Services' West Valley Fuel Reprocessing Plant. I. Tornado Effects on Head-End Cell Airflow, ORNL/NUREG-80/P1 (NUREG/CR-1530, Part 1) (1981).

6. Nuclear Regulatory Staff, NFS-Interim SER I, Docket No. 50-201 (May 1977).

7. Staff of Nuclear Fuel Services, Safety Analysis Report, NFS' Reprocessing Plant, West Valley, New York, Docket 50-201 (1973).

8. W. Davis, Jr., G. A. West, and R. G. Stacy, Oxide Particle Size Distribution from Shearing Irradiated and Unirradiated LWR Fuels in Zircaloy and Stainless-Steel Cladding: Significance for Risk Assessment ORNL/NUREG-60 (NUREG/CR-0866) (October 1979).

9. B. C. Finney, Oak Ridge National Laboratory, personal communication, May 30, 1979.

10. G. Dymmel, Boeing Engineering and Construction Co. (formerly at the West Valley Plant of NFS) personal communication, May 31, 1979.

11. A. G. Croff, M. A. Bjerke, G. W. Morrison, and L. A. Petrie, Revised Uranium-Plutonium Cycle PWR and BWR Models for the ORIGEN Computer Code, ORNL/TM-6051 (September 1978).

12. C. B. Woodall, U.S. LWR Spent Fuel Inventory and Projection, Nuclear Assurance Corporation, Y/OWI/SUB-77/42500 (June 1977).

13. E. D. Arnold and B. F. Maskewitz, SDC, A Shielding-Design Code for Fuel Handling Facilities, ORNL-3041 (March 1966). Also available from the Radiation Shielding Information Center of Oak Ridge National Laboratory as SDC, Kernel Integration Shield Design Code for Radioactive Fuel Handling Facilities, CCC-60 (Nov. 25, 1973).

14. K. Stewart, "The Resuspension of Particulate Material from Surfaces," pp. 63-74 in Proceedings of the International Symposium on Surface Contamination, Gatlinburg, Tenn., June 1964, ed. by B. R. Fish, Pergamon, New York (1967).

15. U.S. Nuclear Regulatory Commission, Reactor Safety Study: An Assessment of Accident Risks in U.S. Commercial Nuclear Power Plants, WASH-1400 (NUREG-75/014) (October 1975).

16. J. W. Healy, Surface Contamination: Decision Levels, Los Alamos Scientific Laboratory, LA-4558-MS (September 1971).

17. M. Corn, "Adhesion of Particles," Aerosol Science, ed. by C. N. Davies, Academic, New York (1966).

18. C. N. Davies, "Deposition from Moving Aerosols," Aerosol Science, ed. by C. N. Davies, Academic, New York (1966).

19. C. N. Davies, "The Sedimentation of Small Suspended Solids," p. 25 in Symposium on Particle Size Analysis, Institution of Chemical Engineers and Society of Chemical Industry, Feb. 4, 1947 (Trans. Inst. Chem. Eng. Suppl. 25, 25-39 1947).

20. C. N. Davies, "Definitive Equations for the Fluid Resistance of Spheres," Proc. Phys. Soc. (London) 57, 259 (1945).

21. J. D. Iversen, J. B. Pollack, R. Greeley, and B. R. White, "Saltation Threshold on Mars: The Effect of Interparticle Force, Surface Roughness, and Low Atmospheric Density," Icarus 29, 381 (1976).

22. J. D. Iversen, R. Greeley, and J. B. Pollack, "Windblown Dust on Earth, Mars, and Venus," J. Atmos. Sci. 33, 2425 (1976).

23. L. D. Cloutman, C. W. Hirt, and N. C. Romero, SOLA-ICE: A Numerical Solution Algorithm for Transient Compressible Fluid Flows, Los Alamos Scientific Laboratory, LA-6236 (July 1976).

24. P. M. Morse and H. Feshback, Methods of Theoretical Physics, McGraw-Hill Book Co., New York, 1953. See particularly Chapter 5 of Part 1, and pp. 1292-1295 of Part 2 of the 3rd edition.

25. D. W. Marquardt, "An Algorithm for Least-Squares Estimation of Nonlinear Parameters," J. Soc. Ind. Appl. Math. 11, 431 (1963).

26. D. W. Marquardt, Least-Squares Estimation of Nonlinear Parameters (NLIN), SHARE Program Library, SDA 3094 01 (Aug. 15, 1966).

27. J. Aitchison and J. A. C. Brown, The Lognormal Distribution, Cambridge University Press, New York, 1957.

NUREG/CR-1530, Part 2
ORNL/NUREG-80/P2

INTERIM DISTRIBUTION

1-3. W. Davis, Jr.

4. D. E. Ferguson

5. E. J. Frederick

6. L. J. Holloway

7. A. L. Lotts

8. C. D. Scott

9. C. H. Shappert

10. V.C.A. Vaughen

11. Laboratory Records, RC

12. Laboratory Records

13. ORNL Patent Section

14-15. Technical Information Center, Oak Ridge, Tenn. 37830

16. Office of Assistant Manager, Energy Research and Development
Department of Energy, Oak Ridge Operations Office,
Oak Ridge, TN 37830